

THE RATIONAL DESIGN OF RECOGNITIVE POLYMERIC
NETWORKS FOR SENSING APPLICATIONS

Except where reference is made to the work of others, the work described in this dissertation is my own or was done in collaboration with my advisory committee. This dissertation does not include proprietary or classified information.

Kimberly RyAnne Dial Noss

Certificate of Approval:

Robert Chambers
Professor
Chemical Engineering

Mark E. Byrne, Chair
Mary and John Sanders
Associate Professor
Chemical Engineering

ZhongYang (Z.-Y.) Cheng
Associate Professor
Material Engineering

Yoon Y. Lee
Alumni Professor
Chemical Engineering

George T. Flowers
Dean
Graduate School

THE RATIONAL DESIGN OF RECOGNITIVE POLYMERIC
NETWORKS FOR SENSING APPLICATIONS

Kimberly RyAnne Dial Noss

A Dissertation

Submitted to

the Graduate Faculty of

Auburn University

in Partial Fulfillment of

the Requirements of the

Degree of

Doctor of Philosophy

Auburn, Alabama
May 9, 2009

THE RATIONAL DESIGN OF RECOGNITIVE POLYMERIC
NETWORKS FOR SENSING APPLICATIONS

Kimberly RyAnne Dial Noss

Permission is granted to Auburn University to make copies of this dissertation at its discretion, upon the request of individuals or institutions and at their expense. The author maintains copyright and retains all publication rights.

Signature of Author

Date of Application

VITA

The author Kimberly RyAnne Dial Noss was born in Birmingham, Alabama. She attended Auburn University from 1998 to 2003 where she earned a Bachelor in Chemical Engineering Degree from Auburn University. RyAnne married Scot Robert Noss on August 2, 2003 and shortly afterwards joined the Chemical Engineering graduate program at Auburn University.

DISSERTATION ABSTRACT
THE RATIONAL DESIGN OF RECOGNITIVE POLYMERIC
NETWORKS FOR SENSING APPLICATIONS

Kimberly RyAnne Dial Noss

Doctor of Philosophy, May 9, 2009
(B.ChE, Auburn University, 2003)

142 Typed Pages

Directed by Mark E. Byrne

Testosterone recognitive networks were synthesized with varying feed crosslinking percentages and length of the bi-functional crosslinking agent to analyze the effect of changing structural parameters on template binding properties such as affinity, selectivity, capacity, and diffusional transport. The crosslinking percentage of the crosslinking monomer ethylene glycol dimethacrylate was varied from 50% to 90% and associated networks experienced a 2 fold increase in capacity and a 4 fold increase in affinity with the equilibrium association constants, K_a , ranging from $0.32 \pm 0.02 \times 10^4 \text{ M}^{-1}$ to $1.3 \pm 0.1 \times 10^4 \text{ M}^{-1}$, respectively. The higher concentration of crosslinking monomer increased the crosslinking points available for inter-chain stabilization creating an increased number of stable cavities for template association. However, by increasing the length of the crosslinking agent and increasing the feed crosslinking percentage from

77% crosslinked poly(methacrylic acid-*co*-ethylene glycol dimethacrylate) (poly(MAA-*co*-EGDMA)) to 50% crosslinked poly(methacrylic acid-*co*-poly(ethylene glycol)200 dimethacrylate) (poly(MAA-*co*-PEG200DMA)), the mesh size of the network increased resulting in an increased template diffusion coefficient from $(2.83 \pm 0.06) \times 10^9 \text{ cm}^2/\text{s}$ to $(4.3 \pm 0.06) \times 10^9 \text{ cm}^2/\text{s}$, respectively, which is approximately a 40% faster template diffusional transport. A 77% crosslinked poly (MAA-*co*-PEG200DMA) recognitive network had an association constant of $(0.20 \pm 0.05) \times 10^4 \text{ M}^{-1}$ and bound $(0.72 \pm 0.04) \times 10^{-2} \text{ mmol testosterone/g dry polymer}$, which was less by 6 and 3 fold, respectively, compared to a similarly crosslinked poly(MAA-*co*-EGDMA) recognitive network. Structural manipulation of the macromolecular architecture illustrates the programmability of recognitive networks for specific template binding parameters and diffusional transport, which may lead to enhanced imprinted sensor materials and successful integration onto sensor platforms.

ACKNOWLEDGEMENTS

I would first like to thank Jesus Christ, the savior of my heart and soul, for granting me the fortitude and strength that has carried me through this journey. I would also like to thank my husband, Scot Noss, who is and will always be the hero of my heart. Scot was always a source of encouragement. Scot's love and dedication to our marriage made life beautiful and for that, I will always be thankful. I would also like to thank my mother, Linda Dial, who is my "constant" and my biggest fan. My mom always believed in me, even when I didn't believe in myself. I would like to thank my best friend and older but much wiser sister, Ceil Harper, whose comedic timing brings relief in situations where they are needed and much appreciated. I would like to thank my Dad, Bill Dial, for always believing his baby girl could reach her dreams. Thank you to all my family and friends for their constant devotion, support, and presence in my life.

I would also like to thank Ron and Nelda Noss and the Noss Family. The Noss Family took me in as their daughter-in-law and has loved me as their own. I would also like to thank my professor, Mark E. Byrne, who saw potential in me and gave me a chance to show my abilities to the world. Also, I thank my committee members for their participation in my dissertation defense and their valuable feedback. I would also like to thank the faculty and staff of the Chemical Engineering Department for their constant support especially the past two years. I would like to thank Asa Vaughan for his support

and friendship during my doctoral work. Thank you to Deborah Bacik for being there for me, even if just for one of our diet coke breaks. Also, thank you to Siddarth Venkatesh and Maryam Ali for their wisdom and friendship. My eyes have forever been opened.

I would also like to thank Ivonne and A.J. Thompson. Without Ivonne, I would not have made it through the past two years. Thank you to all the families at the Fisher House for your love and support. I would also like to thank Col. Russ Kotwal for his encouragement in finishing my degree. Dr. Kotwal saw the importance before I did, and I thank him for his gentle persuasions. To the United States Special Operations Command and the Care Coalition, thank you so much for your support during Scot's injury. If it was not for your wonderful group, Scot would have been lost in the system, and I would be left to fight this battle alone. Thank you.

My deepest gratitude to the funding agencies that supported my research: National Science Foundation (NSF-CBET-0730903, Grant G00003191), US Department of Education (GAANN Grant P200A060184, K.R.N- GAANN Fellow), the USDA-CSREGS under Grant (2006-34394-16953), the Auburn University Detection and Food Safety Center (M.E.B. is a participating member), and an Auburn University Competitive Research Grant.

I DID IT SCOT! I love you! WAR EAGLE AND GOD BLESS AMERICA!

Dr. Kimberly RyAnne Dial Noss

Style manual or journal used American Chemical Society Style.

Computer software used Microsoft Word, Excel, Visual Basic, Endnote

TABLE OF CONTENTS

LIST OF FIGURES.....	xiii
1.0 INTRODUCTION	1
2.0 RECOGNITIVE POLYMERIC NETWORKS COMBINED WITH BIODIAGNOSTICS AND BIOSENSORS	3
2.1 Free-Radical Polymerization	5
2.2 Polymerization Methods	7
2.2.1 Covalent Template Polymerization.....	7
2.2.2 Non-Covalent Template Polymerization	8
2.3 Network Altering Parameters of Templated Polymerization.....	10
2.3.1 Solvent Effect.....	10
2.3.2 Temperature Effect	12
2.3.3 pH and Ion Concentration Effect	14
2.3.4 Crosslinking Agent and Feed Concentration Effect	14
2.4 Polymer Network Mesh Size and Mesh Size Calculation	15
2.5 Template Rebinding and Selectivity Studies	17
2.6 Biomolecular Diagnostics and Sensing	19
2.6.1 Biomolecular Diagnostics	20
2.6.2 Biosensing Platforms for Molecular Detection.....	21
2.6.2.1 Microcantilevers	22

2.6.2.2 Surface Plasmon Resonance	23
2.6.3 Surface Plasmon Resonance Theory	25
2.7 Facilitation of Intelligent Polymers at the Micro/Nano Scale	28
2.7.1 Lithography Techniques	28
3.0 STRUCTURAL DESIGN, SYNTHESIS, AND BINDING PARAMETER	
ANAYLSIS OF RECOGNITIVE NETWORKS.....	48
3.1 Scientific Rationale.....	49
3.2 Synthesis of a Typical Recognitive Polymer for Testosterone.....	50
3.2.1 Materials	50
3.2.2 Polymer Synthesis.....	50
3.2.3 Polymer Recognition Studies: Template Affinity, Capacity, and Selectivity .	52
3.2.4 Double Bond Conversion.....	57
3.3 Results and Discussion	59
<u>3.3.1 Analysis of Template Binding Parameters</u>	<u>59</u>
3.3.2 Double Bond Conversion via Reaction Analysis.....	63
3.4 Conclusions.....	65
3.5 References.....	67
4.0 TRANSPORT CONSIDERATIONS OF RECOGNITIVE NETWORKS	79
4.1 Scientific Rationale.....	79
4.2 Theoretical Model of Diffusion	81
4.3 Synthesis of Recognitive Networks for Template Release Studies	84
4.3.1 Materials	84

4.3.2 Polymer Synthesis.....	85
<u>4.4 Results and Discussion</u>	<u>86</u>
4.5 Conclusions.....	93
4.6 References.....	93
5.0 CONCLUSIONS.....	105
APPENDIX A.....	107
A-1. Data from the Template Rebinding Studies.....	108
A-2 Data from the Template Release Studies.....	120
APPENDIX B	128
B-1. Error Analysis	128

LIST OF FIGURES

Figure 2.1: Template-Mediated Polymerization.	46
Figure 2.2: Illustration of the Surface Plasmon Refractive Theory.	47
Figure 3.1: Functional Monomer and Crosslinking Agent Structure..	70
Figure 3.2: The Molecular Structure of Testosterone and Progesterone..	71
Figure 3.3: Testosterone Equilibrium Binding Isotherms of 77% Crosslinked Poly(MAA- <i>co</i> -EGDMA) Recognitive and Control Networks.....	72
Figure 3.4: Testosterone Equilibrium Binding Isotherms of Poly(MAA- <i>co</i> -EGDMA) and Poly(MAA- <i>co</i> -PEG200DMA) Recognitive Networks at Various Feed Crosslinking Percentages	73
Figure 3.5: Testosterone Equilibrium Binding Isotherms of Poly(MAA- <i>co</i> -EGDMA) and Poly(MAA- <i>co</i> -PEG200DMA) Networks at 77% Feed Crosslinking.....	74
Figure 3.6: Testosterone Binding Affinity Constants for Poly(MAA- <i>co</i> -EGDMA) and Poly(MAA- <i>co</i> -PEG200DMA) Networks at Various Feed Crosslinking Percentages	75
Figure 3.7: Selectivity Study of Poly(MAA- <i>co</i> -EGDMA) Recognitive Networks at 77% Crosslinking	76
Figure 3.8: Heat flow versus Time for the UV Polymerization of 77% Crosslinked poly(MAA- <i>co</i> -EGDMA) Recognitive Network.	77
Figure 3.9: Fractional Double Bond Conversion Versus Feed Crosslinking Percentage using UV Polymerization.....	78

Figure 4.1: Illustration of the Mesh Size in Rigid Networks.	97
Figure 4.2: Mass of Testosterone Released from a 77% Testosterone Recognitive and Control Poly(MAA- <i>co</i> -EGDMA) Network.....	98
Figure 4.3: Fractional Mass of Testosterone Released from a 77% Testosterone Recognitive and Control Poly(MAA- <i>co</i> -EGDMA) Network....	99
Figure 4.4: Mass of Testosterone Released from Testosterone Recognitive Poly(MAA- <i>co</i> -EGDMA) Network at Various Crosslinking Percentages..	100
Figure 4.5: Fractional Mass of Testosterone Released from Testosterone Recognitive Poly(MAA- <i>co</i> -EGDMA) Network at Various Crosslinking Percentages.....	101
Figure 4.6: Mass of Testosterone Released from Testosterone Recognitive Poly(MAA- <i>co</i> -EGDMA) and Poly(MAA- <i>co</i> -PEG200DMA) Networks at 77% Crosslinking.....	102
Figure 4. 7: Fractional Mass of Testosterone Released from Testosterone Recognitive Poly(MAA- <i>co</i> -EGDMA) and Poly(MAA- <i>co</i> -PEG200DMA) Networks at 77% Crosslinking.....	103
Figure 4. 8: Diffusion Coefficients for Testosterone Recognitive and Control Poly(MAA- <i>co</i> -EGDMA) and Poly(MAA- <i>co</i> -PEG200DMA) Network at Various Crosslinking Percentages..	104
Figure A.1.1: Relative Intensity Versus Wavelength..	108
Figure A.1.2: Standard Curve of Testosterone in Chloroform..	109
Figure A.1.3:Rebinding Isotherms of Testosterone Recognitive and Control Poly(MAA- <i>co</i> -EGDMA) at 77% Crosslinking.....	111

Figure A.1.4: Testosterone Equilibrium Binding Isotherms of Poly(MAA- <i>co</i> -EGDMA) at 50% Feed Crosslinking.....	112
Figure A.1.5: Rebinding Isotherm of Testosterone Recognitive and Control Poly(MAA- <i>co</i> -EGDMA) at 50% Crosslinking.....	114
Figure A.1.6: Testosterone Equilibrium Binding Isotherms of Poly(MAA- <i>co</i> -EGDMA) at 90% Feed Crosslinking.....	115
Figure A.1.7: Rebinding Isotherms of Testosterone Recognitive and Control Poly(MAA- <i>co</i> -EGDMA) at 90% Crosslinking.....	117
Figure A.1.8: Testosterone Equilibrium Binding Isotherms of Poly(MAA- <i>co</i> -PEG200DMA) at 77% Feed Crosslinking.....	118
Figure A.1 .9: Progesterone Equilibrium Binding Isotherms of Poly(MAA- <i>co</i> -EGDMA) at 77% Feed Crosslinking.....	119
Figure A.2.1: Linear Regression Fractional Mass of Testosterone Released from Testosterone Recognitive Poly(MAA- <i>co</i> -EGDMA) Network at 77% Crosslinking.....	120
Figure A.2.2: Linear Regression Fractional Mass of Testosterone Released from the Control Poly(MAA- <i>co</i> -EGDMA) Network at 77% Crosslinking.....	121
Figure A.2.3: Linear Regression Mass Fraction of Testosterone Released from Testosterone Recognitive Poly(MAA- <i>co</i> -EGDMA) Network at 50% Crosslinking.....	122
Figure A.2.4: Linear Regression Fractional Mass of Testosterone Released from the Control Poly(MAA- <i>co</i> -EGDMA) Network at 50% Crosslinking.....	123

Figure A.2.5: Linear Regression Fractional Mass of Testosterone Released from Testosterone Recognitive Poly(MAA- <i>co</i> -PEG200DMA) Network at 77% Crosslinking.	124
Figure A.2.6: Linear Regression Fractional Mass of Testosterone Released from the Control Poly(MAA- <i>co</i> -PEG200DMA) Network at 77% Crosslinking.....	125
Figure A.2.7: Linear Regression Fractional Mass of Testosterone Released from Testosterone Recognitive Poly(MAA- <i>co</i> -PEG200DMA) Network at 50% Crosslinking.	126
Figure A.2. 8: Linear Regression Fractional Mass of Testosterone Released from the Control Poly(MAA- <i>co</i> -PEG200DMA) Network at 50% Crosslinking.....	127

1.0 INTRODUCTION

Recognitive networks are synthetic polymeric materials that are rationally designed to recognize or bind target molecules. Non-covalent molecular imprinting can create highly selective recognitive networks by promoting and stabilizing interactions between the chemical functionality of chain building monomers and the functionality of the template or “guest” molecules. Non-covalent interactions such as hydrogen bonding, Van der Waals forces, hydrophobic forces, and ionic interactions ensure the formation of site-specific cavities between monomer(s) and template molecules. The concept of macromolecular recognition manifests itself in two major synergistic effects: (i) shape specific cavities that match the template molecule, which provide stabilization of the chemistry in a crosslinked matrix, and (ii) chemical groups oriented to form multiple complexation points with the template.

In order to facilitate recognitive polymer integration within sensor platforms and optimize the response times, imprinted macromolecular structural parameters need to be studied to determine relationships between network architecture and template binding affinity, capacity, selectivity, and diffusional transport. Recognitive networks typically demonstrate increased affinity and selectivity in a highly crosslinked structure, which significantly limits template diffusion. Thus, the research that is presented within this dissertation focuses on the rational design and characterization of recognitive polymeric

networks by altering parameters that will influence network architecture such as the degree of network crosslinking and the size of the crosslinking monomer (i.e., feed or initial formulation crosslinking percentage and the length of the crosslinking monomer). We hypothesize that by tailoring the network structure, favorable and selective template binding can occur without significantly limiting the diffusion of the template molecule. In effect, imprinted networks can have programmable binding and diffusion parameters by rational design of the network, and this may allow them to integrate quite well in a number of sensing schemes. It is also important to note that depending on the diversity of molecules within a given sample environment (i.e., similarity in size and chemical functionality of other molecules compared to the template molecule) a highly-crosslinked, transport-restrictive, highly-selective network may not be needed to achieve adequate recognition.

Chapter 2.0 comprises of an overview of the literature describing macromolecular recognition and the parameters that affect recognitive polymer properties. This chapter also includes an overview of the field of biosensor platforms and methods to graft polymeric materials to those surfaces. Chapter 3.0 details the synthesis and template binding analysis of a testosterone recognitive polymer in conjunction with studying the effect of changing certain structural parameters. Finally, Chapter 4.0 discusses template diffusion data analysis, and the rational design of recognitive networks for future use as the main sensing element in biosensors.

2.0 RECOGNITIVE POLYMERIC NETWORKS COMBINED WITH BIODIAGNOSTICS AND BIOSENSORS

Recognitive polymeric networks are synthetic intelligent materials that have the ability to recognize or demonstrate selective binding to a target molecule. Another popular name for recognitive networks is molecularly imprinted polymers, implying that the target molecule's opposite molecular configuration and chemical functional groups are imprinted into the polymeric matrix of the network, creating synthetic, site-specific cavities for the target molecule. When the recognitive polymer is introduced into a target molecule environment, the polymer will bind the target molecule with an association constant that is comparable to association constants found in nature. Recognitive networks have been highly studied in recent years¹⁻⁸. For example, theophylline⁹, morphine¹⁰, cholesterol¹¹, and testosterone¹² recognitive networks have been designed with dissociation constants equal to $(8.1 \pm 0.9) \times 10^{-9}$ M, $(1.2 \pm 0.2) \times 10^{-6}$ M, $(5.9 \pm 1.3) \times 10^{-4}$ M, and 0.9×10^{-4} M, respectively. These values are comparable to dissociation constants found in nature. For example, a carbohydrate-protein^{13, 14} binding interaction has a dissociation constant that ranges from 10^{-3} to 10^{-6} M and antigen-antibody¹⁵ interactions have dissociation constants that range from 10^{-8} to 10^{-10} M.

Recognitive materials also exhibit template rebinding efficiency in wide ranges of pHs and temperatures¹⁶⁻²⁰. Mechanical stability and, most importantly, the relatively inexpensive cost of production make the material ideal for commercial applications in the

area of separations, biomaterials, sensors, and drug delivery²¹⁻²⁴. To demonstrate the suitability of cognitive networks in a wide range of environments, a thermal and chemical stability study was conducted on a theophylline cognitive methacrylic acid-ethylene glycol dimethacrylate copolymer²⁰. The network was very resilient withstanding temperatures ranging from 20°C to 350°C for 24 hours. However, at temperatures between 100°C and 350°C, there was an 80% decrease in the binding capacity. The polymers also withstood harsh environments such as acidic, basic, and autoclave environments (121°C) without drastically losing binding affinity for the template molecule²⁰.

It should also be noted that approximately 80% of the cognitive network research field uses the poly(methacrylic acid-*co*-ethylene glycol dimethacrylate) (poly(MAA-*co*-EGDMA)) networks as matrices for macromolecular recognition¹³. The poly(MAA-*co*-EGDMA) network is a crosslinked network which consists of linear MAA chains attached to one another by covalent links formed by the incorporation of a bi-functional crosslinking monomer, EGDMA²⁵. In this case, the crosslinking monomer is a monomer that has two carbon-carbon double bonds that can react and link two growing linear polymer chains together. The resulting macromolecular structure formed by the crosslinking polymer reaction forms the backbone for the three-dimensional template binding cavities. It should be noted that these crosslinked polymer networks do not dissolve and are not soluble in solvent. The crosslinks between linear chains form an interlinked macromolecule that can swell in the solvent, depending on how well the solvent interacts or solvates the polymer chains. The gel point or gelation point during a

polymerization reaction is the point at which the polymer becomes no longer soluble in solvent²⁶.

2.1 Free-Radical Polymerization

The most common method for the polymerization of a cognitive network is by free-radical polymerization. The monomer mixture usually consists of functional monomers, a template molecule, a bi-functional crosslinking agent, solvent, and initiator. The initiator frequently used for highly crosslinked networks is azobisnitrile because of the compound's high degree of initiator fragments or free radicals (R) that are formed after initiation (Eqn. 2.1).



After free-radical formation, the free radicals react with the carbonyl double bonds that are associated with the functional and crosslinking monomers (M) (Eqn. 2.2). For example, the initiator used in the research presented in this dissertation is azobisisobutyronitrile (AIBN). When irradiated with UV light, AIBN breaks into two 2-cyanoprop-2-yl radicals and two nitrogen molecules. The radical produced by the breaking of AIBN reacts with the carbon-carbon double bond within the monomer to form a monomer radical.

Propagation will occur (Eqn. 2.3), which is the addition of monomers to the growing polymer chain. Free radicals are unstable and will find a way to pair with an electron without the formation of other free radicals. Termination begins when two radicals come together to form a dead polymer chain (Eqn. 2.4). This is known as coupling. All the double bonds have reacted within this dead chain to form inter-linking between monomer units. Another form of termination is disproportionation, which is the transfer of one hydrogen atom from one growing polymer chain to another, forming different end groups without forming an inter-linking chain.

The two main reaction initiation mechanisms for free-radical polymerization are thermal and photo initiation. Thermal initiated free-radical polymerization is based upon heat of thermal energy breaking the initiation molecule into radicals from which the polymerization reaction begins. Thermal polymerizations at higher temperatures will have a faster rate of reaction, but double bond conversion is a better indicator of final polymer structure²⁷⁻²⁹. In most cases, thermal initiation takes place above a temperature of 40°C. With increases in temperature for initiation, hydrogen bond strength decreases resulting in weaker non-covalent bonding within the template molecule – functional monomer complex. This gives lower affinity binding sites and lower population density of binding sites within the final recognitive polymer structure³⁰⁻³².

Photoinitiated free-radical polymerization employs a photoinitiator that will form radicals upon irradiation with ultra-violet light. In photo-polymerization reactions, the amount and concentration of incident light plays an important role in the rate of radicals forming within the mixture which directly influences the polymerization rate. An increase

in intensity will yield an increase in the rate of reaction and double bond conversion^{33,34}. A major advantage of using photo-polymerization to create recognitive polymer networks is the ability to have lower temperatures which increase non-covalent bond strengths, which increase the stability of the template molecule–functional monomer complex. This results in the creation of more effective template binding sites^{20-23,26}.

2.2 Polymerization Methods

There are two main polymerization methods that can be used in imprinting a target molecule: covalent and non-covalent polymerization³⁵. We utilized the non-covalent polymerization method for our research; however, it is important to understand the multiple methods in recognitive polymer synthesis.

2.2.1 Covalent Template Polymerization

For the covalent polymerization method, the template molecule is covalently attached to the monomer in a chemical step that is independent of the polymerization. Such molecules as bisphenol A³⁶, testosterone³⁷, and cholesterol³⁸ have been successfully imprinted using the covalent polymerization method. Bisphenol A dimethacrylate was used as the template-monomer along with the crosslinking agent ethylene glycol dimethacrylate to produce a bisphenol A (BPA) recognitive network. After polymerization, the BPA was cleaved by hydrolysis for the creation of site specific cavities. When introduced to a solution of free BPA, the BPA recognitive polymer

recognized and bound the BPA molecules resulting in an association constant, K_a , equal to $1.72 \times 10^5 \text{ M}^{-1}$ ³⁶.

The template to monomer ratio and the feed crosslinking percentage are two important parameters in cognitive network polymerization. For the covalent method, the template to monomer ratio is stoichiometrically set due to the chemically modified step that covalently binds the monomer to the template molecule. Therefore, a known value of template monomers is used for imprinting. The crosslinking percentage of the monomer mixture is also of importance. Highly crosslinked networks create a very rigid structure. When the rigidity of the network is decreased (decreasing the feed crosslinking percentage), template binding decreases³⁹. One of the advantages of using the covalent method for molecular imprinting is that only the functional monomers are associated with the template molecule, decreasing the non specific interactions. However, some disadvantages are the tedious synthetic steps that are needed in the formation of the template monomer, and the chemical treatment to release the template from the network³⁵.

2.2.2 Non-Covalent Template Polymerization

The non-covalent method is the most commonly used method for cognitive polymerization. The rational design of the polymer network using the non-covalent method is to pair a functional monomer with chemical functional groups that will non-covalently bond with target molecule. Van der Waals, ionic, hydrophobic, and hydrogen bonding play a vital role in the functional monomer-template complexation. Figure 2.1

illustrates the non-covalent polymerization method. In Figure 2.1 A, the choice of the monomer is heavily dependent on the functionality of the target biomolecule. The functional monomer to template ratio is usually much higher than unity to ensure a higher probability of complexation between the template and functional monomer. The pre-polymerization solution, Figure 2.1 B, usually consists of the target molecule, functional monomer or monomers, a bifunctional crosslinking agent, solvent, and an initiator. Non-covalent complexation, which in most cases involves hydrogen bonding, will occur between the functional monomer(s) and the target molecule (Figure 2.1 C). After complexation, polymerization occurs usually by a free-radical thermal or UV photopolymerization initiation mechanism, forming a network that entraps the biomolecule (Figure 2.1 D).

A solvent is used to wash the template molecule out of the network disrupting the non-covalent interactions between the template molecule and the polymer. The cavity that is formed has the opposite configuration and chemical functional groups to bind template molecule. When the recognitive network is introduced into a solution of the same template molecule, the network rebinds the template with high selectivity and affinity⁹⁻¹². Typically, a control polymer is polymerized by the same method except the target molecule is not included.

One main advantage of using the non-covalent polymerization method over covalent polymerization is the elimination of synthetic chemistry in preparing the template-monomer complex. The number of target molecules available for imprinting significantly increases with the non-covalent method. The removal of the template is also

easier for non-covalently imprinted polymers which involves a washing step instead of a chemical hydrolysis step.

2.3 Network Altering Parameters of Templated Polymerization

The formation of site-specific cavities during polymerization is a function of the three-dimensional interactions between the functional monomer, the template, and the crosslinking agent⁴⁰. However, different characteristics of the monomer solution and post-polymerization conditions, such as the solvent or porogen used during polymerization and rebinding studies^{35, 41}, the temperature of polymerization and rebinding^{29, 42, 43}, pH and ion concentration^{35, 44}, and the crosslinking agent type and concentration all play a vital role in the binding affinity and selectivity of the polymer.

2.3.1 Solvent Effect

The solvent plays an important role in recognition ability, surface area, swelling capacity, and pore size of the polymer^{21, 45}. The selection of an aprotic solvent will increase the hydrogen bonding capacity between the template and the functional monomer. An aprotic solvent has a small or negligible degree of hydrogen bonding capability, forcing stronger template and functional monomer complexation to occur⁴⁶.

Low to moderately crosslinked polymers will exhibit swelling behavior by absorbing a large quantity of solvent within the network when in contact with a suitable solvent. Swelling behavior within crosslinked polymer networks is very similar to linear polymer chains being solvated by a solvent to form a polymer solution. Swelling

behavior is dictated by the change in Gibbs free energy ΔG , which is a combination of the Gibbs free energy of mixing, G_m , and Gibbs elastic free energy, G_{el} (Eqn. 2.5). The Gibbs free energy of mixing, ΔG_m , is further defined in equation 2.6,

$$\Delta G = \Delta G_m + \Delta G_{el} \quad (2.5)$$

$$\Delta G_m = \Delta H_m - T\Delta S_m \quad (2.6)$$

where ΔH_m is the enthalpy of mixing (i.e., heat of mixing), T is the temperature, and ΔS_m is the entropy of mixing. The elastic free energy is calculated by equation 2.7, where T is temperature and ΔS_{el} is the entropy change associated with the change in configuration of the network.

$$\Delta G_{el} = -T\Delta S_{el} \quad (2.7)$$

The Flory solvent interaction parameter, χ_1 , is a unitless quantity representing the enthalpy of mixing. The free energy of mixing equation using the Flory solvent interaction parameter is shown in equation 2.8, where k is a combination of the universal gas constant, R , multiplied by the temperature, T , N_1 and N_2 are the number of molecules for species 1 and species 2, respectively, and v_1 and v_2 are the volume fractions, where the subscript 1 usually represents the solvent and subscript 2 represents the polymer.

$$\Delta G_m = kT (N_1 \ln v_1 + N_2 \ln v_2 + \chi_1 N_1 v_2) \quad (2.8)$$

Swelling behavior would be augmented by ($\chi_1 < 0$), where complete miscibility is obtained at any temperature, and diminished by ($\chi_1 > 0$), where there is an upper limit where partial miscibility occurs^{25, 47, 48}.

The effect of the interaction energy between the functional monomer and template molecule was studied by varying the porogen for a nicotinamide methacrylic acid (MAA)-co-ethylene glycol dimethacrylate (EGDMA) recognitive polymer⁴⁵. The solvents that were used in the monomer mixture varied by dielectric constants (toluene, 2.4; chloroform, 5.5; methanol, 33.6; and acetonitrile 37.5). The results indicated that with aprotic solvents (i.e., chloroform, acetonitrile, and toluene) the interaction energy between the template and functional monomer was influenced by the dielectric constants of the solvents (e.g., the smaller the dielectric constant, the higher the interaction energy between the template and functional monomer). More complexes were formed with the smaller dielectric constant solvents because of the decreased interference of hydrogen bonding between the solvent and polymeric network. Additionally, protic solvents lowered the interaction energy by interfering with hydrogen bonding between the template and functional monomer, thereby, lowering the amount of complexes that were formed.

2.3.2 Temperature Effect

The temperature of polymerization and template rebinding also plays an important role in the binding affinity of recognitive networks⁴². Lower polymerization temperatures are ideal for non-covalent polymerization because non-covalent interactions, such as

hydrogen bonding, are stronger at lower temperatures, stabilizing the template-monomer complexes in the pre-polymerization solution. For polymerization reactions, conversion follows an Arrhenius relationship with respect to temperature. For acrylate and dimethacrylate copolymer networks, increasing the temperature increases both the polymerization rate and the double-bond conversion. The polymerization temperature can be varied, but the structural characteristics of the polymer product are better described by the final double bond conversion. For example, a polymer polymerized at 70°C with a double bond conversion of 50% has the same glass-transition temperature, T_g , as the same polymer polymerized at 40°C with a double bond conversion of 50%²⁷⁻²⁹. Glass-transition temperature is the temperature where a smaller second order transition occurs at which amorphous portions of a polymer soften and become rubbery⁴⁷. Higher temperatures correspond to higher double bond conversion and are a direct result of increased vibrational energy which translates to more flexibility within the growing network resulting in fewer steric hindrances.

Recently, the temperature of polymerization was varied in the synthesis of a 3-L-phenylalanylaminopyridine poly(MAA-*co*-EGDMA) network⁴². Various azobisnitriles (2,2-azobisisobutyronitrile (AIBN) and azobisdivaleronitrile (ABDV)) were used as the initiator in either thermal or UV polymerization initiation mechanisms with the temperature set at 10°C, 40°C, or 60°C. At the lowest temperature, UV light was utilized for polymerization, and for the higher temperatures, thermal free-radical polymerization was used as the polymerization initiation mechanism. In comparison to a thermally

initiated free-radical polymerization, the UV polymerized network had a higher template capacity (0.7 μmol) than that of the polymer made thermally at 60°C (0.3 μmol).

2.3.3 pH and Ion Concentration Effect

The pH and ion concentration play a vital role in the formation and rebinding of recognitive networks^{35, 44}. pH values either above or below the pKa of monomers (depending on the electrostatic makeup of the monomer backbone of the polymer) can influence the uptake of the template molecule. A study of the pH and the ionic concentration dependence was conducted on an ochratoxin A (OTA) imprinted poly(MAA-*co*-diethyl amino ethyl methacrylate(DEAEM)-*co*-acrylamide(AM)-*co*-EGDMA) network⁴¹. The results indicated that at a more acidic pH, the binding capacity of the template OTA was higher (95%), but at a basic pH the rebinding of the template molecule decreased to approximately 80%. Once the pH was above the pKa of the polymer, around pH 7.4, hindered the template binding due to electrostatic repulsion between the carboxylic acid groups and the template molecule. Thus, the binding capacity of the network decreased⁴¹.

2.3.4 Crosslinking Agent and Feed Concentration Effect

Diffusional transport limitations, which is a function of the concentration and length of the crosslinking agent in the monomer feed solution, also play a role in the design of the polymeric network (especially in respect to sensor design). The higher the feed crosslinking percentage, the more rigid the matrix, which will hinder the template

transport through the polymer. However, this can be overcome slightly by changing the thickness of the polymer. Thickness of the sensing element is a vital factor in the design of a cognitive network based sensor.

The feed concentration of the double bonds does not accurately represent the final double bonds reacted to form the polymeric network². In this paper, reaction analysis of a typical poly(MAA-co-EGDMA) molecularly imprinted network measured via differential scanning calorimetry revealed low double bond conversion ($35 \pm 2.3\%$ at 0°C to $54 \pm 1.9\%$ at 50°C) which is due to severely constrained network formation². In one study, an FT-IR spectroscopic analysis was performed on a polymeric network to relate the amount of carbonyl bonds reacted at different reaction temperatures. At higher temperatures, the number of unreacted double bonds was lower at 4.1% unreacted units compared to 12.9% unreacted units at 0°C ⁴². The unreacted double bonds of the network are due to pendant double bonds that are hindered because of the network.

2.4 Polymer Network Mesh Size and Mesh Size Calculation

The mesh size of a crosslinked polymer network is defined as the average distance between the linear polymer chains, and it is representative of the space available within the polymer network for diffusion⁴⁹. Peppas and Merrill⁵⁰ have developed a model using hydrogels, which are loosely crosslinked, water containing gels, to describe the relationship of average molecular weight between crosslinks (\overline{M}_c) and the polymer volume fraction in the swollen state ($v_{2,s}$) within a swollen crosslinked networks synthesized in the presence of a solvent (Eqn 2.9). The equation allows us to

calculate \overline{M}_c from experimentally determined values such as the polymer volume fraction in the swollen state ($v_{2,s}$); polymer volume fraction in the relaxed state ($v_{2,r}$); specific density of the polymer (\overline{v}); known quantities such as V_1 (molar volume of water); molecular weight of uncrosslinked polymer chains (\overline{M}_n); and the Flory polymer-solvent interaction parameter (χ_1).

$$\frac{1}{\overline{M}_c} = \frac{2}{\overline{M}_n} - \frac{\left(\frac{\overline{v}}{V_1}\right) \left[\ln(1 - v_{2,s}) + v_{2,s} + \chi_1 v_{2,s}^2 \right]}{v_{2,s} \left[\left(\frac{v_{2,s}}{v_{2,r}}\right)^{\frac{1}{3}} - \frac{1}{2} \left(\frac{v_{2,s}}{v_{2,r}}\right) \right]} \quad (2.9)$$

The mesh size (ξ) can be calculated from the (\overline{M}_c) using equation 2.10, where C_n is the rigidity factor, M_r is the molecular weight of the polymer repeating unit, and l is the length of the carbon-carbon bond (1.54Å).

$$\xi = v_{2,s}^{\frac{1}{3}} \left(\frac{2C_n \overline{M}_c}{M_r} \right)^{\frac{1}{2}} l \quad (2.10)$$

The average mesh size of a crosslinked polymer structure can be altered by the feed crosslinking percentage and by the length and branching of crosslinking monomer. In addition, a change in solvent, or pH of the solvent, can alter the Flory interaction parameter and the extent of swelling, which will directly affect the mesh size. High numbers of junction points or crosslinks within a polymer network are the reason that highly crosslinked polymer networks do not exemplify swelling behavior. Increasing the crosslinking monomer length has shown to increase the mesh size^{48, 51}. By changing the

swelling characteristics of the network, the diffusion characteristics of the template molecule through the polymer will change⁵². Recent literature demonstrates that an increase in solvent concentration in the pre-polymerization formulation results in a polymer network with increased mesh size, which would increase the template diffusional transport through the macromolecular structure⁵³⁻⁵⁵. Explanation given for the change in transport properties are as follows: the solvent does not become actively incorporated into the growing polymer chains, and the growing polymer chains have to form around the solvent within the system. Increasing the average mesh size of the macromolecular structure allows for increased diffusional transport through the polymer matrix. In the synthesis of imprinted polymer networks, solvent is used as a porogen to create pores within the macromolecular structure, allowing for faster diffusion of the template molecule through the macromolecular structure⁵⁶.

2.5 Template Rebinding and Selectivity Studies

Batch mode and chromatographic mode template rebinding studies are two main ways to determine the amount of template or substrate bound to the recognitive network. Within the batch mode, a known amount of recognitive polymer is placed in a known concentration of the substrate. After a predetermined amount of time, the polymer is separated and the effluent collected to determine the amount of free substrate in solution. The change in concentration of the free substrate compared to the original substrate concentration is the amount of substrate that is bound to the recognitive network. A binding isotherm is constructed for each polymeric network by obtaining final

equilibrium binding readings for a range of substrate concentrations for both the cognitive network and the control network. The uptake of the substrate molecule by the control polymer is through non specific interactions.

After the binding isotherm is completed, a mathematical analysis, using tools such as the Scatchard Analysis (Eqn. 2.11), the Freundlich Isotherm (Eqn. 2.12), or the Langmuir Isotherm (Eqn. 2.13), is used to analyze the data and the final determination of binding parameters is dependent on the fit of the data. The equations are presented below,

$$\frac{S_b}{C_f} = K_a N - S_b \quad (2.11)$$

$$S_b = AC_f^v \quad (2.12)$$

$$S = \frac{S_b K_a C}{1 + K_a C} \quad (2.13)$$

where S_b is the amount of substrate bound; C_f is the concentration of free substrate; K_a is the template association constant; N is the total number of binding sites; A is the Freundlich binding constant; v is the Freundlich heterogeneity parameter ($0 < v < 1$); S is the equilibrium concentration of the stationary phase; and C is the equilibrium concentration of the mobile phase. The Scatchard plot, however, is not the ideal mathematical analysis tool because it does not work well with hydrogen bonding solid phases. After mathematical analysis, an association constant, K_a , is determined, indicating how well the substrate binds to the network⁵⁷⁻⁵⁹.

The site-specific cavities within the cognitive network are highly selective to the template molecule. However, the cavity could also be selective to a molecule that has a similar configuration, or is the chiral opposite of the target molecule. For example, a

selectivity study was conducted on a α -bilirubin recognitive methacrylic acid poly(MAA-co-EGDMA) network to illustrate how selective the network was toward α -bilirubin compared to biliverdin, progesterone, and testosterone. The bilirubin had a superior binding capacity ratio of 5.3 ± 1.4 over the biliverdin, and a binding capacity ratio of 1.93, 1.37, and 2.89 with bilirubin in a mixture of progesterone, testosterone and biliverdin, respectively⁶⁰. The study demonstrates that the network is highly selective to α -bilirubin, but is capable of binding other molecules at lower selectivity due to the similar shape, size, and configuration of the molecules.

2.6 Biomolecular Diagnostics and Sensing

Biomolecular diagnostics and detection has reached a new frontier in the past decade with the development of micro/nanotechnology that is capable of moving conventional *in-vitro* diagnostic capabilities *in-vivo*. Such progress has led to advancements in cellular imaging and detection of diseases in the early stages, which is beneficial for the early administration of therapeutics. These new developments have led to the tracking of cellular migration, which is a crucial part of understanding the biological phenomena that takes place once transplanted cells have been distributed *in-vivo*^{61, 62}. Also, the development of micro/nanotechnology for biosensing has allowed, among other things, diagnostic tests to be administered at point-of-care instead of sending the sample off to another location for analysis. The general idea of using micro/nanotechnology for diagnostics and detection strategies is to have a faster, more reliable, less expensive means to detect and diagnose illness for early treatment, which

can lead to overall improved health of the patient. The rational design of synthetic cognitive polymers for biomolecular sensing will make such advancements a reality. A brief literature review is presented in the following sections.

2.6.1 Biomolecular Diagnostics

Molecular Resonance Imaging (MRI) is one technique that offers near cellular resolution that has the ability to detect at a molecular level. This is very crucial in cancer diagnostics and therapy⁶¹⁻⁶⁹. Magnetic nanoparticles are used as the reagents in support of imaging cells with MRI. For specific cell targeted imaging, the nanoparticles are modified with molecular ligands (i.e., glycoproteins, saccharides, antibodies) to aid the attachment to the specific cell for imaging (e.g., the T cell response to certain pathogens or cancer cells and the tracking of stem cell migration for the advancement of stem cell research⁶¹). Gadolinium-rhodamine modified nanoparticles were investigated as contrast agents for use with MRI for the tracking of stem cell migration *in-vivo*, tissue procurement, and fluorescence characterization⁶¹. The cells that were labeled with gadolinium-rhodamine had higher resolution not only in the MR imaging, but also in fluorescence and optical imaging, improving the overall imaging capability of the gadolinium-rhodamine nanoparticles⁶¹.

Quantum Dots (QDs) have become a topic of research for their use as biomolecular probes for biomedical application such as targeted imaging⁷⁰⁻⁷⁵. QDs have excellent advantages over the conventional organic dyes and fluorescent tags: size, composition dependent spectrum of wavelengths, large absorption coefficients, and high

levels of brightness and photostability^{72, 73}. QDs are composed of thousand of atoms of semiconducting crystals that have a ‘quantum confinement effect’. This means that, depending on the size and the composition of the nanoparticle, the nanoparticle will contain a certain characteristic emission wavelength and color⁷⁴. QDs are encapsulated inside a transparent shell that is composed of a material similar to the core material of the QDs which is non-emissive and contains a higher band gap²². An example of a high quality QDs was described by Gao et al.⁷². The nanoparticles were coated with poly (ethylene glycol) to prevent the uptake of the nanoparticles by the reticuloendothelial system (RES), thus extending the circulation time of the material inside the blood stream⁷². QDs can have ligands such as antibodies, proteins, or small-molecule inhibitors positioned on the surface creating site-specific nanoparticles that enhance the biological imaging *in-vivo*.

2.6.2 Biosensing Platforms for Molecular Detection

Conventional methods for biomolecular detection and analysis are enzymatic linked immunosorbent assay (ELISA) and polymerase chain reaction (PCR). The major disadvantage is the time required for the analysis (usually 10-28 hour and 4-6 hours, respectively)⁷⁶. Thus, there is need for fast and reliable detection that requires only minimal amount of sample. Nanotechnology has led to the advancement of nanosensors that are capable of monitoring biological signals in real time, and capable of being used in conjunction with therapeutic drug delivery vehicles for the screening and treatment *in-vivo*. Nanosensors involved some type of recognition element such as optical based

systems (i.e., surface plasmon resonance (SPR)), microcantilevers, or florescent based imaging and a transduction element⁷⁷.

2.6.2.1 Microcantilevers

Microcantilevers are the simplest form of micromechanical systems (MEMS) which exhibit reliable, high precision response to molecular absorption in the micro/nano scale⁷⁸. Microcantilevers are composed of materials that resonate when molecules absorb onto the surface of the cantilever. The deflection of the cantilever is a function of the material, the thickness, and the length of the cantilever⁷⁹. Microcantilevers surfaces have been modified with molecular tags such single strand DNA^{80, 81}, pH sensitive hydrogels⁸²⁻⁸⁴, and antibodies for antibody-antigen detection⁸⁵. Biochips that have microcantilevers as the main detecting element do not require external power, labels, signal transduction, or external electronics for the operation of the biosensor. This makes the sensors ideal for point-of-care or implantable devices for the detection of the biological precursors for disease⁸⁶.

Microcantilevers have been designed for the highly selective detection of glucose molecules which is beneficial in the diagnosis and treatment of diabetes^{79, 87}. Pei, et al immobilized glucose oxidase (GOx) enzymes (an enzyme that breaks glucose into gluconic acid) onto the surface of the microcantilever for the detection of glucose. The enzyme is highly selective to GOx, providing an excellent platform for glucose recognition. The bending of the microcantilever due to the absorption of the glucose molecules is detected by a laser beam which is sent to a position sensitive detector⁸⁷. The

microcantilever proved to be a highly sensitive biosensor for the detection of glucose because the deflection of the microcantilever was a strong function of the glucose concentration.

Microcantilevers can also be arranged into microarrays for the detection of multiple molecules within a small sample, even in the picoliter range^{88, 89}. Antibodies or single strand DNA hybrids can be used within each array as the recognition tag with optical detection as the main readout for the system. Microarrays are of great advantage in tests that require multiple reading of molecules that are precursors of certain diseases.

2.6.2.2 Surface Plasmon Resonance

Surface plasmon resonance (SPR) has become a fast growing technology that allows non-invasive and non-destructive techniques to be used in the detection of chemical and biological molecules. The real time detection of molecules using SPR technology has a label-free interaction between the biomolecule and the sensing substrate on the SPR surface⁹⁰. The change of mass or change in thickness of the material on the sensor surface is proportional to the change of the refractive index of the metal⁹¹. This can elude to structural and binding parameters such as diffusion coefficients, kinetics, and association constants for thin polymeric film, as well as absorption rates of certain proteins and nucleotides onto the substrate surface. A rapid, robust sensor, such as point-of-care diagnostics, can be developed using SPR technology.

There have been investigations of recognitive network/SPR sensors in sensing biologically important molecules such domoic acid⁹², sialic acid⁹³, NAD⁺ or NADP⁺

cofactors⁹⁴, adenosine⁹⁵, and cytochrome C⁹⁶. Domoic acid is an important amino acid neurotoxin that is found in seafood such as crabs, mussels and anchovies. If ingested, symptoms such as nausea, vomiting, cramps, diarrhea, headaches, seizures and even memory loss may occur^{93, 97}. Lotierzo and coworkers investigated a recognitive based SPR biosensor that could detect domoic acid. Using a Biacore system, gold was deposited onto a glass surface by vacuum deposition to optimize the grafting of the recognitive network onto the gold coated glass slide before transferring the gold onto the Biacore chip⁹². The gold slide was then soaked in a 1mM solution of the self assembled monolayer (SAM) molecule, 2-mercaptoethylamine, for 24 hours to ensure the attachment and configuration of the SAM on the gold slide. A polymer solution consisting of 2-diethylamino ethyl methacrylate (DEAEM), N,N'-methylenebisacrylamide and the template molecule, domoic acid, was deposited onto the surface of the gold and polymerized using a UV light source. After polymerization, the gold piece was soaked in methanol to wash the template from the grafted polymer⁹².

The domoic acid recognitive SPR sensor was then tested by flowing a solution of domoic acid into the Biacore system. The recognitive network binds the domoic acid which increases the mass of the imprinted polymer, corresponding to an increase in the refractive index. A regeneration step followed with a sodium dodecil sulphate in 10mM HCL wash, stripping the polymer of the domoic acid. It is important to note, that after the regeneration step, the domoic acid solution was injected again and the polymer experienced similar resonance or binding capacity as the first injection. This illustrates

that the polymer does in fact have the capability of multiple regeneration and rebinding steps.

2.6.3 Surface Plasmon Resonance Theory

In order to appreciate the full capacity SPR has for fast and reliable biomolecular detection, the theory behind SPR should be presented. Researchers commonly use a gold substrate SPR sensor for the absorption of molecules, such as RNA, DNA, proteins, and antibodies. Gold is used because of the plasmon state characteristic it exhibits. The absorption of the molecules, however, is strongly influenced by the surface assembly monolayer (SAM) that is absorbed onto the gold surface. Such compounds as silanes and sulfur groups are used because of the strong and stable covalent bond between the silane and sulfur with the gold surface.

Plasmon state for metal is initiated when optical light is absorbed onto the thin substrate and excites the surface plasmon molecules⁹¹. Figure 2.2 illustrates the theory. In a configuration such as the Kretschmann configuration, light is illuminated from a high refractive index medium to a lower refractive index medium with the thin film substrate acting as a boundary between the two layers. The light undergoes a total internal reflection which exhibits an evanescent wave that excites a charge on the substrate. All the optical energy is reflected back to the higher refractive index, while the evanescent field penetrates the lower refractive index⁹¹. In order for the gold film to have a standing charge of excitation, the substrate must be in contact with a sample of lower refractive index than that of the waveguide. This will only occur when the wavevector of the

standing charge, k_{sp} , and the evanescent wave, k_x , are equal, as indicated by the following equations:

$$k_{sp} = k_o \sqrt{\frac{\epsilon_m \epsilon_o}{\epsilon_m + \epsilon_s}} \quad (2.14)$$

$$k_{xc} = k_o \eta_D \sin \theta_{inc} \quad (2.15)$$

where k_o is the wavevector of the incident light; ϵ_m is the dielectric constant of the thin metal substrate; ϵ_s is the dielectric constant of the sample; and η_D is the refractive index of the waveguide. The thickness of the gold substrate also plays a key role in SPR detection affecting the appearance of the SPR as well as the phase detection range and resolution. For example, when the gold substrate is 45nm thick, the resolution of the phase detection reaches as high as 10^{-5} RIU (refractive index unit)⁹⁰.

There are many different ways to detect the output of light when SPR occurs, such as wavelength interrogation, angular interrogation, and intensity measurement. In wavelength interrogation, the polychromatic SPR reflected light (more than one wavelength) is passed through a narrow interference band and the output is measured by some sort of detection camera such as a CCD camera^{90, 93}. For the angular interrogation, a monochromatic (one wavelength) SPR light is reflected and is detected by the CCD camera at assorted angles by rotating the light beam^{90, 94, 95}. Finally, with intensity

measurement, the angle of the monochromatic light is fixed and the output is measured by the CCD camera^{90, 95}.

One of the most common ways to detect SPR is the heterodyne phase detection with the Kretschmann prism configuration. This system follows the Fresnel equation and the equation of reflectivity of single layer membrane to calculate the reflection coefficient, r , and the phase shift of the reflective light, δ ,

$$r_{i,4} = \frac{r_{i,i+1} + r_{i+1,5} e^{2jd_{i+1}k_{zi+1}}}{1 + r_{i,i+1} e^{2jd_{i+1}k_{zi+1}}}, \quad i=2, 1, 0 \quad j = \sqrt{-1} \quad (2.16)$$

$$\delta = \arg(r_{0,4}) \quad (2.17)$$

where k_{zi} is the wave number vectors of the transmission light in the sequenced optical medium; $r_{i,i+1}$ is the reflection ratio of the electric field intensity at the interface between two adjacent mediums; and d_i is the thickness of the sequenced medium.

Heterodyne interferometry has several ways to detect SPR such as single channel, multichannel, or micro-array biosensors. For example, in single channel detection, after SPR excitation, two light rays, p-polarized (extraordinary ray) and s-polarized (ordinary ray) take on two different paths once they go through the prism. The p-polarized light is changed, while the s-polarized light is used as the reference. The change between the p-polarized light and the reference light measures the change in the refractive index on the biological/chemical film on the gold substrate. A photo-detector detects the phase shift between the measured and reference signals converting them into an electric signal⁸⁸.

2.7 Facilitation of Intelligent Polymers at the Micro/Nano Scale

The transfer of intelligent polymeric material onto micro/nano valves and sensors is accomplished by different methods, which include, but are not limited to, lithography, micromachining, and micromolding. The scope of this scope is not to fully detail each process, but to concentrate on the most applicable process for microfabricating intelligent polymers onto these substrates.

2.7.1 Lithography Techniques

One of the first techniques available for manufacturing microfluidic devices was silicon micromachining. Due to the high cost of labor, specialized skills, and equipment, micromachining is not widely used⁹⁸. Soft lithography became the method of choice because it not only offered a less expensive and faster approach, it also required less specialized methods of fabrication⁹⁹. The steps to process a biomicroelectromechanical system (bioMEMS), valve, or sensor with intelligent polymers usually takes places in four distinct steps: (i) thin-film deposition, (ii) lithography, (iii) etching, and (iv) substrate bonding¹⁰⁰.

Thin-film deposition techniques deposit materials on the substrate which are used for masking, isolation, and structural purposes⁹⁹. The four types of techniques include oxidation, chemical vapor deposition (CVD), physical vapor deposition (PVD), and electrodeposition. An oxidation technique takes place in a high temperature range from 800°C to 1200°C in the presence of an oxygen or water atmosphere, resulting in the

oxidation of the substrate. Chemical vapor deposition is the reaction of the material in the gas phase to form the thin film on the substrate. The two most common types of CVD are low pressure CVD and plasma enhanced CVD (PECVD).

Physical vapor deposition involves two types of processes for evaporation and sputtering. During the evaporation process, the substrate is placed inside a vacuum chamber where the film is heated and allowed to form on the surface of the substrate. In sputtering, the material is targeted by high energy inert ions allowing clusters to be removed and ejected towards the substrate⁹⁹. The last technique, electrodeposition or electroplating, involves the substrate being introduced to a solution containing the reducible form of the ion of the desired material and maintained at a negative potential compared to the counter anode electrode¹⁰¹.

The next step in microfabricating is soft lithography which involves the transfer or the molding of the desired image onto the substrate using a photoresist master^{99, 101}. Soft lithography is deemed to be inexpensive and affordable eliminating the need for cleanrooms, specialized equipment, and skills¹⁰². Photolithography refers to the process of stamping a polymer that is photosensitive. The typical substrate used is polydimethylsiloxane (PDMS) which is comprised of two parts: elastomer and curing agent. The photosensitive pre-polymer is placed in the cavity of the PDMS and is exposed to UV light through a mask containing the desired pattern to be transferred. The unreacted or unexposed regions of the substrate are then washed off and then the mold is hard baked for 20-30 minutes at 120-180 °C to improve the adhesion of the polymer to the substrate¹⁰¹.

The next two steps involve etching and substrate bonding^{100, 102-104}. The etching step entails patterning the substrate and selectively removing material from the substrate. The selectivity and directionality of the etching process are the two important characteristics. Selectivity indicates the degree with which the etchant can distinguish between the masking material and the material to be etched. Directionality is the profile of the etch under the mask. An anisotropic etch has dissolution rates that are a function of the specific directions, and an isotropic etch is where the etchant attacks the material in all directions at the same rate. The three most common chemicals for the anisotropic etching process are potassium hydroxide (KOH), ethylene diamine pyrochatechol (EDP), and tetramethyl ammonium hydroxide (TMAH). Substrate bonding (silicon-silicon, silicon-glass, and glass-glass) is used to fabricate 3-dimensional structures. Silicon-silicon fusion or silicon direct bonding is an important technique used to fabricate micromechanical devices and silicon-insulator (SOI) substrates¹⁰⁰. Another technique that is used is silicon-glass anodic bonding or electrostatic bonding, which is used to join the substrates for microsensor packaging and device fabrication¹⁰⁰.

Only recently has the integration of cognitive networks onto sensing substrates been investigated. Through our research that is presented in the next chapters, the evidence that imprinted networks can be programmed for enhanced template binding affinity and diffusion may lead to increases in the use of the materials as the main sensing element in a number of sensing schemes.

2.8 References

1. Noss, K. R.; Vaughan, A. D.; Byrne, M. E., Tailored binding and transport parameters of molecularly imprinted films via macromolecular structure: the rational design of recognitive polymers. *Journal of Applied Polymer Science* **2007**, *6*, 3435-3441.
2. Vaughan, A. D.; Sizemore, S. P.; Byrne, M. E., Enhancing molecularly imprinted polymer binding parameters via controlled/living radical polymerization and reaction analysis. *Polymer* **2007**, *48*, 74-81.
3. Byrne, M. E.; Salian, V., Molecular imprinting within hydrogels II: progress and analysis of the field. *International Journal of Pharmaceutics* **2008**, *364*, 188-212.
4. Venkatesh, S.; Sizemore, S. P.; Byrne, M. E., Novel biomimetic hydrogels for enhanced loading and extended release of ocular therapeutics. *Biomaterials* **2007**, *28*, 717-724.
5. Venkatesh, S.; Saha, J.; Pass, S.; Byrne, M. E., Transport and structural analysis of molecular imprinted hydrogels for controlled drug delivery. *European Journal of Pharmaceutics and Biopharmaceutics* **2008**, *69*, 852-860.
6. Ali, M.; Byrne, M. E., Controlled Release of high molecular weight hyaluronic acid from molecularly imprinted hydrogel contact lenses. *Pharmaceutical Research* **2009**, *26*, 714-726.
7. Ali, M.; Horikawa, S.; Venkatesh, S.; Saha, J.; Hong, J. W.; Byrne, M. E., Zero-order therapeutic release from imprinted hydrogel contact lenses within in-vitro physiological ocular tear flow. *Journal of Controlled Release* **2008**, *124*, 154-162.

8. Byrne, M. E.; Peppas, N. A., Recognitive biomimetic networks with moiety imprinting for intelligent drug-delivery. *Journal of Biomedical Materials Research* **2008**, *84A*, 137-147.
9. Yimaz, E.; Mosbach, K.; Haupt, K., Influence of functional and cross linking monomers and the amount of template on the performance of molecularly imprinted polymers in binding assays. *Analytical Communications* **1999**, *36*, 167-170.
10. Anderson, L. I.; Muller, P.; Vlatakis, G.; Mosbach, K., Mimics of the binding sites of opioid receptors obtained by molecular imprinting of enkephalin and morphine. *Proceedings of the National Academy of Sciences of the United States of America* **1995**, *92*, 4788-4792.
11. Whitecombe, M. J.; Rodriguez, M. E.; Villar, P.; Vulfson, E. N., A new method for the introduction of recognition site functionality into polymers prepared by molecular imprinting: synthesis and characterization of polymeric receptors for cholesterol *Journal of American Chemical Society* **1995**, *117*, 7105-7111.
12. Cheong, S. H.; Rachov, A.; Park, J. K.; Yano, K.; Karube, I., Synthesis and binding properties of a noncovalent molecularly imprinted testosterone-specific polymer. *Journal of Polymer Science Part A: Polymer Chemistry* **1997**, *36*, 1725-1732.
13. Hilt, J. Z.; Byrne, M. E., Configurational biomimesis in drug delivery: molecular imprinting of biologically significant molecules. *Advanced Drug Delivery Reviews* **2004**, *56*, 1599-1620.
14. Roy, R., Syntheses and some applications of chemically defined multivalent glycoconjugates. *Current Opinion of Structural Biology* **1996**, *6*, 692-702.

15. Roost, H.; Bachmann, M. F.; Hang, A.; Kalinke, U.; Pliska, H.; Hengartner, H.; Zinkemagel, R. M., Early high-affinity neutralizing anti-viral IgG responses without further overall improvements of affinity. *Proceedings of the National Academy of Science of the United States of America* **1995**, *92*, 1257-1261.
16. Wuff, G., A way towards artificial antibodies. *Angewandte Chemie International Edition in English* **1995**, *34*, 1812-1832.
17. Lin, L. Q.; Li, Y. C.; Fu, Q.; He, L.; Zhang, J.; Zhang, Q. Q., Molecularly imprinted polymer for sinomenine and study on its molecular recognition mechanism. *Polymer* **2006**, *47*, 3792-3798.
18. Shi, X.; Wu, A.; Qu, G.; Li, R.; Zhang, D., Development and characterisation of molecularly imprinted polymers based on methacrylic acid for selective recognition of drugs. *Biomaterials* **2007**, *28*, 3741-3749.
19. Hedin-Dahlstrom, J.; Rosengren-Holmberg, J. P.; Legrand, S.; Wikman, S.; Nicholls, I. A., A class II aldolase mimic. *Journal of Organic Chemistry* **2006**, *71*, 4845-4853.
20. Svenson, J.; Nicholls, J. A., On the thermal and chemical stability of molecularly imprinted polymers. *Analytica Chimica Acta* **2001**, *435*, 19-24.
21. Lavignac, N.; Allender, C. J.; Brain, K. R., Current status of molecularly imprinted polymers as alternatives antibodies in sorbent assays. *Analytica Chimica Acta* **2004**, *510*, 139-145.

22. Lin, L.; Zhang, J.; Fu, Q.; He, L.; Li, Y., Concentration and extraction of sinomenine from herb and plasma using a molecularly imprinted polymer as the stationary phase. *Analytica Chimica Acta* **2006**, *561*, 178-182.
23. Piletsky, S. A.; Alcock, S.; Turner, A. P. F., Molecular imprinting: at the edge of the third millennium. *Trends in Biotechnology* **2001**, *19*, 9-12.
24. Sellergen, B.; Shea, K. J., Influence of polymer morphology on the ability of imprinted network polymers to resolve enantiomers. *Journal of Chromatography A* **1993**, (635), 31-49.
25. Alcock, H. R.; Lampe, F. W., *Contemporary Polymer Chemistry*. 2nd ed.; Prentice Hall: Englewood Cliffs, **1990**.
26. Vaughan, A. D. Reaction analysis of templated polymer systems. Auburn University, Auburn, **2008**.
27. Cook, W. D.; Simon, G. P.; Burchill, P. J.; Lau, M.; Fitch, T. J., Curing kinetics and thermal properties of vinyl ester resins. *Journal of Applied Polymer Science* **1997**, *64*, 769-781.
28. Lecamp, L.; Yousseff, B.; Bunel, C.; P, L., Influence of photoinitiator concentration, temperature and light intensity. *Polymer* **1997**, *38*, 6089-6096.
29. Lovell, L. G.; Lu, H.; Elliot, J. E.; Stansbury, J. W.; Bowman, C. N., The effect of cure rate on the mechanical properties of dental resins. *Dental Materials* **2001**, *17* (504-511).
30. Rampey, A.; Umpleby, R. J.; Rushton, G. T.; Iseman, J. C.; Shad, R. N.; Shimizu, K. D., Characterization of the imprinted effect and the influences of imprinting

conditions on affinity, capacity and heterogeneity in molecularly imprinted polymers using the Freundlich isotherm-affinity distribution analysis. *Analytical Chemistry* **2004**, *76*, 1123-1133.

31. Piletsky, S. A.; Piletsky, E. V.; Karim, K.; Freebairn, K. W.; Legge, C. H.; Turner, A. P. F., Polymer Cookery: influence of polymerization conditions on the performance of molecularly imprinted polymers. *Macromolecules* **2002**, *35*, 7499-7504.

32. Piletsky, S. A.; Mijangos, I.; Guerreiro, A.; Piletsky, E. V.; Chianella, U.; Karim, K.; Turner, A. P. F., Polymer cookery: influence of polymerization time and different initiation conditions on performance of molecularly imprinted polymers. *Macromolecules* **2005**, *38*, 1410-1414.

33. Bowman, C. N.; Peppas, N. A., Coupling of kinetics and volume relaxation during polymerizations of multiacrylates and multimethacrylates. *Macromolecules* **1991**, *24*, 1914-1920.

34. Anseth, K. S.; Kline, L. M.; Walker, T. A.; Anderson, K. J.; Bowman, C. N., Reaction kinetics and volume relaxation during polymerization of multiethylene glycol dimethacrylates. *Macromolecules* **1995**, *28*, 2491-2499.

35. Mayes, A. G.; Whitecombe, M. J., Synthetic strategies for the generation of molecularly imprinted organic polymers. *Advanced Drug Delivery Reviews* **2005**, *57*, 1742-1778.

36. Ikegami, T.; Mukawa, T.; Nariai, H.; Takeuchi, T., Bishphenol A recognition polymers prepared by covalent molecular imprinting. *Analytica Chimica Acta* **2004**, *504*, 131-135.

37. Cheong, S. H.; McNiven, S.; Rachov, A.; Levi, R.; Yano, K.; Karube, I., Testosterone receptor binding mimic constructed using molecular imprinting. *Macromolecules* **1997**, *30*, 1371-1322.
38. Hwang, C. C.; Lee, W. C., Chromatographic characteristics of cholesterol-imprinted polymers prepared by covalent and non-covalent imprinting methods. *Journal of Chromatography A* **962**, 962 (69-78), 69.
39. Karlsson, J. G.; Anderson, L. I.; Nicholls, J. A., Probing the molecular basis for ligand-selective recognition in molecularly imprinted polymers selective for the local anesthetic bupivacaine. *Analytica Chimica Acta* **2001**, *435*, 57-64.
40. Spivak, D. A., Optimization, evaluation and characterization of molecularly imprinted polymers. *Advanced Drug Delivery Reviews* **2006**, *57*, 1779-1794.
41. Turner, N. W.; Piletsky, E. V.; Karim, K.; Whitecombe, M. J.; Malecha, M.; Magan, N.; Baggiani, C.; Piletsky, S. A., Effect of the solvent on recognition properties of molecularly imprinted polymer specific for ochratoxin A. *Biosensors and Bioelectronics* **2004**, *20*, 1060-1067.
42. Lu, Y.; Li, C.; Wang, X.; Sun, P.; Xing, X., Influence of polymerization temperature on the molecular recognition of imprinted polymers. *Journal of Chromatography B* **2004**, *804*, 53-59.
43. Lu, H.; Lovell, L. G.; Bowman, C. N., Exploiting the heterogeneity of cross-linked photopolymers to create high-Tg polymers from polymerization performed at ambient conditions. *Macromolecules* **2001**, *34*, 8021-8025.

44. Xinglong, Y.; Dingxin, W.; Xing, W.; Xiang, D.; Wei, L.; Xinsheng, Z., A surface plasmon resonance imaging interferometry for protein micro-array detection. *Sensors and Actuators B-Chemical* **2005**, *108*, 765-77.
45. Wu, L.; Zhu, K.; Zhao, M.; Li, Y., Theoretical and experimental study of nicotinamide molecularly imprinted polymers with different porogens. *Analytica Chimica Acta* **2005**, *549*, 39-44.
46. Hwang, C. C.; Lee, W. C., Chromatographic characteristics of cholesterol-imprinted polymers prepared by covalent and non-covalent imprinting methods. *Journal of Chromatography A* **2002**, *962*, 69-78.
47. Sperling, L. H., *Introduction to Physical Polymer Science*. 4th ed.; John Wiley & Sons, Inc: Hoboken, **2005**.
48. Flory, P. J., *Principles of Polymer Chemistry*. 1st ed.; Cornell University Press: Ithaca, **1953**.
49. Brazel, C. S.; Peppas, N. A., Synthesis and characterization of thermo- and chemomechanically responsive poly(N-isopropylacrylamide-co-methacrylic acid) hydrogels. *Macromolecules* **1995**, *24*, 8016-8020.
50. Peppas, N. A., *Hydrogels in Medicine and Pharmacy*. CRC Press: **1987**.
51. Odian, G., *Principles of Polymerization*. 2nd ed.; John Wiley & Sons: New York, **1982**.
52. Small, H., Chemical modification of crosslinked polymers: new approach to synthesis of ion exchange and chelating resins. *Industrial Engineering Chemical Production Research Development* **1967**, *3*, 147-150.

53. Watkins, A. W.; Anseth, K. S., Investigation of molecular transport and distributions in poly(ethylene glycol) hydrogels with confocal laser scanning microscopy. *Macromolecules* **2005**, *38*, 1326-1334.
54. Saha, B.; Streat, M., Adsorption of trace heavy metals: applications of surface complexation theory to a macroporous polymer and a weakly acidic ion-exchange resin. *Industrial Engineering Chemical Research* **2005**, *44*, 8671-8681.
55. Figuly, G. D.; Royce, S. D.; Khasat, N. P.; Schick, L. E.; Wu, S. D.; Davidson, F.; Campbell, G. C.; Keating, M. Y.; Chen, H. W.; Shimshick, E. J.; Fischer, R. T.; Grimminger, L. C.; Thomas, B. E.; Smith, L. H.; Gilles, P. J., Preparation and characterization of novel poly (alkylamine) based hydrogels designed for use as bile acid sequestrants. *Macromolecules* **1997**, *30*, 6174-6184.
56. Spizzirri, U. G.; Peppas, N. A., Structural analysis and diffusional behavior of molecularly imprinted polymer networks for cholesterol recognition. *Chemical Materials* **2005**, *17*, 6719-6727.
57. Umpleby, R. J.; Baxter, S. C.; Bode, M.; Berch, J. K.; Shah, R. N.; Shimizu, K. D., Application of the freundlich adsorption isotherm in the characterization of molecularly imprinted polymers. *Analytica Chimica Acta* **2001**, *425*, 11269-11275.
58. Kim, H.; Spivak, D. A., New insights into modeling non-covalently imprinted polymers. *Journal of American Chemical Society* **2003**, *125*, 11269-11575.
59. Szabelski, P.; Kaczmarek, K.; Cacazzini, A.; Chen, Y. B.; Sellergen, B.; Guiochon, G., Energetic heterogeneity of the surface of molecularly imprinted polymer

studied by high-performance liquid chromatography. *Journal of Chromatography A* **2002**, *964*, 99-111.

60. Syu, M. J.; Deng, J. H.; Nian, Y. M.; Chiu, T. C.; Wu, A. H., Binding specificity of α -bilirubin-imprinted poly(methacrylic acid-co-ethylene glycol dimethylacrylate) toward α -bilirubin. *Biomaterials* **2005**, *26*, 4684-4692

61. Vuu, K.; Xie, J.; McDonald, M. A.; Bernado, M.; Hunter, F.; Zhang, Y.; Li, K.; Bednarski, M.; Guccione, S., Gadolinium-rhodamine nanoparticles for cell labeling and tracking via magnetic resonance and optical imaging. *Bioconjugate Chemistry* **2005**, *16*, 995-999.

62. Winter, P.; Athey, P.; Kiefer, G.; Gulya, G.; Frank, K.; Fuhrhop, R.; Roberston, D.; Wickline, S.; Lanza, G., Improved paramagnetic chelate for molecular imaging with MRI. *Journal of Magnetism and Magnetic Materials* **2005**, *293*, 540-545.

63. Peira, E.; Marzola, P.; Podio, V.; Aime, S.; Sbarbati, A.; Gasco, M. R., *In vitro* and *in vivo* study of lipid nanoparticles loaded with superparamagnetic iron oxide. *Journal of Drug Targeting* **2003**, *11*, 19-24.

64. Bulte, J. W. M., Magnetic nanoparticles as markers for cellular MR imaging. *Journal of Magnetism and Magnetic Materials* **2005**, *289*, 423-427.

65. Bomati-Miguel, O.; Morales, M. P.; Tartaj, P.; Ruiz-Cabello, J.; Bonville, R.; Santos, M.; Zhao, X.; Veintemillas-Verdaguer, S., Fe-based nanoparticulate metallic alloys as contrast agents for magnetic resonance imaging. *Biomaterials* **2005**, *26*, 5695-5707.

66. Shieh, D. B.; Cheng, F. Y.; Su, C. H.; Yeh, C. S.; Wu, M. T.; WU, Y. N.; Tsai, C. Y.; Wu, C. L.; Chen, D. H.; Chou, C. H., Aqueous dispersions of magnetite nanoparticles with NH₃⁺ surfaces for magnetic manipulations of biomolecules and MRI contrast agents. *Biomaterials* **2005**, *26*, 7183-7191
67. Veish, O.; Sun, C.; Gunn, J.; Kohler, N.; Gabikian, P.; Lee, D.; Bhattarai, N.; Ellenbogen, R.; Sze, R.; Hallahan, A.; Olson, J.; Zhang, M., Optical and MRI multifunctional nanoprobe for targeting gliomas. *Nano Letters* **2005**, *5*, 1003-1008.
68. Sahoo, Y.; Goodarzi, A.; Swihart, M. T.; Ohulchansky, T. Y.; Kaur, N.; Furlarni, E. P.; Prasad, P. N., Aqueous ferrofluid of magnetite nanoparticles: fluorescence labeling and magnetophoretic control. *Journal of Physical Chemistry B* **2005**, *109* 3879-3885.
69. Stroh, A.; Faber, C.; Neuberger, T.; Lorenz, P.; Sieland, K.; Jakob, P. M.; Webb, A.; Pilgrim, H.; Schober, R.; Pohl, E. E.; Zimmer, C., *In vivo* detection limits of magnetically labeled embryonic stem cells in the rat brain using high-field (17.6T) magnetic resonance imaging. *Neuroimage* **2005**, *24*, 635-645.
70. Bailey, R. E.; Smith, A. M.; Nie, S., Quantum dots in biology and medicine. *Physica E* **2004**, *25*, 1-12.
71. Jaing, W.; Papa, E.; Fisher, H.; Mardyani, S.; W, C. W. C., Semiconductor quantum dots as contrast agents for whole animal imaging. *Trends in Biotechnology* **2004**, *22*, 607-609.
72. Gao, X.; Yang, L.; Petros, J. A.; Marshall, F. F.; Simons, J. W.; Nie, S., *In vivo* molecular and cellular imaging with quantum dots. *Current Trends in Biotechnology* **2005**, *16*, 63-72.

73. Arya, J.; Kaul, Z.; Wadhwa, R.; Taira, K.; Hirano, T.; Kaul, S., Quantum dots in bio imaging: revolution by the small. *Biochemical and Biophysical Research Communications* **2005**, *329*, 1173-1177.
74. Hasegawa, U.; Nomura, S. M.; Kaul, S. C.; Hirano, T.; Akiyoshi, K., Nanogel-quantum dot hybrid nanoparticles for live cell imaging. *Biochemical and Biophysical Research Communications* **2005**, *331*, 917-921.
75. Chang, E.; Miller, J. S.; Sun, J.; Yu, W. W.; Colvin, V. L.; Drezek, R.; West, J. L., Protease-activated dot probes. *Biochemical and Biophysical Research Communications* **2005**, *334*, 1317-1321.
76. Veseashta, A.; Dimova-Malinovska, D., Nanostructured and nanoscale devices, sensors and detectors. *Science and Technology of Advanced Materials* **2005**, *6*, 312-318.
77. Austin, M. J.; Sadana, A., A fractal analysis of analyte-receptor binding and dissociation kinetics in microcantilever biosensors. *Sensors and Actuators B* **2002**, *82*, 186-199.
78. Ji, H. F.; Thundat, T.; Dabestani, R.; Brown, G. M.; Britt, P. F.; Bonnesen, P. V., Ultrasensitive detection of CrO using a microcantilever sensor. *Analytical Chemistry* **2001**, *73*, 1572.
79. Yan, X.; Ji, H. F.; Lvov, Y., Modification of microcantilevers using layer-by-layer nanoassembly film for glucose measurement. *Chemical Physics Letters* **2004**, *396*, 34-37.

80. Calleja, M.; Nordstrom, M.; Alvarez, M.; Tamayo, J.; Lechuga, L. M.; Boisen, A., Highly sensitive polymer-based cantilevers-sensors for DNA detection. *Ultramicroscopy* **2005**, *105*, 215-222.
81. Lui, F.; Zhang, Y.; Ou-Yang, Z., Flexoelectric origin of nanomechanic deflection in DNA microcantilevers system. *Biosensors and Bioelectronics* **2003**, *18*, 655-690.
82. Bashir, R.; Hilt, J. Z.; Elibol, O.; Gupta, A.; Peppas, N. A., Micromechanical cantilever as an ultrasensitive pH microsensor. *Applied Physics Letters* **2003**, *16*, 3091-3092.
83. Hilt, J. Z.; Gupta, K. A.; Bashir, R.; Peppas, N., Ultrasensitive biomems sensors based on microcantilevers patterned with environmentally responsive hydrogels. *Biomedical Microdevices* **2003**, *5*, 177-184.
84. Ji, H. F.; Hansen, K. M.; Hu, Z.; Thundat, T., Detection of pH variation using modified microcantilever sensors. *Sensors and Actuators B* **2001**, *72*, 233-238.
85. Grogan, C. R.; Raiter, R.; O'Connor, G. M.; Glynn, T. J.; Cunningham, V.; Kane, O.; Charlton, M.; Leech, D., Characterization of an antibody coated microcantilever as a potential immuno-based biosensor. *Biosensors and Bioelectronics* **2002**, *17*, 201-207.
86. Khaled, A. R. A.; Vafai, K.; Yang, N. M.; Zhang, X.; Ozkan, C. S., Analysis, control and augmentation of microcantilever deflections in bio-sensing systems. *Sensors and Actuators B* **2003**, *94*, 103-115.
87. Pei, J.; Tian, F.; Thundat, T., Glucose biosensor based on the microcantilever. *Analytical Chemistry* **2004**, *76*, 292-297.

88. Alvarez, M.; Tamayo, J., Optical sequential readout of microcantilever arrays for biological detection. *Sensors and Actuators B* **2005**, *106*, 687-690.
89. Belaubre, P.; Guirardel, M.; Leberre, V.; Pourciel, J. B.; Bergaud, C., Cantilever based microsystem for contact and non-contact deposition of picoliter biological samples. *Sensors and Actuators A* **2004**, *110*, 130-135.
90. Junfeng, L.; Xiang, D.; Zinglong, Y.; Dongsheng, W., Data analysis of surface plasmon resonance biosensor based on phase detection. *Sensors and Actuators B* **2005**, *108*, 778-783.
91. Xinlong, Y.; Dingxin, W.; Xing, W.; Xiang, D.; Wei, L.; Xinsheng, Z., A surface plasmon resonance imaging interferometry for protein micro-array detection. *Sensors and Actuators B-Chemical* **2005**, *108*, 765-771.
92. Lotierzo, M.; Henry, O. Y. F.; Piletsky, S.; Tothill, I.; Cullen, D.; Kania, M.; Hock, B.; Turner, A. P. F., Surface plasmon resonance sensor for domoic acid based on grafted imprinted polymer. *Biosensors and Bioelectronics* **2004**, *20*, 145-152.
93. Kugimiya, A.; Takeuchi, T., Surface Plasmon resonance sensor using molecularly imprinted polymer for detection of sialic acid. *Biosensors and Bioelectronics* **2001**, *16*, 1059-1062.
94. Raitman, O.; Chegel, V. I.; Kharitonov, A. B.; Zayats, M.; Katz, E.; Willner, I., Analysis of NAD(P)⁺ and NAD(P)H cofactors by means of imprinted polymers associated with Au surfaces: A surface plasmon resonance study. *Analytica Chimica Acta* **2004**, *504*, 101-111.

95. Taniwaki, K.; Hyakutake, A.; Aoki, T.; Yoshikawa, M.; Guiver, M. D.; Roberston, G. P., Evaluation of the recognition ability of molecularly imprinted materials by surface plasmon resonance (SPR) spectroscopy. *Analytica Chimica Acta* **2003**, *489*, 191-198.
96. Ishihara, T.; Arakawa, T., Detection of cytochrome C by means of surface plasmon resonance sensor. *Sensors and Actuators B* **2003**, *92*, 262-265.
97. Falconer, I. R., Algal toxins in seafood and drinking water. *Medical Journal of Australia* **1993**, *159*, 423-432.
98. Beebe, D. J.; Mensing, G. A.; Walker, G. M., Physics and applications of microfluidics in biology *Annual Review of Biomedical Engineering* **2002**, *4*, 261-286.
99. Ziaie, B.; Baldi, A.; Gu, Y.; Siegel, R. A., Hard and soft micromachining of biomems: review of techniques and examples of applications in microfluidics and drug delivery. *Advanced Drug Delivery Reviews* **2004**, *56*, 145-172.
100. Eddington, D. T.; Beebe, D. J., Flow controls with hydrogels. *Advanced Drug Delivery Review* **2004**, *56*, 199-210.
101. Razzacki, S. Z.; Thwar, P. K.; Yang, M.; Ugaz, V. M.; Burns, M. A., Integrated Microsystems for controlled delivery. *Advanced Drug Delivery Reviews* **2004**, *56*, 185-198.
102. Yu, Q.; Bauer, J. M.; Moore, J. S.; Beebe, D. J., Responsive biomimetic hydrogel valve for microfluidics. *Applied Physics Letters* **2001**, *78*, 2589-2591.

103. Beebe, D. J.; Moore, J. S.; Bauer, J. M.; Yu, Q.; Lui, R. H.; Devadoss, C.; Jo, B. J., Functional hydrogels structures for autonomous flow control insished microfluidic channels. *Nature* **2000**, *404*, 588-590.
104. Li, R. H.; Yu, Q.; Beebe, D. J., Fabrication and characterization of hydrogel based microvalves. *Journal of Microelectromechanics* **2001**, *11*, 45-53.

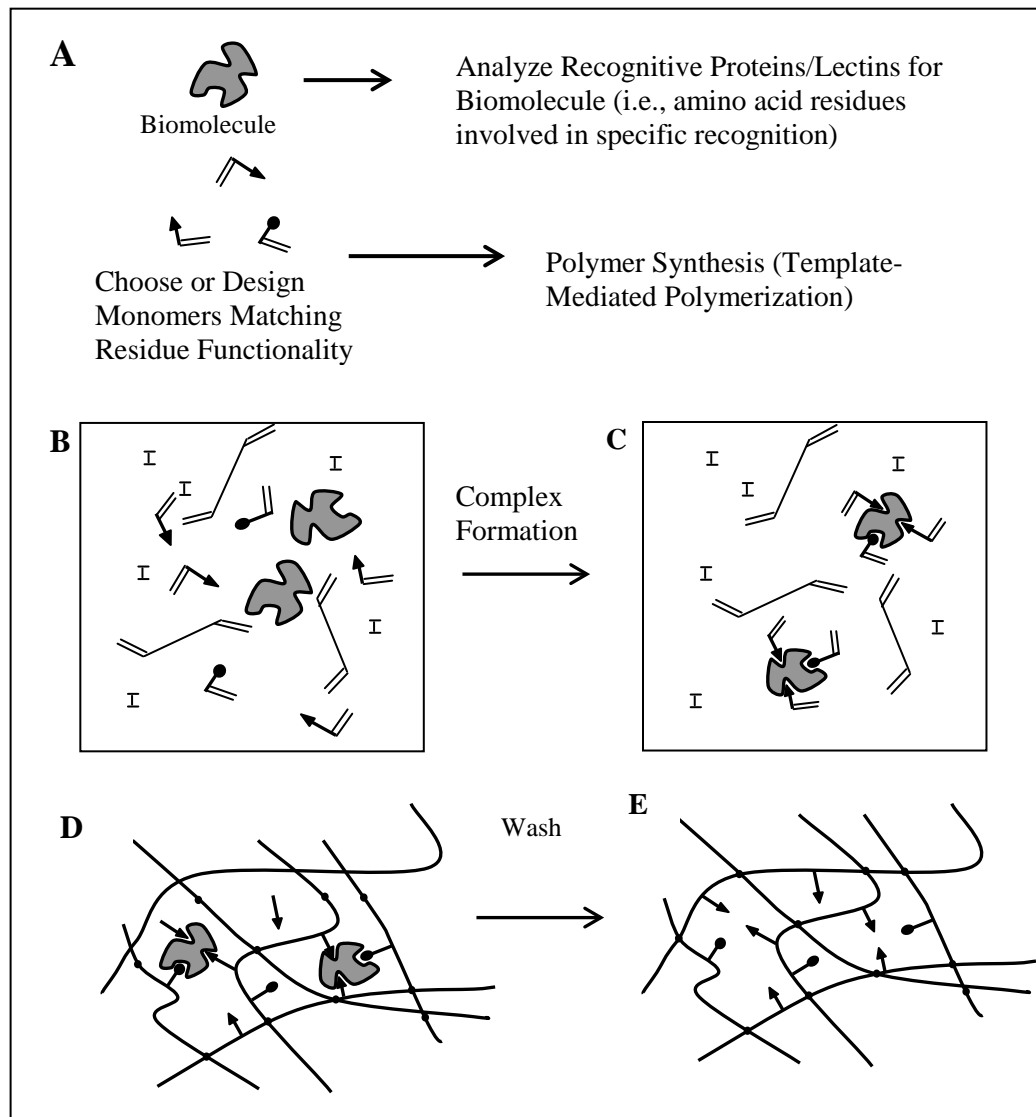


Figure 2.1: Template-Mediated Polymerization. A schematic of the non-covalent, template-mediated polymerization steps.

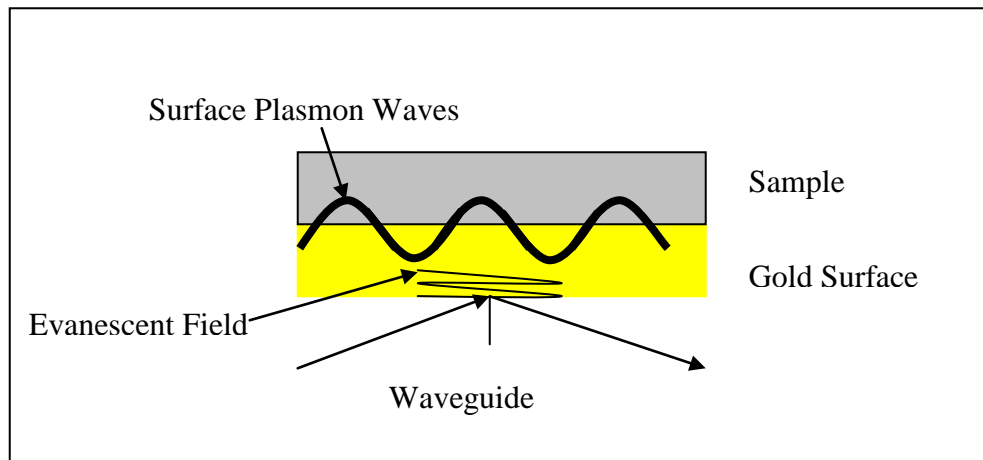


Figure 2.2: Illustration of the Surface Plasmon Refractive Theory. Illustration of the excitation of a standing charge on a thin gold substrate which corresponds to the SPR theory .

3.0 STRUCTURAL DESIGN, SYNTHESIS, AND BINDING PARAMETER ANAYLSIS OF RECOGNITIVE NETWORKS

The design, synthesis, and template binding parameter analysis of recognitive networks are presented and discussed in this chapter. Different structural parameters, such as the length and feed concentration of the crosslinking monomer, were varied to program binding parameters such as template binding capacity, affinity, and selectivity. The specific aims presented in this chapter include: (i) the synthesis of testosterone selective recognitive networks with variations in macromolecular structure; and (ii) the characterization of recognitive testosterone networks via reaction analysis. Template diffusional transport will be discussed in detail in Chapter 4.0.

The macromolecular structure was altered by varying the feed crosslinking monomer concentration (mole percent of crosslinking monomer in feed, mole of crosslinking monomer/moles of total monomers) from 50%-90%. The length of the crosslinking monomer was also varied by using ethylene glycol dimethacrylate and poly(ethylene glycol)200 dimethacrylate (which have 1 and 4.5 ethylene glycol units, respectively). The characterization of the different networks involved dynamic and equilibrium binding studies to elucidate binding parameters such as binding affinity, capacity, and selectivity. Polymerization reaction analysis was also conducted to find the relationship between the number of double bonds in the feed and the number of double bonds reacted or the fractional double bond conversion of the macromolecular structure.

3.1 Scientific Rationale

The results presented in this chapter are the subject of a published research article¹. A pre-existing testosterone recognitive poly(methacrylate-*co*-ethylene glycol dimethacrylate) network (poly(MAA-*co*-EGDMA)) with well documented binding parameters^{2,3} was used as the basis and starting point of this research. The main objective was to synthesize the literature network, determine the binding parameters, compare the binding parameters to the literature values, and then vary structural components of the network to analyze the effect of structural differences on the template binding parameters. We hypothesized that by varying the feed concentration of the crosslinking monomer, the affinity of the network to testosterone would vary. We also hypothesized that by increasing the length of the crosslinking monomer, the macromolecular structure would become more mobile, decreasing the binding capacity and affinity to testosterone. Therefore, in this chapter, we provide a detailed analysis on the effects of changing multiple structural parameters of the polymeric network on the template binding parameters. Finally, the rates of polymerization and degree of double bond conversion of the different polymeric systems were also studied to obtain a more precise understanding of the post-polymerization macromolecular structure of the network in comparison to the feed crosslinking percentage. Previous studies on similar systems indicate that the post-polymerization structure does not accurately represent the feed concentration of the crosslinking monomer, which may also play a key role in the binding enhancement and template diffusion through templated polymeric networks⁴.

3.2 Synthesis of a Typical Recognitive Polymer for Testosterone

Described in this section is the synthesis of a testosterone recognitive poly(methacrylate-*co*-ethylene glycol dimethacrylate), poly(MAA-*co*-EGDMA), network with a 77% feed crosslinking percentage (i.e., moles of crosslinking monomer divided by the total moles of monomers in feed solution). Also described is the synthesis of networks with different feed crosslinking percentages (varied from 50-90%) as well as the incorporation of crosslinking monomers differing in linear size.

3.2.1 Materials

In this work, we synthesized methacrylate copolymer networks imprinted for testosterone using ethylene glycol dimethacrylate (EGDMA) and poly(ethylene glycol)200dimethacrylate (PEG200DMA) as crosslinking agents, which have approximately 1 and 4.5 ethylene glycol units, respectively. Methacrylic acid (MAA), testosterone, chloroform, azobisisobutyronitrile (AIBN), and EGDMA were purchased from Sigma Aldrich (Milwaukee, WI) (Figure 3.1). PEG200DMA was purchased from Polysciences Inc. (Warrington, PA). All chemicals were analytical grade and used as received except for MAA which had inhibitor removed by vacuum distillation prior to use.

3.2.2 Polymer Synthesis

An 8:1 functional monomer to template molar ratio was used to produce testosterone recognitive networks with MAA as the functional monomer, testosterone as

the template molecule dissolved in chloroform, AIBN as the initiator, and EGDMA or PEG200DMA as the crosslinking monomer. Control polymers were produced by the same method as the imprinted polymers but without testosterone. Monomer solutions were prepared with the molar ratio of initiator to double bonds held constant at 0.015 and the weight percentage of the solvent constant at 50% (w/v). The feed crosslinking percentage was varied from 50%, 77%, and 90%, and the length of the crosslinking monomer was varied.

In a typical experiment, the functional monomer, template molecule, crosslinking monomer, and solvent were added to a glass vial and sonicated for 30 minutes to make certain the solution was well mixed. For example, a solution to form a 50% crosslinked poly(MAA-*co*-EGDMA) cognitive network consisted of EGDMA (9.40 mmole), MAA (9.40 mmole), testosterone (1.20 mmole), AIBN (0.41 mmole), and chloroform (25.0 mmole). It should be noted that the order in which the individual components were added to the solution was very important. The monomer and crosslinker agent were mixed together first, then the template molecule was added, followed by solvent and initiator. Failure to follow the appropriate sequence resulted in the template not dissolving completely in the pre-polymerization solution. Since this experiment dealt with a very hydrophobic template molecule, testosterone, it was advantageous to dissolve the template in the solvent separately before adding to the monomer/crosslinking agent solution.

Oxygen acts as a free-radical scavenger and hinders the polymerization reaction. To eliminate dissolved oxygen, nitrogen was slowly bubbled through the solution for 30

minutes. Separate experiments were conducted to determine optimum nitrogen purge times. The nitrogen was bubbled very slowly through the solution to prevent significant evaporation of the solvent during the nitrogen purge step.

The nitrogen-purged pre-polymerization solution was then transferred to an aluminum mold with a cooling system that held the temperature constant at 0°C and maintained a nitrogen atmosphere. A Novacure 2100 (Exfo, Ontario, Canada) mercury spot cure lamp was used as the light source with intensity of 50 mW/cm², as determined via a radiometer, for 17 minutes. The intensity versus wavelength spectrum can be found in Appendix A-1, Figure A.1.1. After synthesis, the polymer was crushed using a mortar and pestle to produce particles that were separated using molecular sieves. Particle sizes ranged between 53µm-150µm, which was determined to be the optimal particle size for template rebinding³. The polymer particles were washed using a Soxhlet apparatus with ethanol for 1 week or until testosterone and unreacted monomers were not detected in the effluent via spectrophotometric monitoring (Biotek Synergy, Winooski, VT). The particles were then dried in a vacuum oven (T=30°C at 27mm Hg) for 24 hours in preparation for the template rebinding studies.

3.2.3 Polymer Recognition Studies: Template Affinity, Capacity, and Selectivity

Prior to template binding studies, a standard curve for testosterone in chloroform was developed. The results indicated a linear absorbance versus concentration region until 0.18mM and a concentration-independent region after 0.18mM where the absorbance did not change with increasing concentration of testosterone (Appendix 1-1,

Figure A.1.2). Therefore, a 0.025mM to 0.167mM concentration range or serial sample dilution was used in all experiments.

The testosterone recognitive networks were thoroughly washed with 100% ethanol solution in a Soxhlet apparatus to remove the template. After one week of rigorous washing, the effluent was analyzed for testosterone by measuring the absorbance ($\lambda_{\text{Testosterone,max}}=238\text{nm}$) via Synergy UV-Vis spectrophotometer (BioTeck Instruments, Winooski, Vermont). The polymers were washed until testosterone was no longer detected in the effluent. The appropriate time needed to wash the recognitive networks was a function of the structural components. For example, the 90% crosslinked poly(MAA-co-EGDMA) recognitive network washed for 3 weeks. The higher the feed concentration of the crosslinking agent, a more constricted network was formed, requiring more time to wash away the template molecule.

Dynamic binding studies were performed in quadruplicate by introducing 5 mg of recognitive or control polymer particles into 2.5ml of varying concentrations of testosterone in chloroform for a pre-determined equilibrium time of 24 hours. Dynamic binding studies were conducted on separate samples measuring the supernatant at various time intervals. Final equilibrium values of testosterone concentration were obtained by spectrophotometric analysis at a wavelength of 238 nm (i.e., the wavelength of maximum absorbance of testosterone). A mass balance was used to determine the bound testosterone within the polymeric network.

Various binding isotherms were utilized to analyze the rebinding data. The equations for Scatchard, Langmuir, and Freundlich isotherms are shown in equations 3.1, 3.2, and 3.3, respectively. The linear form of the Scatchard equation is shown below

$$\frac{Q}{C_e} = -K_a Q + Q_{\max} \quad (3.1)$$

where Q is the bound amount of template, C_e is the equilibrium concentration of template in the solution, the template equilibrium binding affinity is represented by K_a , and Q_{\max} is the maximum template binding capacity. The affinity and the maximum template loading capacity are calculated via linear regression of the data.

The Langmuir isotherm is represented by the equation 3.2,

$$Q = \frac{K_a Q_{\max} C_e}{1 + K_a C_e} \quad (3.2)$$

where Q is the bound amount of template, C_e is the equilibrium concentration of the template in solution, the template binding affinity is K_a , and Q_{\max} is the maximum template loading capacity. Linearized form of the equation was used to determine the affinity and capacity. The Langmuir isotherm assumes that there is uniform one-layer adsorption of the template molecule, equilibrium conditions, and that the surface is homogeneous.

The Freundlich isotherm is an empirical equation can be applied to heterogeneous surfaces with a multiplicity of sites. Equation 3.3 is the Freundlich Isotherm,

$$Q = k_f C_e^n \quad (3.3)$$

where Q is the amount bound by the recognitive polymer, the equilibrium template concentration is C_e , the Freundlich affinity is k_f , and n is the exponent value. At $n=1$, the Freundlich isotherm is in linear form. The R^2 values for the Freundlich isotherms indicated that the Freundlich isotherms were the best fit for the recognitive networks studied (95% confidence). It is a statistical measuring tool that represents how well the regression line fits the data points where R^2 values range between zero and one with one indicating a perfect fit. The Freundlich isotherm analysis has been validated in literature for the characterization of molecularly imprinted polymers⁵⁻⁸.

Association affinities or constants describe how well a molecule (ligand) is attracted to a receptor site. Molecularly imprinted networks have been reported with binding affinities comparable to biological systems. For example, theophylline⁹, morphine¹⁰, cholesterol¹¹, and testosterone³ recognitive networks have been designed with dissociation constants equal to $(8.1 \pm 0.9) \times 10^{-9}$ M, $(1.2 \pm 0.2) \times 10^{-6}$ M, $(5.9 \pm 1.3) \times 10^{-4}$ M, and 0.9×10^{-4} M, respectively. These values are comparable to dissociation constants found in nature. For example, carbohydrate-protein^{12,13} dissociation constants range from 10^{-3} to 10^{-6} M and antigen-antibody¹⁴ dissociation constants range from 10^{-8} to 10^{-10} M.

Linear regression analysis of the Freundlich isotherm was used to calculate the average affinity and capacity for the recognitive polymers as discussed by Rampey et al⁸. Equation 3.4 and 3.5 give the maximum affinity (K_{max}) and minimum affinity (K_{min}).

K_{\max} and K_{\min} represent the limits of the affinity spectrum and are determined from the maximum ($C_{e \max}$) and minimum equilibrium concentrations ($C_{e \min}$).

$$K_{\max} = \frac{1}{C_{e \min}} \quad (3.4)$$

$$K_{\min} = \frac{1}{C_{e \max}} \quad (3.5)$$

The number of binding sites, ($N_{K_1-K_2}$), (Eqn 3.6) was taken between K_1 and K_2 . K_1 and K_2 are affinity values between K_{\min} and K_{\max} .

$$N_{K_1-K_2} = k_f (1 - n^2) (K_1^{-n} - K_2^{-n}) \quad (3.6)$$

The average affinity (K_{avg}) is calculated by equation 3.7.

$$K_{\text{avg}} = \left(\frac{n}{n-1} \right) \cdot \left[\frac{K_1^{1-n} - K_2^{1-n}}{K_1^{-n} - K_2^{-n}} \right] \quad (3.7)$$

When weighted-average affinity values are high, the molecules, on average, bind tightly to the receptor. Conversely, low weighted-average affinity values are indicative of weak binding systems. The reciprocal of the equilibrium association constant is the dissociation constant.

Selectivity studies followed a similar procedure as the template binding studies except progesterone dissolved in chloroform (wavelength of maximum absorbance equal

to 240 nm) was used as the rebinding solution. Progesterone was chosen because of the similar structure of progesterone compared to testosterone, where progesterone differs only by the carbonyl group located at the C17 chemistry (Figure 3.2).

The selectivity, α , for the testosterone cognitive network was determined by equation 3.8,

$$\alpha = \frac{K_{avg, template}}{K_{avg, other molecule}} \quad (3.8)$$

where, K_{avg} is the equilibrium, weighted-average affinity or association constant determined by Freundlich analysis.

3.2.4 Double Bond Conversion

The UV polymerization mechanism was investigated to determine the extent of double bond conversion within each network. As indicated in the literature, the final crosslinking content does not accurately represent the feed concentration of the crosslinking monomer, with less double bond conversion than expected⁴. For UV photopolymerization, the double bond conversion for each polymer system was determined via Differential Photo Calorimetry (DPC) (TA Instruments). The instrument measures the heat flow from the monomer solution sample relative to a reference pan. The heat evolved was measured as a function of time and the theoretical reaction enthalpy of the monomer solution was used to calculate the rate of polymerization, R_p , in the units of fractional double bond conversion per second. Integration of the rate of polymerization curve versus time yielded the experimental heat of reaction. The experimental heat of reaction and the theoretical heat of reaction are used to determine the final double bond

conversion. The calculations were analyzed by a Microsoft Excel Visual Basic program created by Vaughan¹⁵.

The assumptions in the copolymerization of multiple monomers (i.e., two types in this case, functional and crosslinking monomer) were that each monomer had equal reactivity and the theoretical reaction enthalpy derived for a co-monomer mixture was calculated by the summation of component mole fraction multiplied by the monomer heat of reaction. The theoretical enthalpy of methacrylate double bonds was equal to 13.1 kcal mole^{-17 4,16}. The majority of the heat of reaction was due to the double bonds reacting from the high amount of EGDMA present in the monomer solution. EGDMA has two moles of double bond per mole of monomer; therefore, this system can be considered EGDMA in chloroform with a dilute amount of MAA.

For photo-polymerization, a recognitive polymer disk was produced by placing 12.5 μL of pre-polymerization solution within an aluminum hermetic pan, and placing it in the cell of the DPC. The solution was allowed to purge with nitrogen for 5 minutes at a 40 mL/min purge rate and a temperature of 20°C. To prevent possible evaporation of the solvent, a small quartz plate was placed on top of the pan after the 5 minute purge time. Nitrogen continued to flow for the duration of the experiment at a purge rate of 40 mL/min. The solution was then cooled to the polymerization temperature of 0°C and was held at 0°C for 15 minutes. The shutter on the UV light source (Novacure 2100, Exfo, Canada, with a 100 Watt mercury arc light bulb) was opened and the solution was irradiated by 52.5 mW/cm² UV light (checked with internal radiometer) for 17 minutes at which time the polymerization reaction was ensured to be over (i.e., the typical

polymerization time was on the order of a few minutes). The temperature of the sample was held between 0°C to 1°C throughout the reaction, and the end point of each reaction was determined when the heat flow changed less than 1%.

3.3 Results and Discussion

In this section, detailed analysis of template binding parameters such as the binding affinity, binding capacity, selectivity, as well as fractional double bond conversions of testosterone recognitive poly(MAA-*co*-EGDMA) and poly(MAA-*co*-PEG200DMA) networks are discussed. The results show that by changing structural parameters, such as the length of the crosslinking agent and feed crosslinking percentage, the binding capacity and affinity of the networks change. Also, results clearly demonstrated that the crosslinking percentage of the polymeric network does not accurately represent the feed crosslinking percentage of the polymer solution. Template diffusional analysis is presented in Chapter 4.

3.3.1 Analysis of Template Binding Parameters

Figure 3.3 highlights the differences in binding capacity for a 77% crosslinked testosterone recognitive poly(MAA-*co*-EGDMA) network and a 77% crosslinked control poly(MAA-*co*-EGDMA) network. To reiterate, the control network was synthesized by the same method as the recognitive network but without the template molecule. As seen in Figure 3.3, the poly(MAA-*co*-EGDMA) recognitive network bound 3.6 fold more testosterone, $(1.8 \pm 0.4) \times 10^{-2}$ mmol testosterone /g dry polymer, compared to the

corresponding control network, which bound $(0.5 \pm 0.2) \times 10^{-2}$ mmol testosterone /g dry polymer. The increased template loading by the recognitive network compared to the control provides evidence that three-dimensional cavities are formed during the imprinting polymerization process and the macromolecular structure provides “memory” for the template rebinding. When the imprinted networks are introduced into a template solution, the polymers bind the free testosterone molecules by non-covalent forces such as hydrogen bonding, van der Waals forces, and hydrophobic forces¹⁷. It is expected that the template molecule binds non-specifically to the control network because the macromolecular chains of the network provide some opportunity for non-specific interaction.

We then investigated the effects of changing the three-dimensional macromolecular structure of the recognitive polymer network on the template binding parameters. The first structural change was achieved by varying the feed crosslinking percentage of the crosslinking monomer. We hypothesized that by increasing the feed crosslinking percentage of crosslinking monomer, a more constrictive polymeric network would form, corresponding to an increased formation of three-dimensional cavities available for template binding. By lowering the feed crosslinking percentage, effective cavities may not be able to form during polymerization and for the ones that do form, there would be more mobility within the chains leading to less stable three-dimensional cavities and less template binding. Different monomer solutions were prepared with varying crosslinking percentage, ranging from 50%-90%. Figure 3.4 highlights the variation of the feed crosslinking percentage of the poly(MAA-*co*-EGDMA) network,

from 50%-90%. The highest crosslinked cognitive network, 90% poly(MAA-*co*-EGDMA), bound approximately 2 fold more testosterone ($(0.22 \pm 0.03) \times 10^{-1}$ mmol testosterone /g dry polymer) compared to the least crosslinked cognitive network, 50% poly(MAA-*co*-EGDMA) ($(0.13 \pm 0.03) \times 10^{-1}$ mmol testosterone /g dry polymer). Increasing the crosslinking percentage of the network increases the amount of crosslinking points available for inter-chain stabilization, creating more effective cavities for template binding.

To analyze the effect of a longer bi-functional crosslinking monomer on the template binding parameters, poly(ethylene glycol)200dimethacrylate (PEG200DMA) was used as the crosslinking monomer. This bi-functional crosslinking monomer has approximately 4.5 more ethylene glycol repeating units than the EGDMA monomer resulting in a longer, more flexible crosslinking monomer. By increasing the length of the crosslinking monomer, it is expected that there will be more chain mobility introduced into the network which would result in the formation of fewer, less effective three-dimensional cavities. As seen in Figure 3.5, a decrease in binding capacity is evident when utilizing a longer bi-functional crosslinking monomer. The 77% crosslinked poly(MAA-*co*-PEG200DMA) cognitive network had a 2.5 fold lower binding capacity ($(0.72 \pm 0.02) \times 10^{-2}$ mmol testosterone/g dry polymer) than the 77% crosslinked poly(MAA-*co*-EGDMA) cognitive network. By increasing the linear size of the crosslinking monomer, the mobility of the network increases as well as the spacing between the functional chemistry, creating fewer, less effective cavities with decreased stability for template binding.

By varying the crosslinking percentage of the poly(MAA-*co*-PEG200DMA) network, we see a similar trend in the variation of the binding capacities as compared to the poly(MAA-*co*-EGDMA) networks (Fig. 3.4). The 77% crosslinked poly(MAA-*co*-PEG200DMA) bound 1.5 more testosterone than the 50% crosslinked poly(MAA-*co*-PEG200DMA) recognitive network ($(0.51 \pm 0.03) \times 10^{-2}$ mmol testosterone/g dry polymer). With fewer crosslinking monomers available for inter-chain stabilization, fewer three-dimensional cavities are formed which lowers the binding capacity for the network. This analysis demonstrates that by varying structural components, the macromolecular structure can be rationally tailored to specific template binding capacities.

The linearized form of the Freundlich isotherm (Eqn 3.3) was used to calculate the template binding affinity for each network (Figure 3.6). Comparing the 77% crosslinked polymers, the recognitive poly(MAA-*co*-EGDMA) network had an association constant of $(1.20 \pm 0.07) \times 10^4 \text{ M}^{-1}$ which was 6 fold more compared to the recognitive poly(MAA-*co*-PEG200DMA) network ($K_a = (0.20 \pm 0.05) \times 10^4 \text{ M}^{-1}$). It also should be noted that the 77% crosslinking poly(MAA-*co*-EGDMA) recognitive network ($K_a = (1.20 \pm 0.07) \times 10^4 \text{ M}^{-1}$) is in experimental agreement with a literature value³ ($K_a = 1.10 \times 10^4 \text{ M}^{-1}$).

Equilibrium selectivity studies were conducted to determine how selective the testosterone recognitive poly(MAA-*co*-EGDMA) network was to progesterone, a molecule similar in size, functionality, and configuration to testosterone. Progesterone differs from testosterone only at the C17 chemistry (Fig. 3.2). The 77% crosslinked

testosterone recognitive poly(MAA-*co*-EGDMA) polymer demonstrated 2.3 fold lower binding capacity for progesterone (0.80 ± 0.20) $\times 10^{-2}$ mmol progesterone /g dry polymer) compared to testosterone (1.8 ± 0.4) $\times 10^{-2}$ mmol testosterone /g dry polymer) (Fig. 3.7). The selectivity ratio, α , was calculated using equation 3.8, and for the 77% crosslinked testosterone recognitive poly(MAA-*co*-EGDMA) network the selectivity ratio was equal to 1.2. The selectivity ratio is based upon the template binding affinities of the network in the different molecule solution (i.e., testosterone and progesterone). The binding affinity of the 77% recognitive poly(MAA-*co*-EGDMA) network in testosterone solution was $(1.20 \pm 0.07) \times 10^4 \text{ M}^{-1}$, while the 77% recognitive poly(MAA-*co*-EGDMA) network in progesterone solution was $(0.98 \pm 0.03) \times 10^4 \text{ M}^{-1}$. The cavities formed during the imprinting process have chemical functional groups as testosterone to promote non-covalent interactions with testosterone. This macromolecular memory for testosterone allows for the testosterone recognitive poly(MAA-*co*-EGDMA) network to decipher between the progesterone and testosterone molecules. There is some non-specific interaction between progesterone and the network. It should be noted that the 77% crosslinked testosterone recognitive poly(MAA-*co*-PEG200DMA) polymer did not demonstrate a statistically different selectivity ratio.

3.3.2 Double Bond Conversion via Reaction Analysis

Polymerization reaction analysis was performed on each network to determine if the feed crosslinking concentration accurately represents the post-polymerization network or macromolecular structure. A better understanding of the recognitive network's

macromolecular structure will support our hypothesis that the macromolecular memory changes when certain structural parameters (i.e., the feed crosslinking percentage and the length of the crosslinking agent) are varied. Is the final product as highly crosslinked as indicated by the feed crosslinking percentage? And, if not, does the macromolecular structure correlate with our template rebinding analysis?

A DPC was used in the double bond conversion analysis. The DPC measures the heat flow from the exothermic free-radical polymerization reaction, and the fractional double bond conversion of each network was calculated by integrating the rate of polymerization, which is a function of the theoretical enthalpies both of the methacrylic groups and acrylate groups in the monomer solution. A visual basic program developed by Vaughan¹⁵ was used to calculate the final double bond conversion.

The fractional double bond conversion for the testosterone recognitive and control networks with varying structural parameters (i.e., varying feed crosslinking percentages and length of the crosslinking agent) are shown in Figure 3.9. The fractional double bond conversion for the 77% crosslinked testosterone recognitive poly (MAA-*co*-EGDMA) network was approximately 45 ± 0.5 %, while the 77% crosslinked testosterone recognitive poly(MAA-*co*-PEG200DMA) network had a slightly higher fractional double bond conversion of approximately 60 ± 0.5 %. The shorter length of the bi-functional crosslinking monomer, EGDMA, limits the diffusion of the chains around pendant double bonds in the severely constraint network. However, increasing the length of crosslinking agent increases the mobility of the bi-functional crosslinking monomer to

react with free radicals. This decreases the amount of pendant double bonds or unreacted double bonds in the network.

This study reveals viable information on the true macromolecular structure of the network; the macromolecular structure is not as crosslinked as indicated by the feed crosslinking percentage. One would suspect that higher double bond conversion would correspond to a higher binding capacity and affinity. However, this is not the case as seen with the recognitive and control poly(MAA-*co*-PEG200DMA) networks. The networks had a higher fractional double bond conversion but lower binding capacity and affinities compared to the EGDMA networks. Also, varying the crosslinking percentage from 50% to 77% of the testosterone recognitive and control poly(MAA-*co*-EGDMA) did not show a significant statistical change in the fractional double bond conversion ($40\pm 3\%$ and $45\pm 5\%$, respectively), but binding analysis indicated a decrease in binding capacity and affinity when the feed crosslinking percentage is decreased. The fractional double bond conversion does not change for networks that have the same crosslinking monomer, but there is still an increase in the number of reacted double bonds as the feed crosslinking percentage is increased. Thus, a higher feed amount of crosslinking monomer corresponds to a larger amount of crosslinker incorporated in the network structure.

3.4 Conclusions

In this work, recognitive polymeric networks that are selective to testosterone were prepared using crosslinking molecules differing in size and concentration to program the binding characteristics of the network. By manipulating these structural

parameters, the macromolecular architecture can be rationally tailored to have tuned capacity, affinity, and selectivity. In this chapter, we have shown that a highly crosslinked recognitive network, 90% crosslinked poly(MAA-*co*-EGDMA), had a 2 fold increase in the binding capacity and a 4 fold increase in binding affinity compared to a similar, but lower crosslinked recognitive network, 50% crosslinked poly(MAA-*co*-EGDMA). Also, by increasing the length of the crosslinking monomer within recognitive networks (i.e., comparing 77% crosslinked poly(MAA-*co*-EGDMA) to poly(MAA-*co*-PEG200DMA)), there was approximately a 3 fold decrease in the amount of testosterone bound. The longer crosslinking agent has more flexibility, resulting in fewer effective three dimensional cavities and less stable cavities. Selectivity studies indicated that at a crosslinking percentage of 77%, the testosterone recognitive polymer had a higher affinity for testosterone ($(1.2 \pm 0.7) \times 10^4 \text{ M}^{-1}$) than that of progesterone ($(0.98 \pm 0.03) \times 10^4 \text{ M}^{-1}$). Reaction analysis performed on the networks showed the fractional double bond conversion for networks with the same crosslinking agents are statistically the same, but however, there is still an increase in the number of reacted double bonds as the feed crosslinking percentage is increased. This is an indication that the feed crosslinking percentage does not accurately represent the post-polymerization macromolecular structure.

Since the recognitive networks have been shown in this research to have programmable binding affinities, the next area that needs to be explored is the diffusional transport of the template molecule through the network. Ultimately, in any sensor design incorporating recognitive thin films, there will be trade-off involving binding parameters

(e.g., affinity, selectivity, capacity) and transport considerations. A more structurally open network will have faster template transport, allowing for a decrease in response time. The affinity and selectivity may be lower; however, depending on the size, shape, and configuration of molecules in the sample fluid (i.e., how difficult a sensing environment), the lower values may be a workable tradeoff for a faster response time.

3.5 References

1. Noss, K. R.; Vaughan, A. D.; Byrne, M. E., Tailored binding and transport parameters of molecularly imprinted films via macromolecular structure: the rational design of recognitive polymers. *Journal of Applied Polymer Science* **2007**, *6*, 3435-3441.
2. Cheong, S. H.; Rachov, A.; Park, J. K.; Yano, K.; Karube, I., Synthesis and binding properties of a noncovalent molecularly imprinted testosterone-specific polymer. *Journal of Polymer Science Part A: Polymer Chemistry* **1997**, *36*, 1725-1732.
3. Cheong, S. H.; McNiven, S.; Rachov, A.; Levi, R.; Yano, K.; Karube, I., Testosterone receptor binding mimic constructed using molecular imprinting. *Macromolecules* **1997**, *30*, 1371-1322.
4. Vaughan, A. D.; Sizemore, S. P.; Byrne, M. E., Enhancing molecularly imprinted polymer binding parameters via controlled/living radical polymerization and reaction analysis. *Polymer* **2007**, *48*, 74-81.
5. Umpleby, R. J.; Baxter, S. C.; Bode, M.; Berch, J. K.; Shah, R. N.; Shimizu, K. D., Application of the freundlich adsorption isotherm in the characterization of molecularly imprinted polymers. *Analytica Chimica Acta* **2001**, *425*, 11269-11275.

6. Kim, H.; Spivak, D. A., New insights into modeling non-covalently imprinted polymers. *Journal of American Chemical Society* **2003**, *125*, 11269-11575.
7. Szabelski, P.; Kaczmarek, K.; Cacazzini, A.; Chen, Y. B.; Sellergen, B.; Guiochon, G., Energetic heterogeneity of the surface of molecularly imprinted polymer studied by high-performance liquid chromatography. *Journal of Chromatography A* **2002**, *964*, 99-111.
8. Rampey, A.; Umpleby, R. J.; Rushton, G. T.; Iseman, J. C.; Shad, R. N.; Shimizu, K. D., Characterization of the imprinted effect and the influences of imprinting conditions on affinity, capacity and heterogeneity in molecularly imprinted polymers using the Freundlich isotherm-affinity distribution analysis. *Analytical Chemistry* **2004**, *76*, 1123-1133.
9. Yilmaz, E.; Mosbach, K.; Haupt, K., Influence of functional and cross linking monomers and the amount of template on the performance of molecularly imprinted polymers in binding assays. *Analytical Communications* **1999**, *36*, 167-170.
10. Anderson, L. I.; Muller, P.; Vlatakis, G.; Mosbach, K., Mimics of the binding sites of opioid receptors obtained by molecular imprinting of enkephalin and morphine. *Proceedings of the National Academy of Sciences of the United States of America* **1995**, *92*, 4788-4792.
11. Whitecombe, M. J.; Rodriguez, M. E.; Villar, P.; Vulfson, E. N., A new method for the introduction of recognition site functionality into polymers prepared by molecular imprinting: synthesis and characterization of polymeric receptors for cholesterol. *Journal of American Chemical Society* **1995**, *117*, 7105-7111.

12. Hilt, J. Z.; Byrne, M. E., Configurational biomimesis in drug delivery: molecular imprinting of biologically significant molecules. *Advanced Drug Delivery Reviews* **2004**, *56*, 1599-1620.
13. Roy, R., Syntheses and some applications of chemically defined multivalent glycoconjugates. *Current Opinion of Structural Biology* **1996**, *6*, 692-702.
14. Roost, H.; Bachmann, M. F.; Hang, A.; Kalinke, U.; Pliska, H.; Hengartner, H.; Zinkemagel, R. M., Early high-affinity neutralizing anti-viral IgG responses without further overall improvements of affinity. *Proceedings of the National Academy of Science of the United States of America* **1995**, *92*, 1257-1261.
15. Vaughan, A. D. Reaction analysis of templated polymer systems. Auburn University, Auburn, **2008**.
16. Ward, J. H.; Sharar, A.; Peppas, N. A., Kinetics of living radical polymerization of multifunctional monomers. *Polymer* **2002**, *43*, 1745-1752.
17. Byrne, M. E.; Salian, V., Molecular imprinting within hydrogels II: progress and analysis of the field. *International Journal of Pharmaceutics* **2008**, *364*, 188-212.

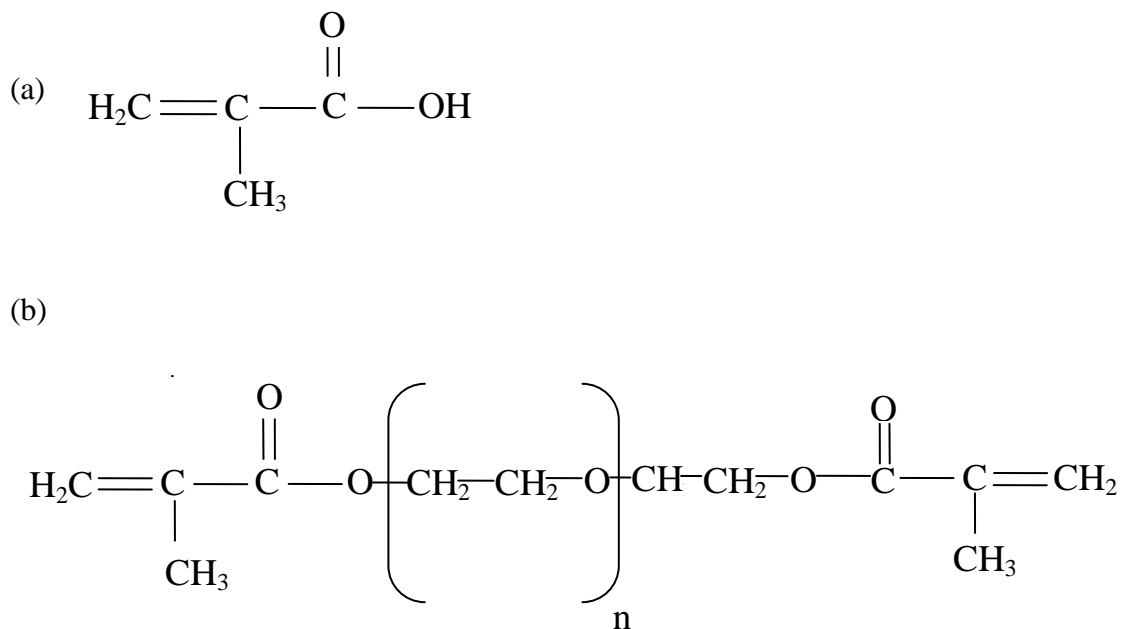


Figure 3. 1: Functional Monomer and Crosslinking Agent Structure. The structures of a) the functional monomer, methacrylic acid and b) the crosslinking agent, poly(ethylene glycol) n dimethacrylate, where n is the molecular weight of the ethylene glycol repeating units. To see the effect of the length of the crosslinking agent on the binding affinity and selectivity, the molecular weight (MW) of the ethylene repeating unit was increased to approximately 200 (PEG200DMA).

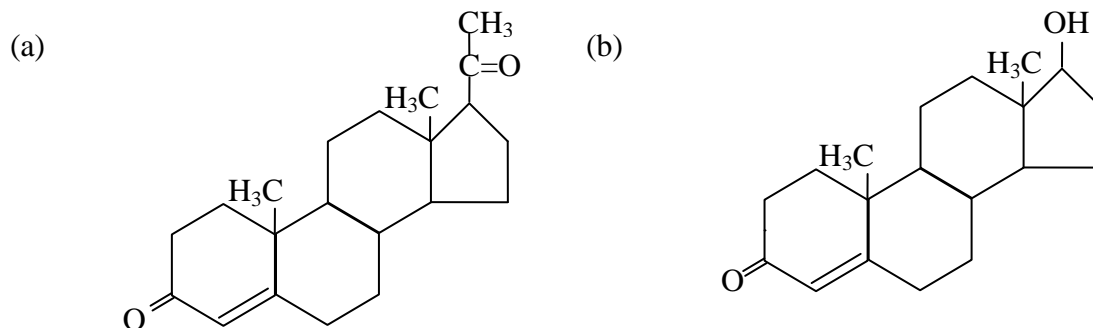


Figure 3. 2: The Molecular Structure of Testosterone and Progesterone.

Progesterone (a) was used in the selectivity studies because of the similar structure as compared to testosterone (b) where the only difference is at the C17 chemistry.

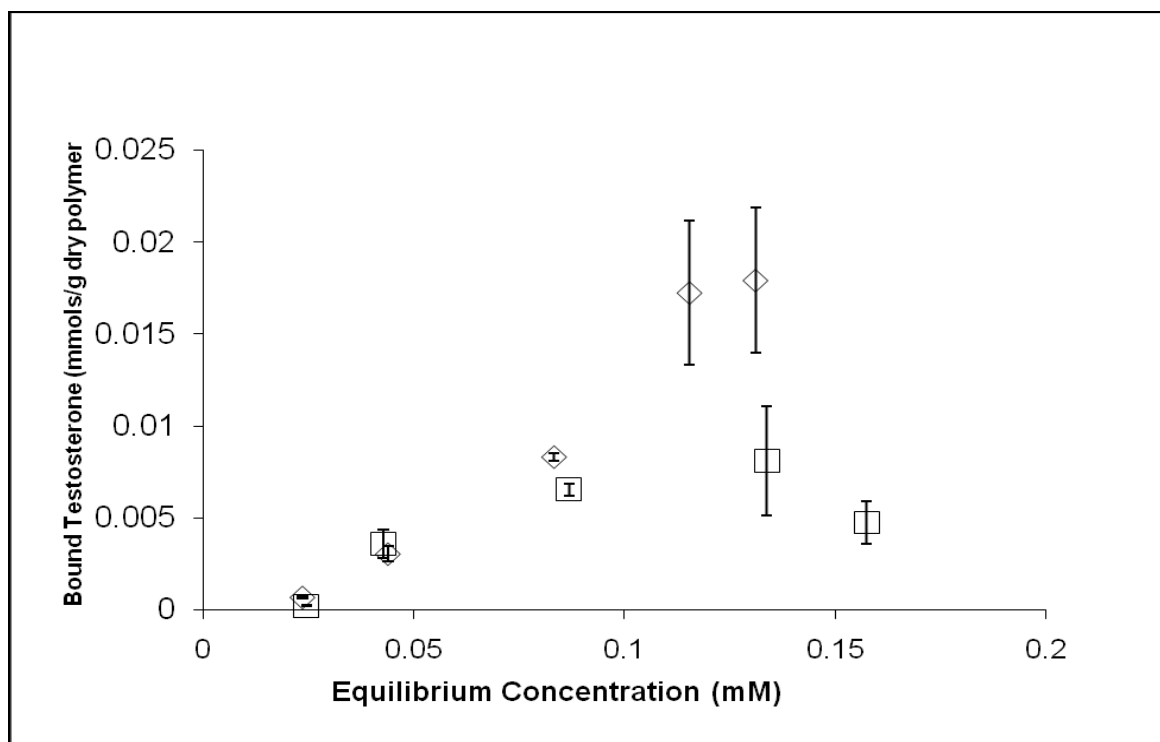


Figure 3.3: Testosterone Equilibrium Binding Isotherms of 77% Crosslinked Poly(MAA-co-EGDMA) Recognitive and Control Networks. Poly(MAA-co-EGDMA) Recognitive Network (◇) and Control Network (□). The recognitive network binds more testosterone compared to the control network illustrating that the recognitive network forms cavities during polymerization that have the configuration and functionality to promote non-covalent bonding to the template molecule. Error bars represent the standard deviation with four replicates at T=25°C

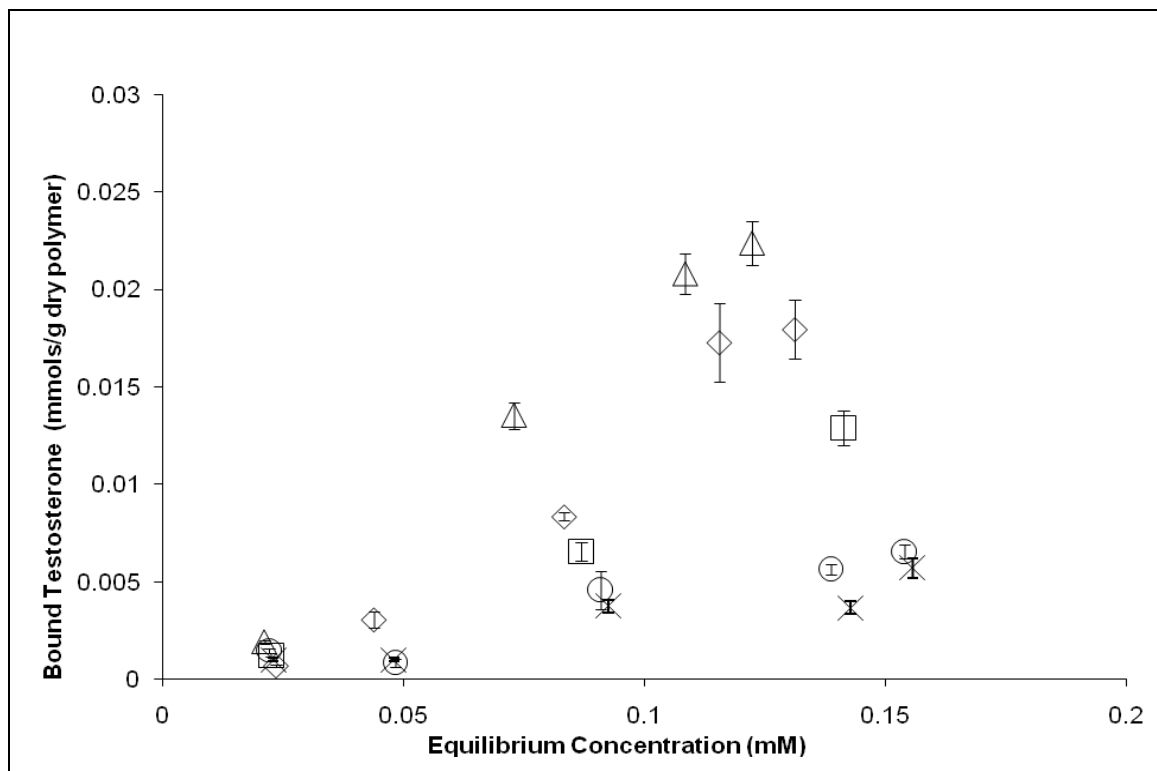


Figure 3.4: Testosterone Equilibrium Binding Isotherms of Poly(MAA-*co*-EGDMA) and Poly(MAA-*co*-PEG200DMA) Recognitive Networks at Various Feed Crosslinking Percentages. Poly(MAA-*co*-EGDMA) networks: 90% (Δ), 77% (\diamond), and 50% (\square). Poly(MAA-*co*-PEG200DMA) networks: 77% (\circ) and 50% (\times). A higher crosslinking percentage increases the binding capacity and affinity of the network. An increase in length of the crosslinking monomer lowers the binding capacity and affinity of the network. Error bars represent standard deviation with four replicates at $T=25^{\circ}\text{C}$.

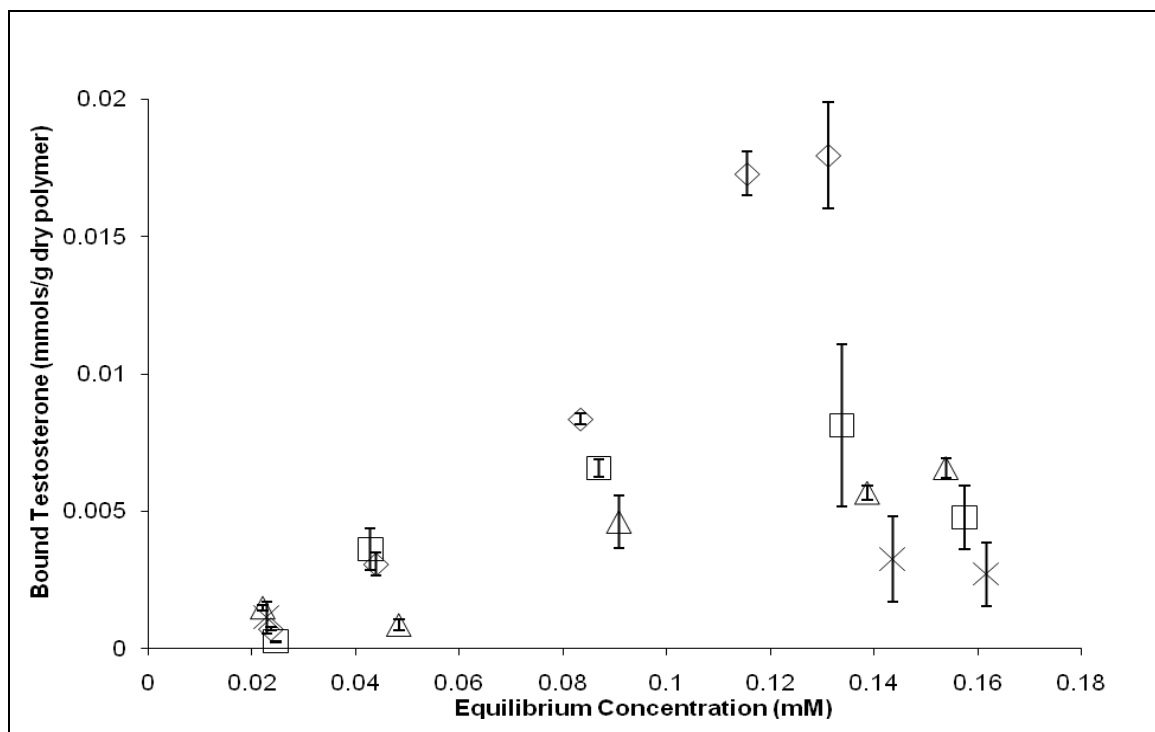


Figure 3.5: Testosterone Equilibrium Binding Isotherms of Poly(MAA-*co*-EGDMA) and Poly(MAA-*co*-PEG200DMA) Networks at 77% Feed Crosslinking. Poly(MAA-*co*-EGDMA) Recognitive Network (\diamond) and Control Network (\square). Poly(MAA-*co*-PEG200DMA) Recognitive Network (Δ) and Control Network(\times). As the length of the crosslinking agent increases, the binding capacities of the networks decrease. Error bars represent standard deviation with four replicates at $T=25^{\circ}\text{C}$.

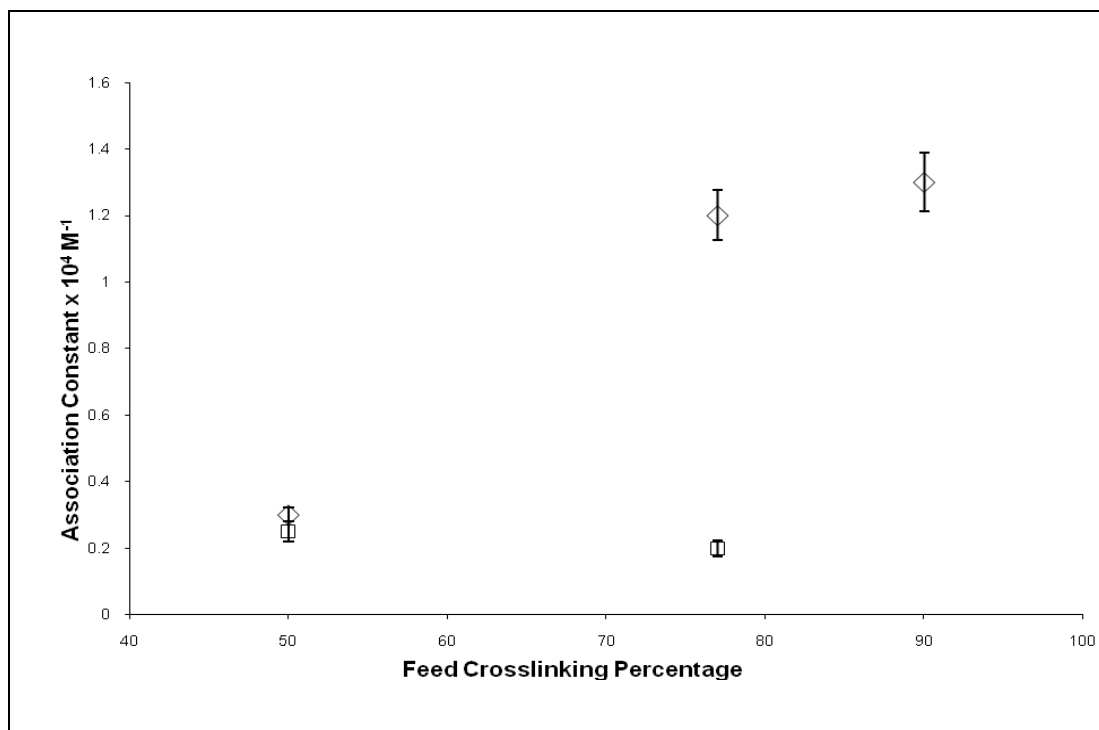


Figure 3.6: Testosterone Binding Affinity Constants for Poly(MAA-co-EGDMA) and Poly(MAA-co-PEG200DMA) Networks at Various Feed Crosslinking Percentages. Poly(MAA-co-EGDMA) networks, (\diamond), and poly(MAA-co-PEG200DMA) networks, (\square). The higher the feed crosslinking percentage, the higher the association constant due to the increase stability of binding sites. Error bars represent standard deviation with four replicates at $T=25^\circ\text{C}$.

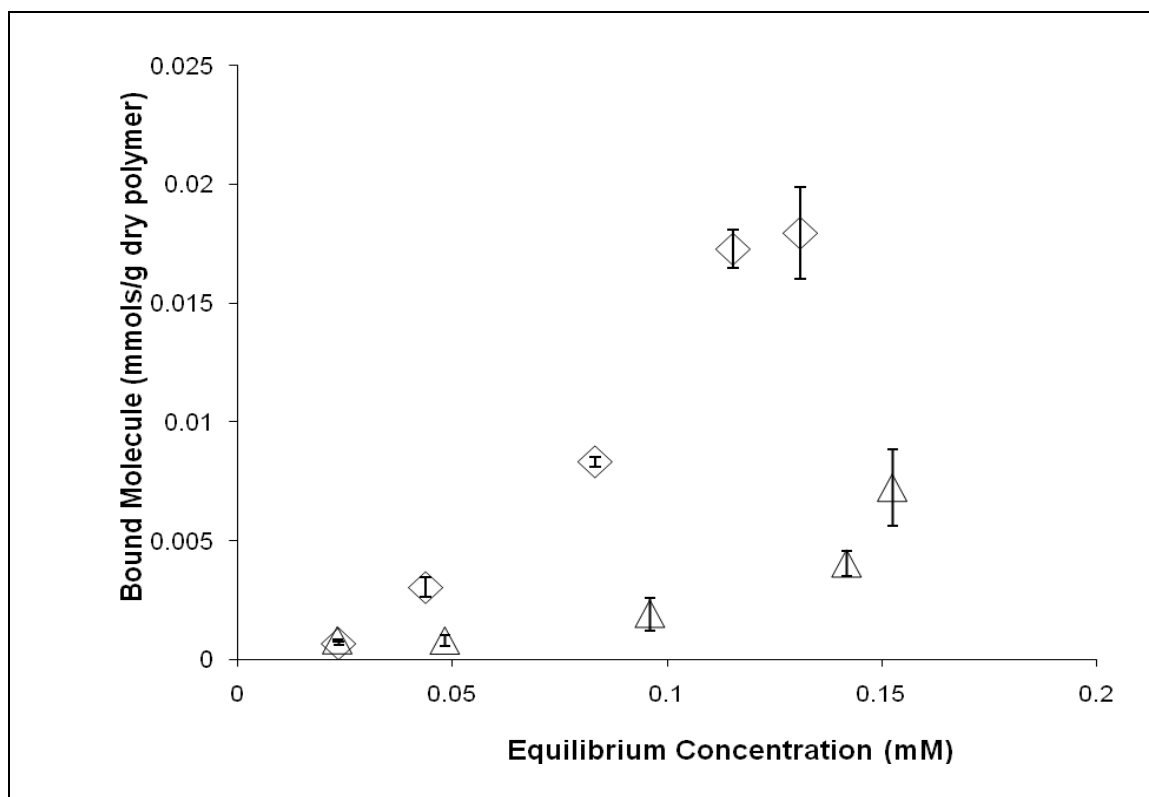


Figure 3.7: Selectivity Study of Poly(MAA-co-EGDMA) Recognitive Networks at

77% Crosslinking. Recognitive network in a concentration of testosterone solution, (◇), and the recognitive network in a concentration of progesterone solution, (△). The testosterone recognitive network binds more testosterone than progesterone illustrating that the imprinted network is more selective and has a higher affinity for testosterone. Error bars represent standard deviation with four replicates at T=25°C.

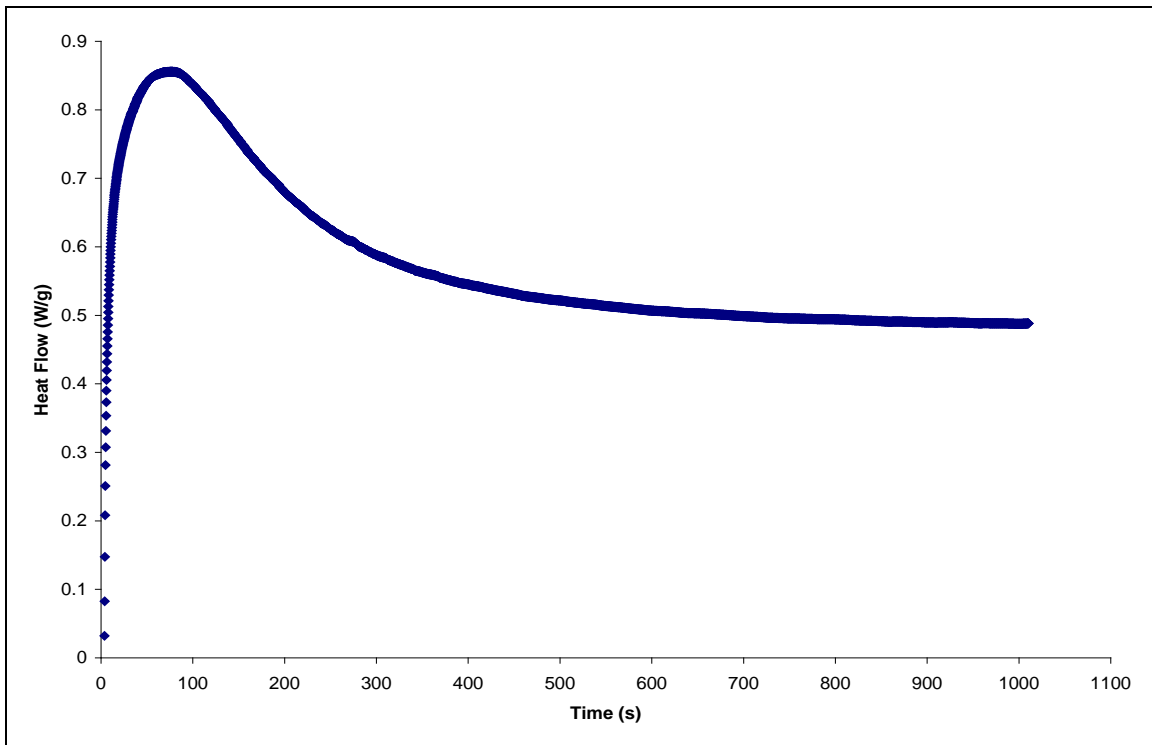


Figure 3.8: Heat flow versus Time for the UV Polymerization of 77% Crosslinked poly(MAA-co-EGDMA) Recognitive Network. The area underneath the curve represents the final bond conversion.

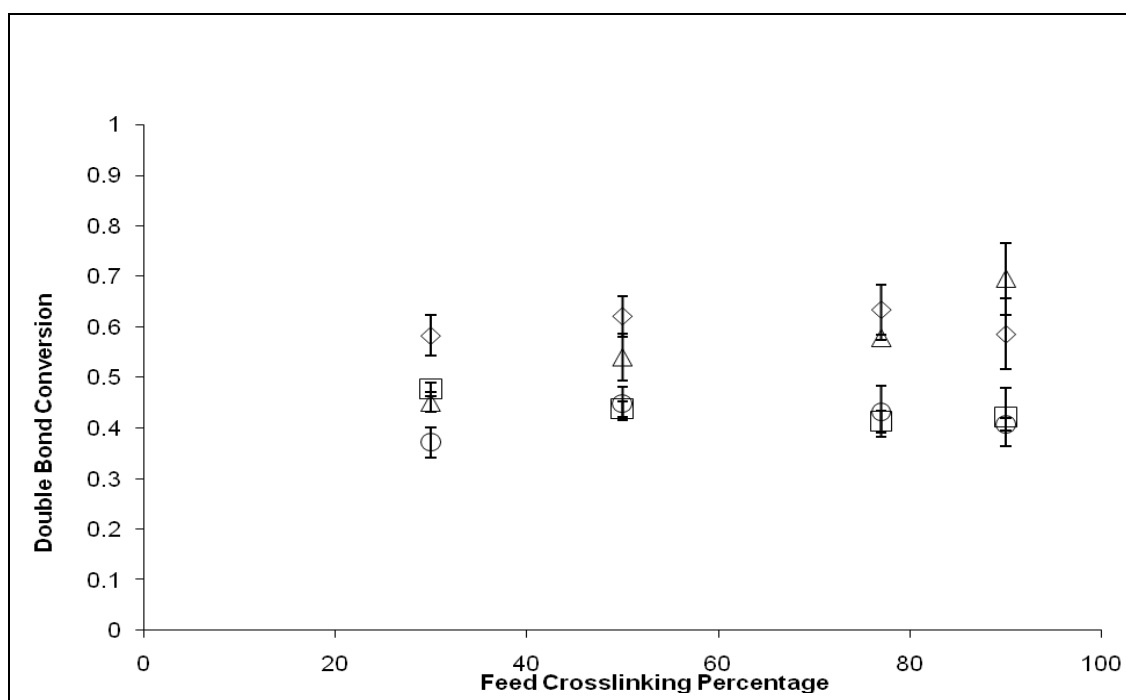


Figure 3.9: Fractional Double Bond Conversion Versus Feed Crosslinking Percentage using UV Polymerization where (o) is the poly(MAA-co-EGDMA) recognitive network, (□) is the poly(MAA-co-EGDMA) control network, (Δ) poly(MAA-co-PEG200DMA) Recognitive Network, (◇) poly(MAA-co-PEG200DMA) Control Network . The DPC studies indicate that the feed crosslinking composition does not accurately represent the final product .

4.0 TRANSPORT CONSIDERATIONS OF RECOGNITIVE NETWORKS

The fabrication of selective, inexpensive, robust biosensors has become a topic of major interest in the past decade. Our laboratory is interested in the creation of thin film recognitive structures for use in point-of-care (POC) diagnostic sensors that can function away from the hospital bed or clinical laboratory. With the use of these polymer structures, there is significant potential to drastically decrease analysis time and improve medicinal therapy. The design and fabrication of new POC sensors will depend on and benefit from the development of synthetic recognitive networks. The rational design and synthesis, along with template rebinding analysis of imprinted polymer networks, was discussed in Chapter 3 which led to an understanding of how the macromolecular memory can influence template binding parameters. In this chapter, the focus is to study template transport through recognitive networks to explore the potential of those materials for biosensing.

4.1 Scientific Rationale

As discussed in Chapter 2, recognitive networks are synthetic, robust materials that can operate in a wide spectrum of environments such as differing pH and temperature ranges. This robust behavior and ability to rebind a template molecule multiple times without loss of affinity makes these networks strong candidates as the

main sensing element of biosensors. Recognitive networks are expected to increase sensor shelf life, facilitate sensor use in a variety of environments, and decrease sensor production costs as compared to biological-containing sensing elements.

Researchers have recently utilized imprinted networks on sensor platforms such as quartz crystal microbalance (QCM)¹⁻¹² and surface plasmon resonance (SPR)^{13,14}. When the target molecule binds to the recognitive network, there is an increase in the acoustic frequency or an increase in the refractive index, respectively, providing a real-time, label-free analysis. However, the use of imprinted films has had a number of limitations¹⁵. One limitation is a slow equilibrium response time that is due to thick films from inadequate polymer grafting techniques. Also, lack of research on the rational design of recognitive networks limits their utilization in the design of a synthetic biosensor.

The multiple sensor platforms available for recognitive network integration were discussed in Chapter 2 (e.g. SPR, Microcantilevers and QCM-D). The best sensor platform for recognitive polymer integration would be the sensor that measures the change in resonance frequency as a function of mass absorption such as the quartz crystal microbalance with dissipation (QCM-D). The QCM-D has the ability to measure the mass absorption in a liquid environment, therefore eliminating any solvent constraints that the highly crosslinked networks require. For example, a highly crosslinked film will crack if it is not remained solvated. Also, with the dissipation measurement, the QCM-D can measure the structural properties (i.e., rigidity, viscoelasticity) and the thickness of the film. These features would be advantageous for sensor design.

Promising studies have been conducted grafting exact patterns of cognitive networks onto silicon surfaces using photolithography methods^{16,17}, but the thickness of the film yielded large response times. Theoretical calculations predict that cognitive networks less than 1 μm thick will give a response time of seconds¹⁷. However, even considering a thin film, the imprinted network structure is very important and should be designed to allow sufficient diffusional transport of template. For example, the film thickness of a bilirubin cognitive polymer-QCM system was approximated (determined by frequency shift) to be 150 nm thick. Despite this thin film, the sensor had an equilibrium response and regeneration time of 41 minutes, which is an inadequate response for a diagnostic sensor¹⁷. One reason for the slow response was the slow diffusion of the template molecule through the highly crosslinked network. While solvent is typically used in imprinted polymer formulations to create porous networks and increase the transport of template, many grafting techniques limit the use of solvent. Therefore, it would be advantageous to investigate the template diffusion through our testosterone imprinted networks to further program the polymeric system for future biosensing purposes. This chapter will discuss in detail the transport properties of the template molecule through the various networks that were discussed previously in Chapter 3.

4.2 Theoretical Model of Diffusion

The transport of a template through a hydrogel can be a mathematically modeled¹⁸. We consider the case in which the hydrogel is shaped like a slab. The aspect

ratio of the exposed surface diameter to the thickness is greater than 10 so one can assume diffusion is occurring in one dimension. By application of Fick's Second Law, we assume the given initial and boundary conditions where,

$$\frac{\partial C}{\partial t} = D \frac{\partial^2 C}{\partial x^2} \quad (4.1)$$

$$C(x, t) = C_0 \text{ when } t = 0 \quad (4.2)$$

$$\frac{\partial C}{\partial x} = 0 \text{ while } t > 0 \text{ and } x = 0 \quad (4.3)$$

$$C = C_s \text{ while } t > 0 \text{ and } x = \pm L \quad (4.4)$$

We describe a system in which a planer hydrogel undergoes one-dimensional diffusion over time in an environment in which the template concentration is very small (i.e., the concentration of template is negligible in the bulk fluid), where C_0 represents the initial template concentration (assumed to be uniform) in the homogeneous gel, x represents the distance from the central, length-wise axis of the hydrogel to the surface, C is the concentration of the template within the gel at any given position and time, C_s is the concentration at the surface of the gel, D represents the constant template diffusion coefficient which is independent of position and concentration, t is time, and L is the thickness of the gel. At $x = 0$, the flux of the template is effectively zero.

The solution of the PDE is given by equation 4.5,

$$\frac{C - C_0}{C_s - C_0} = 1 - \frac{4}{\pi} \sum_{n=0}^{\infty} \frac{(-1)^n}{2n+1} e^{-\frac{(2n+1)^2 \pi^2 D t}{4L^2}} \cos \frac{(2n+1)\pi x}{2L} \quad (4.5)$$

An effective way of comparing the release kinetics from different gels is to compare the fractional release of the template at time t relative to the total drug released at infinite time, expressed as M_t/M_∞ , where M_t is the total cumulative mass of template released at time t , and M_∞ is the total cumulative mass of template released at infinite time.

$$\frac{M_t}{M_\infty} = 1 - \sum_{n=0}^{\infty} \frac{8}{(2n+1)^2 \pi^2} e^{-\frac{(2n+1)^2 \pi^2 D t}{4L^2}} \quad (4.6)$$

The above expression can be expressed in terms of error functions.

$$\frac{M_t}{M_\infty} = 4 \left[\frac{Dt}{L^2} \right]^{\frac{1}{2}} \left[\frac{1}{\pi^{\frac{1}{2}}} + 2 \sum_{n=1}^{\infty} (-1)^n \operatorname{ierfc} \left(\frac{nL}{2\sqrt{Dt}} \right) \right] \quad (4.7)$$

At short times ($M_t/M_\infty < 0.65$) the expression can be simplified to

$$\frac{M_t}{M_\infty} = 4 \left[\frac{Dt}{L^2} \right]^{\frac{1}{2}} \quad (4.8)$$

By plotting the fractional release of testosterone versus $(t^{0.5}/L)$, we can calculate the diffusion coefficient from the slope. We can also measure how well the data matched a Fickian release profile by the empirical Power Law equation:

$$\frac{M_t}{M_\infty} = kt^n \quad (4.9)$$

By plotting the log of fractional release versus the log of time and calculating the slope, we can determine the order of release of the particle from the network. The order of release is equal to $|n-1|$. For Fickian release in slab geometry, the order is 0.5. For time-independent release, the order is 0.

4.3 Synthesis of Recognitive Networks for Template Release Studies

In this section, the synthesis and the template transport analysis of the testosterone recognitive poly(MAA-*co*-EGDMA) and poly(MAA-*co*-PEG200DMA) networks are discussed. The materials used to synthesis the polymers are the same as discussed in Chapter 3; however the synthesis protocol is slightly different as thin-films were needed for template transport studies.

4.3.1 Materials

In this work, we synthesized methacrylate copolymer networks imprinted for testosterone using ethylene glycol dimethacrylate (EGDMA) and poly(ethylene glycol)200dimethacrylate (PEG200DMA) as crosslinking agents, which have approximately 1 and 4.5 ethylene glycol units, respectively. Methacrylic acid (MAA), testosterone (template molecule), chloroform, azobisisobutyronitrile (AIBN), and EGDMA were purchased from Sigma Aldrich (Milwaukee, WI). PEG200DMA was

purchased from Polysciences, Inc. (Warrington, PA). All chemicals were analytical grade and used as received except for MAA which had inhibitor removed by vacuum distillation prior to use.

4.3.2 Polymer Synthesis

An 8:1 functional monomer to template molar ratio was used to produce testosterone recognitive networks with MAA as the functional monomer, testosterone as the template molecule dissolved in chloroform, AIBN as the initiator, and EGDMA or PEG200DMA as the crosslinking monomer. Control polymers were produced by the same method as the imprinted polymers but without testosterone. Monomer solutions were prepared with the molar ratio of initiator to double bonds held constant at 0.015 and the weight percentage of the solvent constant at 50% (w/v). The crosslinking percentage, defined as the moles of crosslinking monomer divided by the total moles of all monomers including crosslinking monomer, was varied from 50%, 77%, and 90%.

In a typical experiment, functional monomer, template molecule, crosslinking monomer, and solvent were added to a glass vial and sonicated for 30 minutes to make certain the solution was well mixed. After the nitrogen purge, the monomer solution was transferred to an aluminum disc mold that created discs of diameter 28mm with thicknesses ranging from 0.8 to 1.0 mm. The aluminum disc mold was held constant by circulating ethylene glycol/water mixture 0°C through the body of the aluminum mold. In the presence of a nitrogen atmosphere, a Novacure 2100 (Exfo, Ontario, Canada) mercury spot cure lamp was used as the light source with intensity of 50 mW/cm², as

determined via radiometer, for 17 minutes. The disks were washed in a modified Soxhlet extraction device to ensure the disks were immersed in solvent at all times. After the washing procedure, the disks were placed in 0.18 mM of testosterone in chloroform and allowed to reach equilibrium. Release studies were performed using 50mL polypropylene vials with 10mL of chloroform. To ensure an infinite sink for the release studies, the fluid was changed every 8 hours for the first 36 hours and thereafter every 24 hours. At every fluid change, a 200 μ L aliquot of the solution was taken and the testosterone concentration was measured at 238 nm using UV-Vis spectrophotometer.

4.4 Results and Discussion

Template transport analysis was conducted on the testosterone recognitive and control poly(MAA-*co*-EGDMA) and poly(MAA-*co*-PEG200DMA) networks. We hypothesized that the diffusion coefficients of the polymeric materials are a function of both the structural parameters and the macromolecular recognition capability of the polymeric network. The recognitive networks will have slower template transport through the network compared to the control networks due template rebinding via macromolecular memory within the recognitive network. Also, the transport of the template molecule will be a function of the macromolecular structure of the polymeric network. Two parameters that can change the macromolecular structure are the feed crosslinking percentage and the length of the bi-functional crosslinking monomer. Within a highly crosslinked network, the template transport will be slower compared to a less crosslinked network because of the structural hindrance, smaller mesh size, and the

decrease in free volume for template transport (Fig. 4.1). Consequently, with a longer crosslinking monomer, the mobility and free volume of the network increases, resulting in a faster template transport through the network (Fig. 4.1).

In order to calculate the diffusion coefficient of the template molecule through the network, a one-dimensional flow cell experiment was designed to measure time dependent flow of testosterone through the recognitive and control networks. However, the experiment was not successful because the gels cracked due to the fast evaporation of chloroform from the poly(MAA-*co*-EGDMA) networks. The polymer chains would desolate quickly and constrict producing significant strain within the network, causing cracks within the gel. The cracks led to solvent leaking out of the side-by-side diffusion cell as well as transport of template through the cracks. Therefore, the one-dimensional flow experiment was not feasible for determining template permeability through the network. Instead, a fractional template release study was used to calculate the diffusion coefficients of template within the networks. Also, because of the high amount of crosslinking within the networks, the mesh size of the network was not calculated since this analysis is based on rubber elasticity theory. However, as discussed in Chapter 2, there has been experimental evidence of decreased mesh sizes in highly crosslinked networks with more appropriate statistical analysis available for the more rigid networks²¹⁻²³.

As seen in Figure 4.2 and Figure 4.3, the release of testosterone was measured from both the testosterone recognitive and control poly(MAA-*co*-EGDMA) networks in relation to time. It is important to note that the release profiles of both networks were

measured for over 100 hours. Also, there was no short time burst effect that is typically seen with a large number of drug delivery systems. Also, there is a linear region of release for both the recognitive and control networks. At 100 hours, the control network recognitive network released approximately 3 fold more testosterone ($(1.5 \pm 0.075) \times 10^{-3}$ mg of testosterone) than the recognitive network ($(5.0 \pm 0.25) \times 10^{-4}$ mg of testosterone). Even though the control network released more testosterone at a given time than the recognitive network, the testosterone rate of release does not correlate with the testosterone loading capacity of the network. The binding capacities of the networks were presented in Chapter 3 and to reiterate, the recognitive network had a larger template binding capacity compared to the control network. If the measurements were taken past 150 hours, the testosterone release from the control network would reach equilibrium much sooner than the release of testosterone from the recognitive network.

In order to demonstrate the testosterone release rates for each network, the testosterone release data was normalized (testosterone fractional release) and plotted versus time (Fig.4.3). The recognitive network has a slower rate of release as compared to the control network. At a value of the x-axis 350, the control network had released approximately 60% of its testosterone released at infinite time (M_{∞}) as compared to 30% of the recognitive network's testosterone released at infinite time (M_{∞}). The mass infinity value for each network was taken as the last data point in the respective linear release profile. Using the slope from the linear regression of the fractional release along with equation 4.8, the template diffusion coefficients were calculated. The 77% crosslinked control network had 67% faster template diffusion coefficient ((4.24 ± 0.08)

$\times 10^{-9} \text{ cm}^2/\text{s}$) than the 77% testosterone recognitive network ($(2.83 \pm 0.06) \times 10^{-9} \text{ cm}^2/\text{s}$) (Fig. 4.8). There are three potential reasons for differing template release rates: (i) change in size of template molecule; (ii) change in the macromolecular structure and free-volume; and (iii) the macromolecular memory within the testosterone imprinted network. The template molecule remained constant and, as discussed in Chapter 3, the macromolecular structure of the recognitive and control network for a given crosslinking monomer did not have a significant statistical difference in the final double bond conversion. Therefore, the slower testosterone release rate in the 77% crosslinked testosterone recognitive network, compared to the 77% crosslinked control network, is due to the macromolecular memory formed during polymerization.

In Figure 4.4 and Figure 4.5, the release of testosterone was measured from both the 50% and 77% crosslinked testosterone recognitive poly(MAA-*co*-EGDMA) network in relation to time. It is important to reiterate that the same trends such as the no short time burst effect, the template release profile measured for more than 100 hours, and the linear release profile were also apparent in the testosterone release data for the 50% recognitive network. As seen in Figure 4.4, the 50% crosslinked recognitive poly(MAA-*co*-EGDMA) network released approximately 2 fold more testosterone ($(2.0 \pm 0.2) \times 10^{-3} \text{ mg}$) than compared to 77% crosslinked network ($(1.0 \pm 0.1) \times 10^{-3} \text{ mg}$). The fractional release, as seen in Figure 4.5, demonstrated that the 50% crosslinked recognitive poly(MAA-*co*-EGDMA) network released the testosterone at a slightly faster rate compared to the 77% crosslinked recognitive poly(MAA-*co*-EGDMA) network. For example, at an x-axis value of 400, the 50% crosslinked recognitive network released

50% of its testosterone released at infinite time compared to 40% from the 77% crosslinked cognitive network's testosterone released at infinite time. Again, the mass at infinite time for both cases was taken as the last point in the respective linear profile. From Appendix A-2, Figure A.2.4 illustrates that the 50% crosslinked control network, has a faster rate of template release than the cognitive network. Because the double bond reaction analysis indicated similar post-polymerization macromolecular structures for both networks, the faster release rate reiterates the concept previously discussed that the slower rate of release is from the imprinting effect within the cognitive network. Also, the 50% crosslinked cognitive network had a 1.2 times higher diffusion coefficient ($(3.32 \pm 0.16) \times 10^{-9} \text{ cm}^2/\text{s}$) compared to the 77% cognitive network ($(2.83 \pm 0.06) \times 10^{-9} \text{ cm}^2/\text{s}$). Since the template molecular size remained constant, the reason for the faster template diffusion coefficient from the 50% cognitive network compared to the 77% cognitive network is from both the change in the macromolecular structure and the template binding capacity and affinity of the network. The less crosslinked network has fewer bi-functional monomers incorporated within the network for intra-chain polymerization, increasing the template holding mesh size, increasing the free volume available for template transport. Also, fewer effective cavities are formed during polymerization, which will decrease the testosterone competitive binding resulting in faster transport of testosterone through the network.

Figures 4.6 and 4.7 demonstrate the effects of changing the length of the crosslinking monomer on the testosterone release rate. At 150 hours, the 77% testosterone cognitive poly(MAA-*co*-EGDMA) network released more testosterone

(($1.0 \pm 0.83 \times 10^{-3}$) mg of testosterone) in comparison to the 77% testosterone recognitive poly(MAA-*co*-PEG200DMA) network ((7.0 ± 0.34) $\times 10^{-4}$ mg of testosterone). However, at an x-axis value of 420, the fractional analysis indicates, as seen in Figure 4.7, the fractional mass release from the 77% testosterone recognitive poly(MAA-*co*-PEG200DMA) network is 1.5 times higher than the 77% testosterone recognitive poly(MAA-*co*-EGDMA) network. Also, the 77% testosterone recognitive poly(MAA-*co*-PEG200DMA), the network has a 1.4 times faster template diffusion coefficient, (3.85 ± 0.08) $\times 10^{-9}$ cm²/s, as compared to the 77% testosterone recognitive poly(MAA-*co*-EGDMA) network ((2.83 ± 0.06) $\times 10^{-9}$ cm²/s). The only variable that was changed was the length of the bifunctional crosslinking monomer, which directly affects the binding parameters and the macromolecular structure. We know by the double bond conversion studies, that the 77% testosterone recognitive poly(MAA-*co*-PEG200DMA) network had a final double bond conversion of approximately 65 \pm 5% compared to 40 \pm 5% final double bond conversion of the 77% testosterone recognitive poly(MAA-*co*-EGDMA) network. However, the 77% testosterone recognitive poly(MAA-*co*-PEG200DMA) network has more network mobility and free volume for faster template transport. This mobility also, as described in Chapter 3, decreased the binding capacity and affinity for the 77% testosterone recognitive poly(MAA-*co*-PEG200DMA) network.

The template binding affinities calculated by the Freundlich isotherm analysis for the recognitive poly(MAA-*co*-EGDMA) and poly(MAA-*co*-PEG200DMA) networks were discussed in Chapter 3. For the 77% testosterone recognitive network, the

poly(MAA-*co*-PEG200DMA) network had an association constant of $(0.20 \pm 0.05) \times 10^4 \text{ M}^{-1}$, which was a 6 fold decrease compared to the poly(MAA-*co*-EGDMA) cognitive network ($K_a = (1.20 \pm 0.07) \times 10^4 \text{ M}^{-1}$). The 50% testosterone cognitive poly(MAA-*co*-EGDMA) network and the 50% testosterone cognitive poly(MAA-*co*-PEG200DMA) had a slightly higher association coefficient ($K_a = (0.25 \pm 0.07) \times 10^4 \text{ M}^{-1}$).

To reiterate the transport analysis, the 77% crosslinked testosterone cognitive poly(MAA-*co*-EGDMA) network had a slower diffusion coefficient ($(2.83 \pm 0.06) \times 10^{-9} \text{ cm}^2/\text{s}$), as seen in Figure 4.8, compared to the diffusion of the template through the 77% testosterone cognitive poly(MAA-*co*-PEG200DMA) network ($(3.85 \pm 0.08) \times 10^{-9} \text{ cm}^2/\text{s}$) and the 50% testosterone cognitive poly(MAA-*co*-PEG200DMA) network ($(3.32 \pm 0.16) \times 10^{-9} \text{ cm}^2/\text{s}$). It should be noted that all the control networks had faster diffusion coefficients compared to their respective cognitive network supporting our hypothesis that the imprinting process slows the template transport through the network. Not only are the macromolecular structure and template molecular size important to the template diffusional transport, but they are also important to template binding affinity. The increase in binding affinity influences the diffusion coefficient through stronger intrinsic macromolecular recognition sites. Therefore, both the binding (i.e., capacity and affinity) and structural parameters (i.e., crosslinking percentage and length of crosslinking agent) should be taken in consideration into tailoring the network for a given application.

4.5 Conclusions

In this work, we demonstrated that higher crosslinked networks had lower template diffusion coefficients, and the diffusion coefficients increased with an increase in the crosslinking monomer size. Also, the imprinting process affected the diffusion of testosterone. All control networks had higher diffusion coefficients than corresponding recognitive networks, suggesting that imprinting decreased the template diffusion coefficient. For each feed crosslinking percentage, poly(MAA-*co*-EGDMA) recognitive networks had approximately a 1.4 fold or 40% lower testosterone diffusion coefficient compared to poly(MAA-*co*-PEG200DMA) recognitive networks. It is important to note that lower crosslinking percentages for recognitive EGDMA and PEG200DMA based copolymers resulted in 17% and 12% higher diffusion coefficients, respectively. Also, the binding affinities influence the template transport rate through the network, indicating that a “tailorable” polymeric network can be designed to fit certain template transport profiles.

4.6 References

1. Kiruchi, M.; Tsuru, N.; Shiratori, S., Recognition of terpenes molecular imprinted polymer coated quartz crystal microbalance in air phase. *Science and Technology of Advance Materials* **2006**, *7*, 165-161.
2. Das, K.; Penelle, J.; Rotello, V. M., Selective picomolar detection of hexachlorobenze in water using a quartz crystal microbalance coated with a molecularly imprinted polymer thin film. *Langmuir* **2003**, *19*, 3921-3925

3. Ersoz, A.; Denizili, A.; Ozcan, A.; Say, R., Molecularly imprinted ligand-exchange recognition assay of glucose by quartz crystal microbalance. *Biosensors and Bioelectronics* **2005**, *20*, 2197-2202.
4. Fu, Y.; Finklea, H. O., Quartz crystal microbalance sensor for organic vapor detection based on molecularly imprinted polymers. *Analytical Chemistry* **2003**, *75*, 5387-5393.
5. Kugimiya, A. L.; Takeuchi, T., Surface Plasmon resonance sensor using molecularly imprinted polymer for detection of sialic acid. *Biosensors and Bioelectronics* **2001**, *16*, 1059-1062.
6. Lin, T. Y.; Hu, C. H.; Chou, T. C., Determination of albumin concentration by MIP-QCM sensor. *Biosensors and Bioelectronics* **2004**, *20*, 75-81.
7. Matsuguchi, M.; Uno, T., Molecular imprinting strategy for solvent molecules and its application for QCM-based VOC vapor sensing. *Sensors and Actuators B* **2006**, *113*, 94-99.
8. Shoji, R. T.; Takeuchi, T.; Kubo, I., Atrazine sensor based molecularly polymer-modified gold electrode. *Analytical Chemistry* **2003**, *75*, 4882-4886.
9. Tai, D. R.; Lin, C. y.; Wu, T. Z.; Chen, L. K., Recognition of dengue virus protein using epitope-mediated molecularly imprinted film. *Analytical Chemistry* **2005**, *77*, 5140-5143.
10. Tsuru, N.; Kiruchi, M.; Kawaguchi, H.; Shiratori, S., A quartz crystal microbalance sensor coated with MIP for Bisphenol A and its properties. *Thin Solid Films* **2006**, *499*, 380-385.

11. Wu, A. H.; Syu, M. J., Synthesis of bilirubin imprinted polymer thin film for the continuous detection of bilirubin in an MIP/QCM/FIA system. *Biosensors and Bioelectronics* **2006**, *21*, 2345-2353.
12. Zhang, Z.; Lui, Y.; Long, Y.; Nie, L.; Yao, S., Effect of the size of molecularly imprinted polymers sensing materials on piezoelectric quartz crystal sensor performance. *Analytical Science* **2004**, *20*, 291-295.
13. Matsui, J.; Akamatsu, K.; Hara, N.; Miyoshi, D.; Nawafune, H.; Tamaki, K.; Sugimoto, N., SPR sensor chip for detection of small molecules using molecularly imprinted polymer with embedded gold nanoparticles. *Analytical Chemistry* **2005**, *77*, 4282-4285.
14. Yilmaz, E.; Mosbach, K.; Haupt, K., Influence of functional and cross linking monomers and the amount of template on the performance of molecularly imprinted polymers in binding assays. *Analytical Communications* **1999**, *36*, 167-170.
15. Pilestky, S. A.; Turner, N. W.; Laitenberger, P., Molecularly imprinted polymers in clinical diagnostics-Future potential and existing problems. *Medical Engineering & Physics* **2006**, *28*, 971-977
16. Byrne, M. E.; Oral, E.; Hilt, J. Z.; Peppas, N. A., Networks for recognition of biomolecules, molecular imprinting and micropatterning poly(ethylene glycol)-containing films. *Polymers of Advanced Technologies* **2002**, *12*, 798-816.
17. Hilt, J. Z.; Byrne, M. E.; Peppas, N. A., Microfabrication of intelligent biomimetic networks for recognition of D-glucose. *Chemistry of Materials* **2006**, *18*, 5869-5875.

18. Crank, J., *The Mathematics of Diffusion*. Oxford University Press: New York, **1975**.
19. Cheong, S. H.; McNiven, S.; Rachov, A.; Levi, R.; Yano, K.; Karube, I., Testosterone receptor binding mimic constructed using molecular imprinting. *Macromolecules* **1997**, *30*, 1371-1322.
20. Bell, C. L.; Peppas, N. A., Solute and protein diffusion in physiologically responsive hydrogels of poly(methacrylic acid-g-ethylene glycol). *Biomaterials* **1996**, *17*, 1203-1218.
21. Flory, P. J., *Principles of Polymer Chemistry*. 1st ed.; Cornell University Press: Ithica, **1953**.
22. Hariharan, D.; Peppas, N. A., Characterization, dynamic swelling behavior and solute transport in cationic networks with applications to the development of swelling-controlled release systems. *Polymer* **37**, *37*, 149-161.
23. Peppas, N. A.; Merrill, N. A., Crosslinked poly(vinyl alcohol) hydrogels as swollen elastic networks. *Journal of Applied Polymer Science* **1977**, *21*, 1764-1770.
24. Torres-Lugo, M.; Peppas, N. A., Molecular design and in vitro studies of novel pH-sensitive hydrogels for the oral delivery of calcitonin. *Macromolecules* **1999**, *32*, 6646-6651.

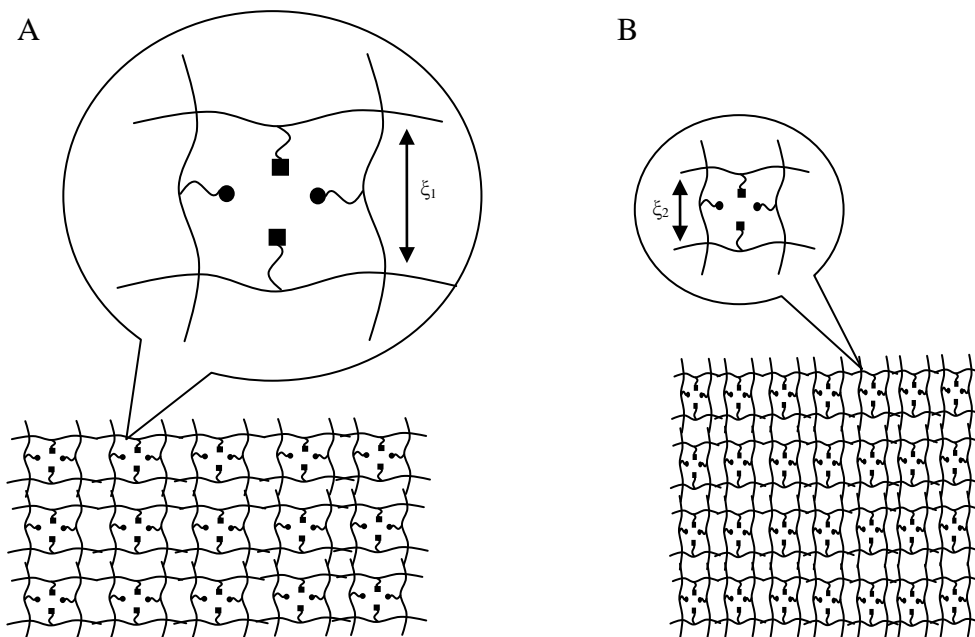


Figure 4.1: Illustration of the Mesh Size in Rigid Networks. When the structural components of a polymeric network are altered, the mesh size of the network is changed which effects the template diffusional transport. A) When a longer crosslinking monomer or less crosslink monomer solution is used in the synthesis, the network is more mobile and less rigid with increased free volume allowing for a faster diffusional transport. B) When a short and more concentrated crosslinking monomer solution is used in the synthesis, the mesh size and free volume are decreased, slowing the template diffusional transport through the network.

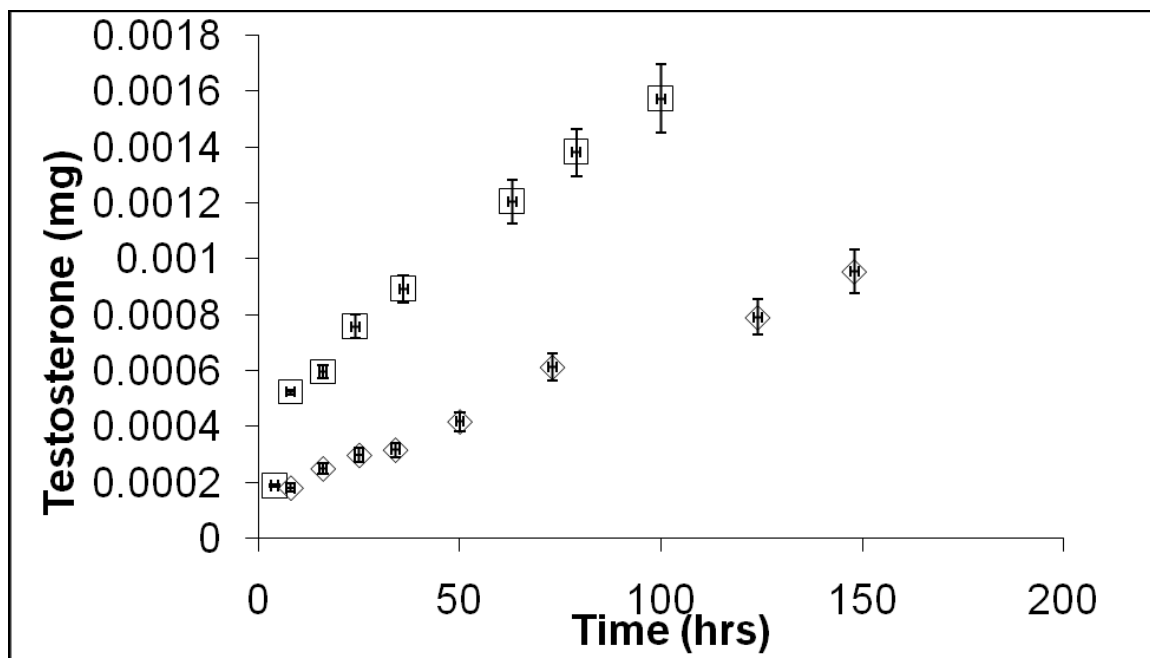


Figure 4.2: Mass of Testosterone Released from a 77% Testosterone Responsive and Control Poly(MAA-co-EGDMA) Network. (\diamond) 77% testosterone responsive poly(MAA-co-EGDMA) network; (\square) 77% control poly(MAA-co-EGDMA). Error bars represent standard deviation of three replicates.

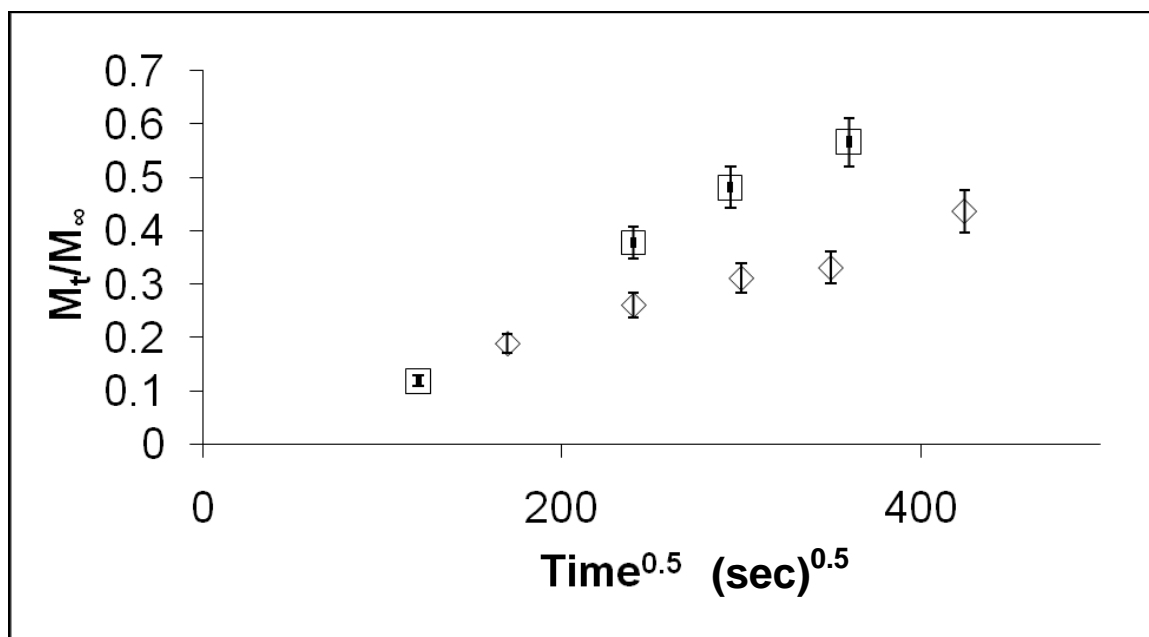


Figure 4.3: Fractional Mass of Testosterone Released from a 77% Testosterone Recognitive and Control Poly(MAA-*co*-EGDMA) Network. (◇) 77% testosterone recognitive poly(MAA-*co*-EGDMA) network; (□) 77% control poly(MAA-*co*-EGDMA). Error bars represent standard deviation in of three replicates.

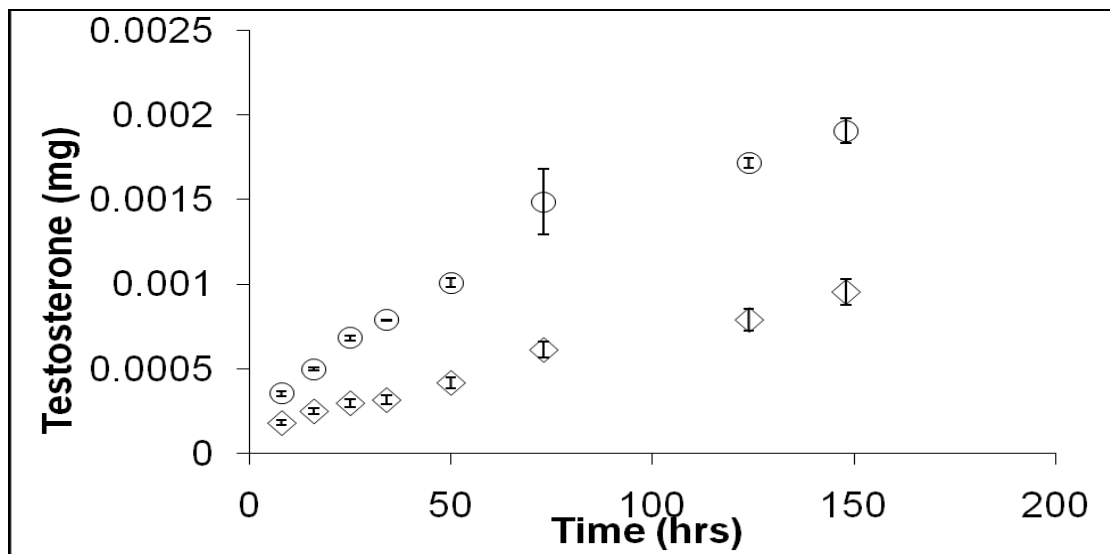


Figure 4.4: Mass of Testosterone Released from Testosterone Recognitive Poly(MAA-*co*-EGDMA) Network at Various Crosslinking Percentages. (◇) 77% testosterone recognitive poly(MAA-*co*-EGDMA) network; (o) 50% testosterone recognitive poly(MAA-*co*-EGDMA). Error bars represent standard deviation in three replicates.

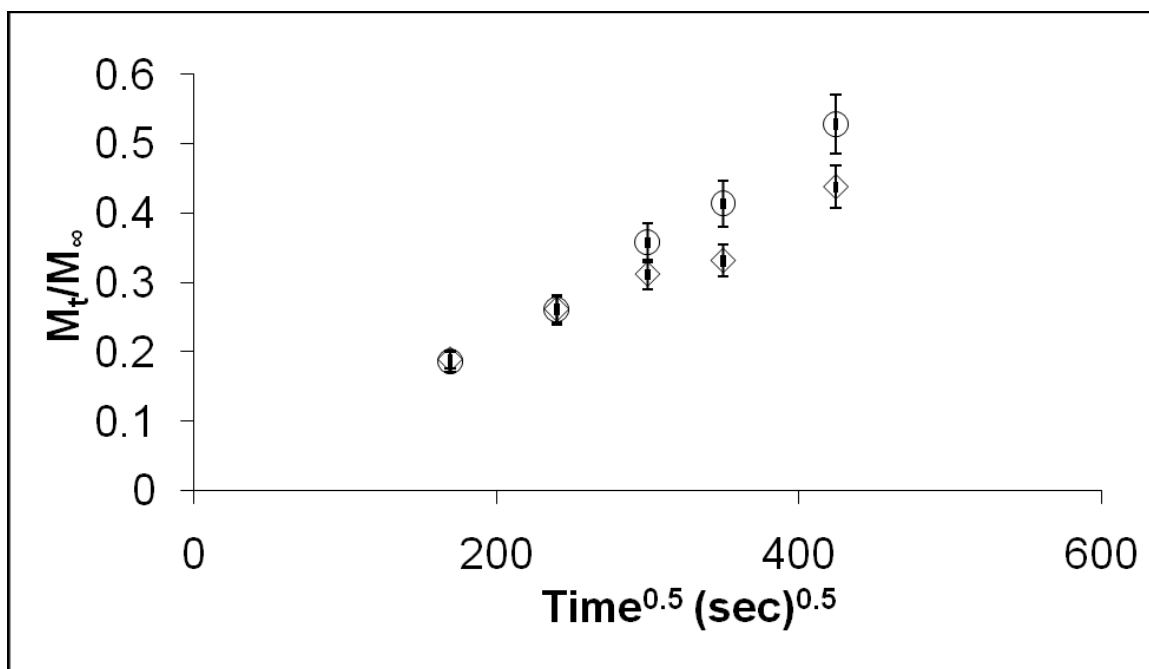


Figure 4.5: Fractional Mass of Testosterone Released from Testosterone Recognitive Poly(MAA-*co*-EGDMA) Network at Various Crosslinking Percentages. (◇) 77% testosterone recognitive poly(MAA-*co*-EGDMA) network; (○) 50% testosterone recognitive poly(MAA-*co*-EGDMA) network. Error bars represent standard deviation of three replicates.

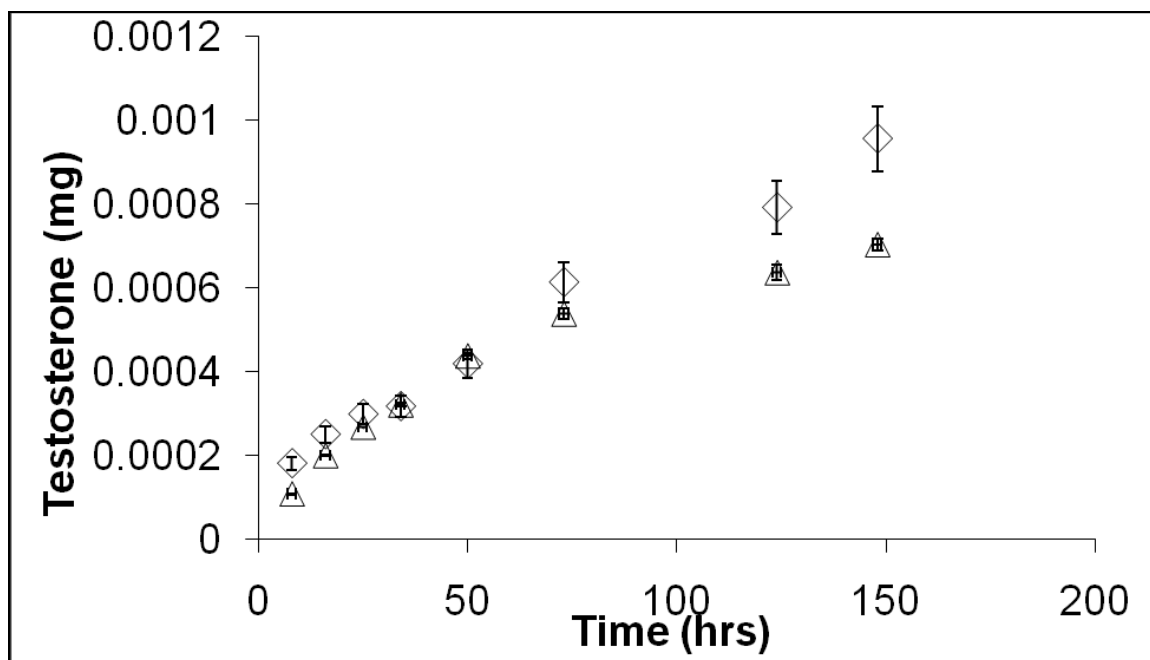


Figure 4.6: Mass of Testosterone Released from Testosterone Recognitive Poly(MAA-co-EGDMA) and Poly(MAA-co-PEG200DMA) Networks at 77% Crosslinking. (◇) testosterone recognitive poly(MAA-co-EGDMA) network; Δ testosterone recognitive poly(MAA-co-PEG200DMA); Error bars represent standard deviation of three replicates.

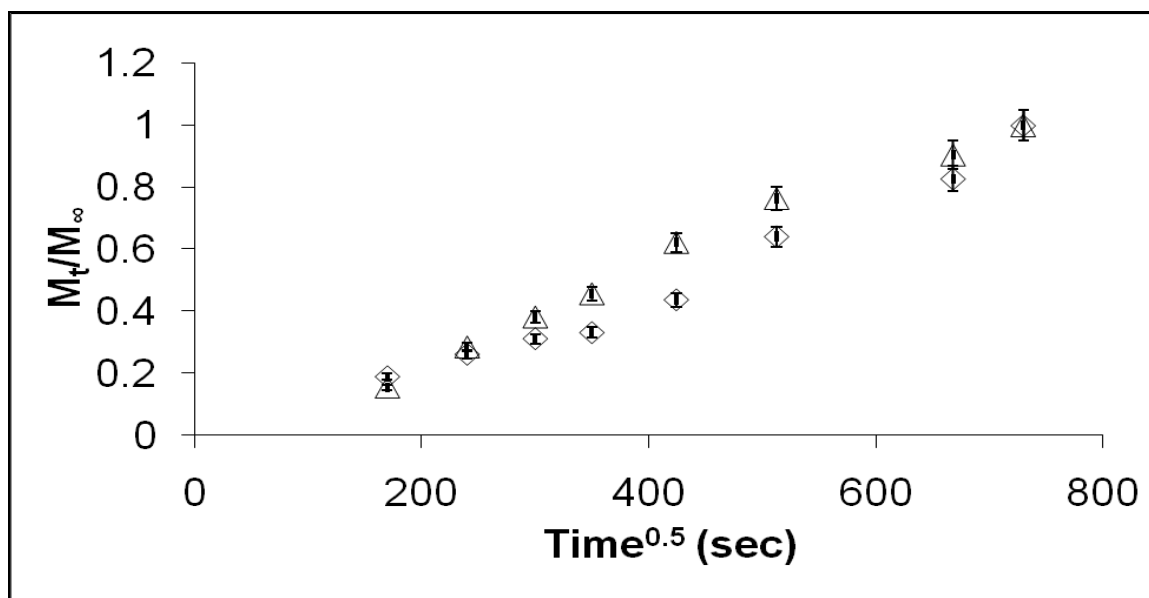


Figure 4.7: Fractional Mass of Testosterone Released from Testosterone Recognitive Poly(MAA-co-EGDMA) and Poly(MAA-co-PEG200DMA) Networks at 77% Crosslinking. (\diamond) 77% testosterone recognitive poly(MAA-co-EGDMA) network; (Δ) 77% testosterone recognitive poly(MAA-co-PEG200DMA). Error bars represent standard deviation of three replicates.

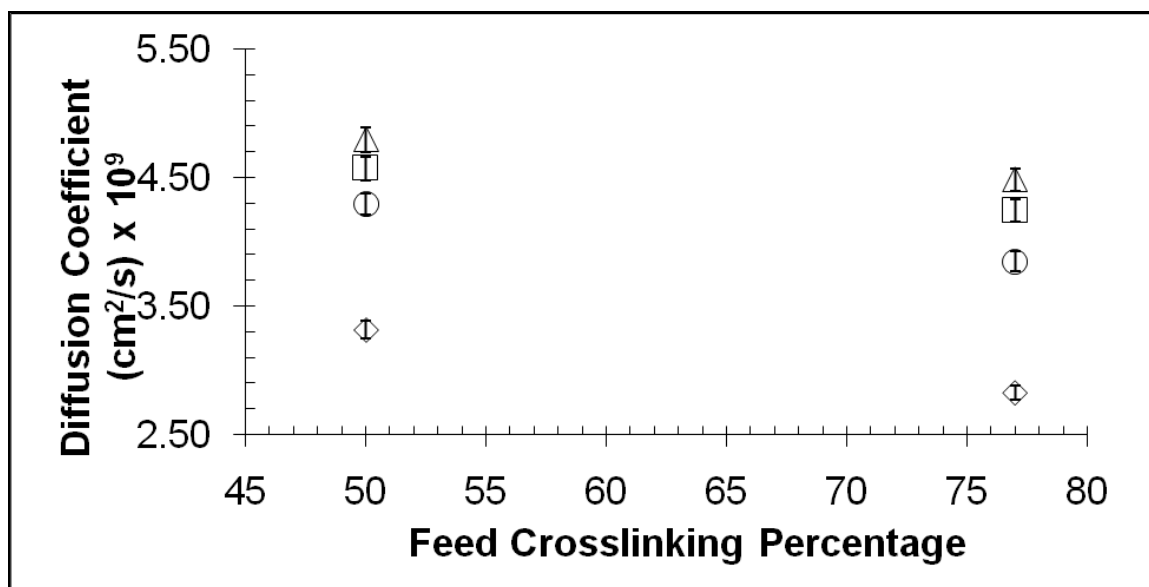


Figure 4.8: Diffusion Coefficients for Testosterone Recognitive and Control Poly(MAA-co-EGDMA) and Poly(MAA-co-PEG200DMA) Network at Various Crosslinking Percentages. (◇) testosterone imprinted poly(MAA-co-EGDMA) network; (○) testosterone imprinted poly(MAA-co-PEG200DMA); (□) control poly(MAA-co-EGDMA) network; (Δ) control poly(MAA-co-PEG200DMA) network. Error bars represent standard deviation of three replicates.

5.0 CONCLUSIONS

This work demonstrates the rational design, synthesis, and characterization of synthetic, intelligent polymeric materials that display tremendous potential for application as recognitive films in micro/nano-scale sensor applications such as point-of-care diagnostics. By manipulating key structural parameters such as the feed concentration and length of the crosslinking agent, the macromolecular architecture can be rationally tailored to have tuned template capacity, affinity, selectivity, and diffusional transport. In this work, we have shown that a highly crosslinked recognitive network, 90% crosslinked poly(MAA-*co*-EGDMA), had a 2 fold increase in the binding capacity and a 4 fold increase in binding affinity compared to a similar lower crosslinked recognitive network, 50% crosslinked poly(MAA-*co*-EGDMA). We have also demonstrated that by increasing the length of the crosslinking monomer within recognitive networks (i.e., comparing 77% crosslinked poly(MAA-*co*-EGDMA) to poly(MAA-*co*-PEG200DMA), there was a 4 fold decrease in the amount of testosterone bound. However, the longer crosslinking agent increased the mesh size and mobility of the macromolecular network allowing for a 40% increase in the diffusional transport. It is important to note that lower crosslinking percentages for recognitive EGDMA and PEG200DMA based copolymers resulted in 17% and 12% higher diffusion coefficients, respectively.

Ultimately, in any sensor design incorporating cognitive thin films, there will be trade-off involving binding parameters (e.g., affinity, selectivity, capacity) and transport considerations. A more structurally open network will have faster template permeation allowing for a decrease in response time. Also, a more structurally open network may provide bulk template binding rather than only surface binding, which would increase binding capacity and lower template affinity and selectivity. However, depending on the size, shape, and configuration of molecules in the sample fluid (i.e., how difficult the sensing environment), the lower values may be a viable tradeoff for a faster response time.

APPENDIX A

Appendix A contains supplemental data that is needed in verification of data presented in the main chapters of the document. A-1 represents the standard curve for the rebinding experiments. The ‘best fit’ analysis of the various isotherms (Scatchard, Langmuir and Freundlich isotherms) are also presented in A-1, along with supplemental data comparing the binding capacity of the control networks to the corresponding cognitive networks. A-2 presents the linear regression of the fractional mass of testosterone released versus to determine the slope of the lines for calculation of the diffusion coefficients. Appendix B contains the error analysis used in the dissertation.

A-1. Data from the Template Rebinding Studies

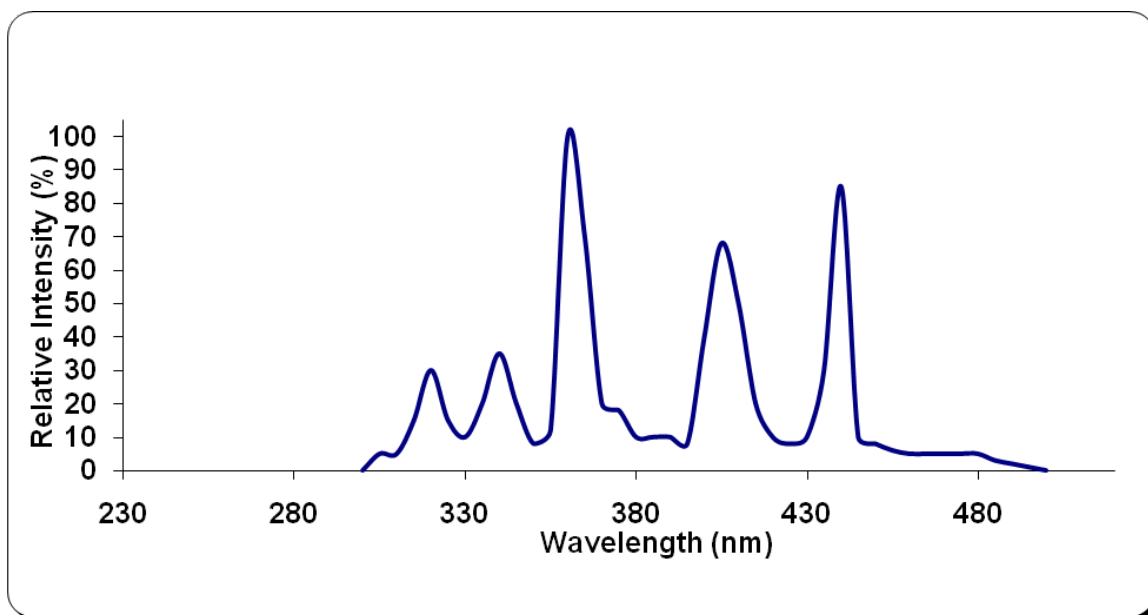


Figure A.1.1: Relative Intensity Versus Wavelength. The relative intensity vs. wavelength for the Novacure 2100 (Exfo, Ontario, Canada) mercury spot cure lamp light source with a 320-500nm wavelength filter.

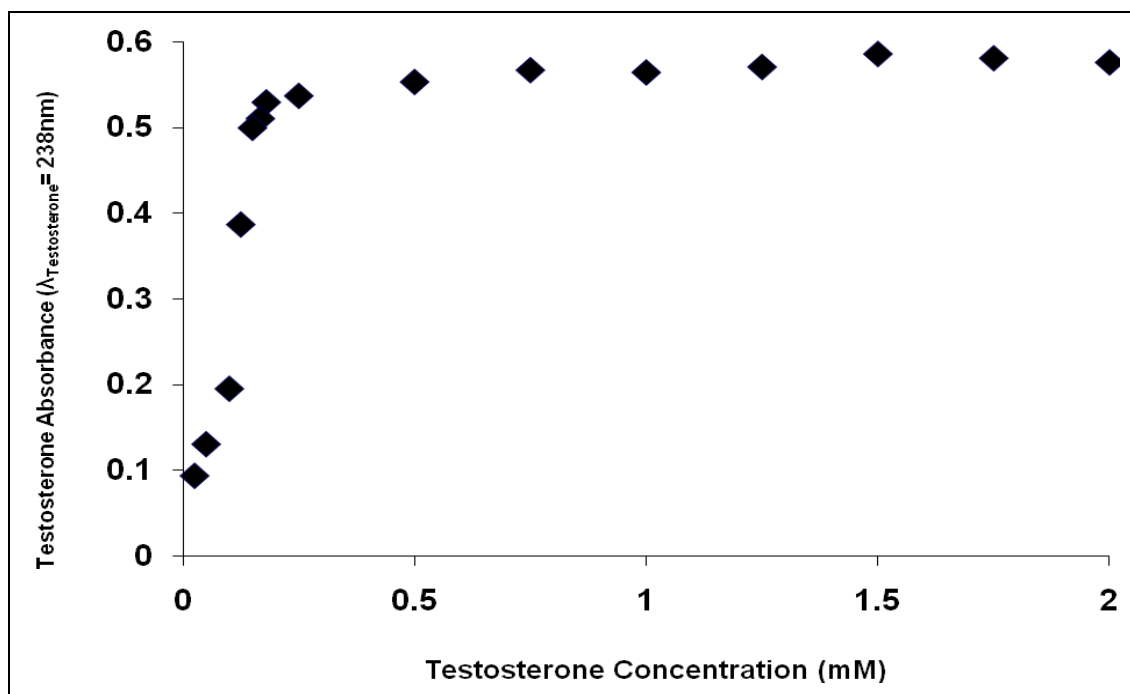
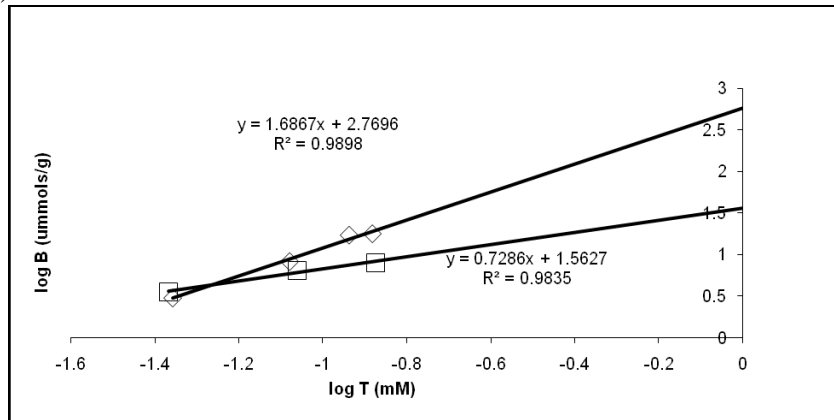
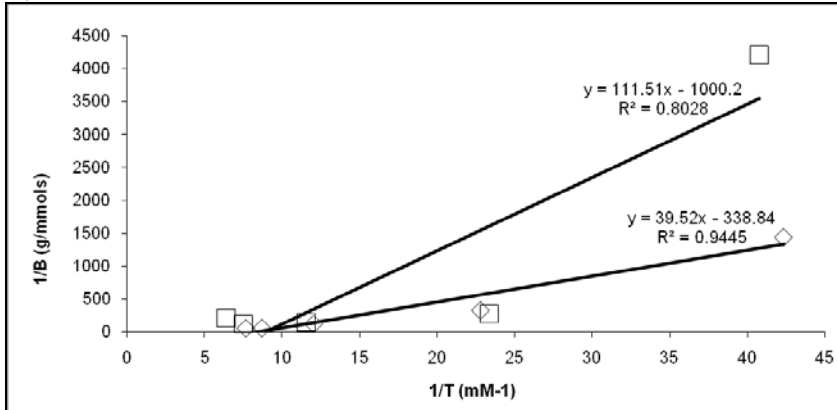


Figure A.1.2: Standard Curve of Testosterone in Chloroform. The non-linear region begins around 0.2 mmol, therefore the concentration range for our experiments did not exceed 0.187 mmol testosterone or used serial dilution methods ($T = 25^{\circ}\text{C}$).

a)



b)



c)

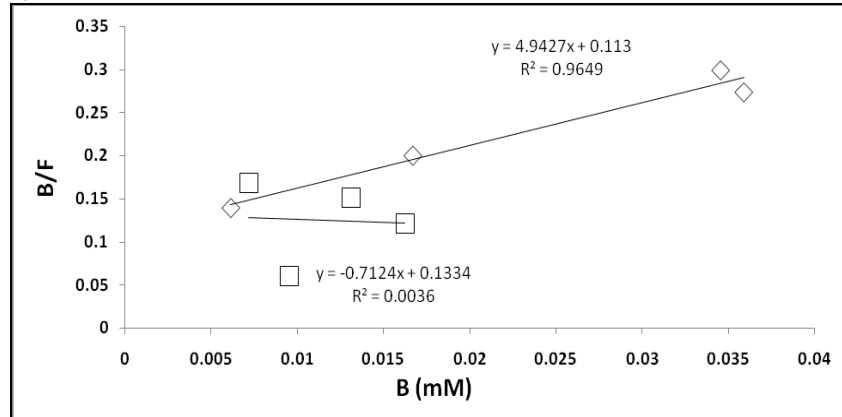


Figure A.1.3:Rebinding Isotherms of Testosterone Recognitive and Control Poly(MAA-co-EGDMA) at 77% Crosslinking. a) The Freundlich Isotherm; b) Langmuir Isotherm; c) Scatchard Plot, where (\diamond) is the recognitive network and (\square) is the control network. According to the R^2 values for both the testosterone and control networks, the Freundlich Isotherm was used to analyze the rebinding data to obtain the affinity constants for each system. B is the bound concentration of Testosterone, F and T represents the equilibrium concentration of Testosterone (T= 25°C).

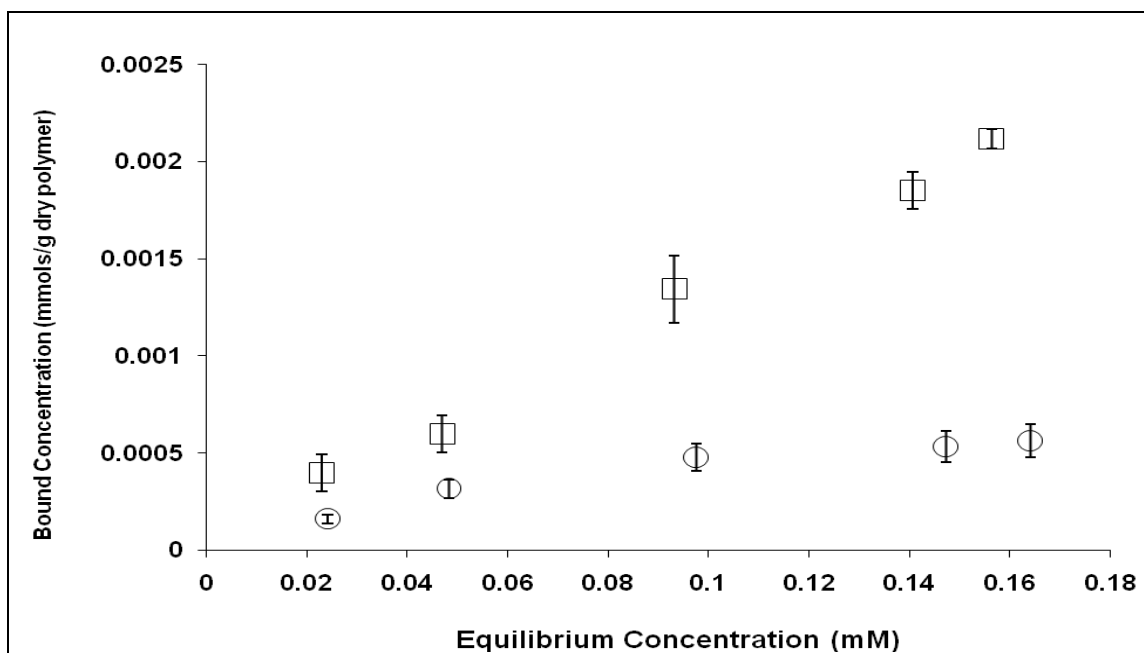
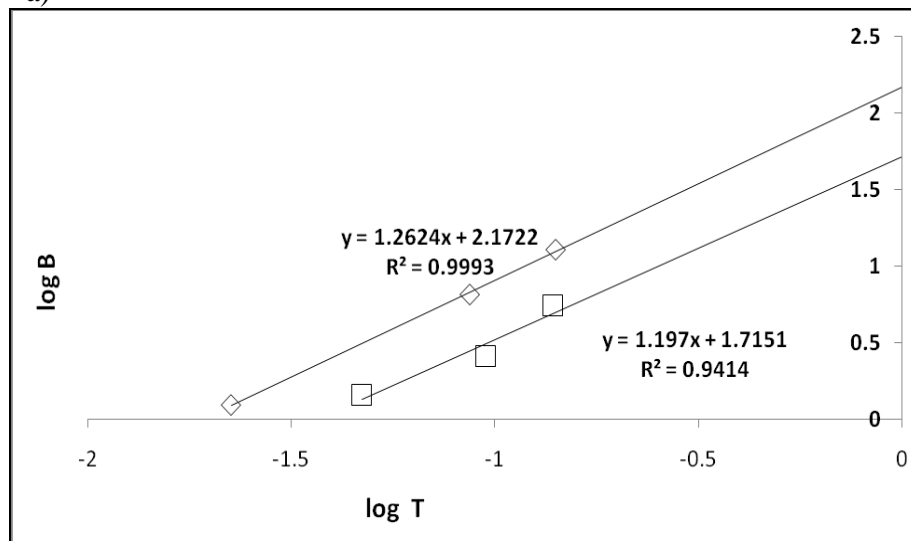
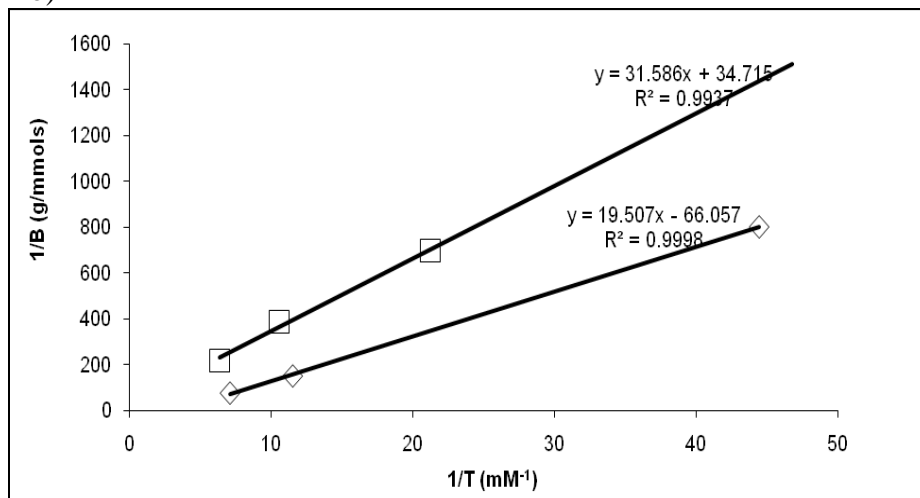


Figure A.1.4: Testosterone Equilibrium Binding Isotherms of Poly(MAA-*co*-EGDMA) at 50% Feed Crosslinking. Poly(MAA-*co*-EGDMA) Recognitive Network (□) and Control Network (○). Error bars represent standard deviation of four replicates (T= 25°C).

a)



b)



c)

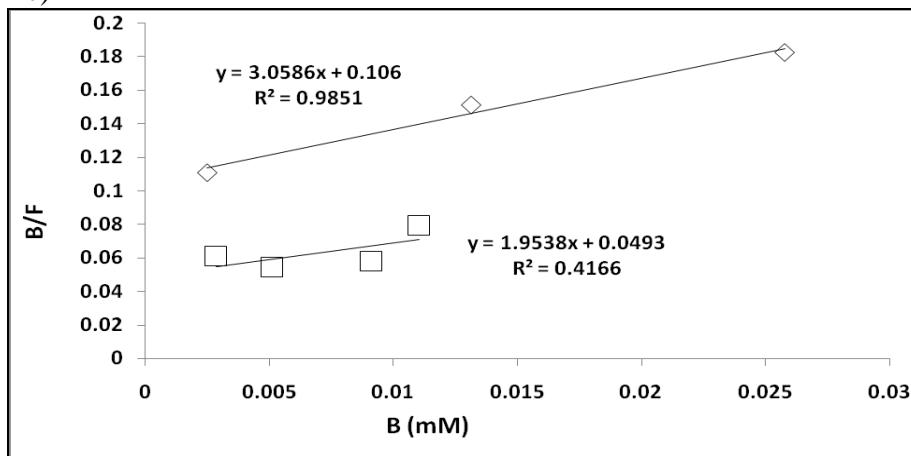


Figure A.1.5: Rebinding Isotherm of Testosterone Recognitive and Control Poly(MAA-co-EGDMA) at 50% Crosslinking. Poly(MAA-co-EGDMA) Recognitive Network (\diamond) and Control Network (\square). a) The Freundlich Isotherm; b) Langmuir Isotherm; c) Scatchard Plot. According to the R^2 values for both the testosterone and control networks, the Freundlich Isotherm was used to analyze the rebinding data to obtain the affinity constants for each system. B is the bound concentration of testosterone, F and T represent the equilibrium concentration of testosterone ($T= 25^\circ\text{C}$).

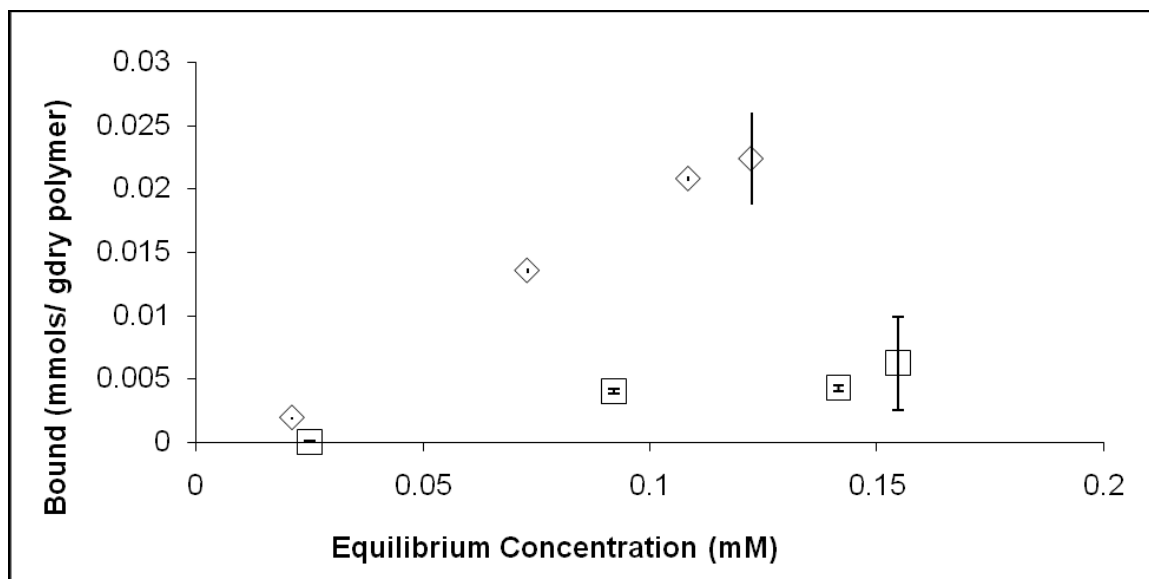
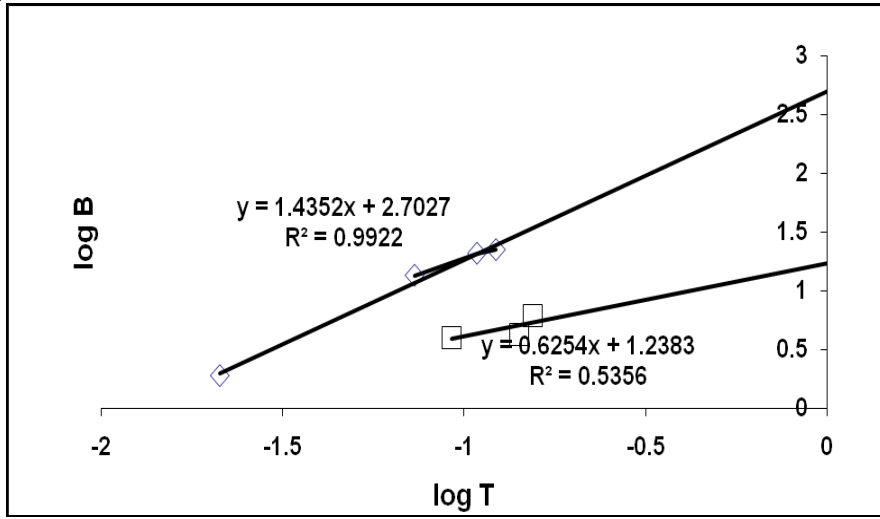
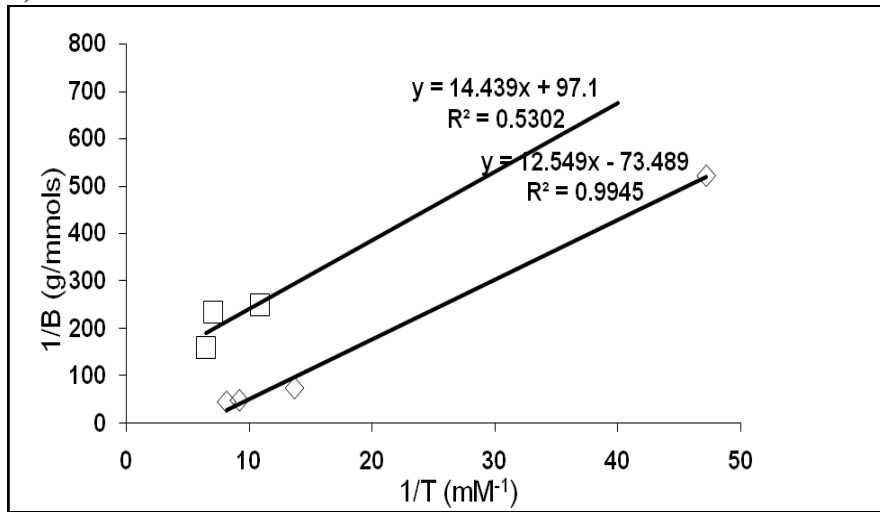


Figure A.1.6: Testosterone Equilibrium Binding Isotherms of Poly(MAA-*co*-EGDMA) at 90% Feed Crosslinking. Poly(MAA-*co*-EGDMA) Recognitive Network (◇) and Control Network (□). Error bars represent standard deviation of four replicates (T= 25°C).

a)



b)



c)

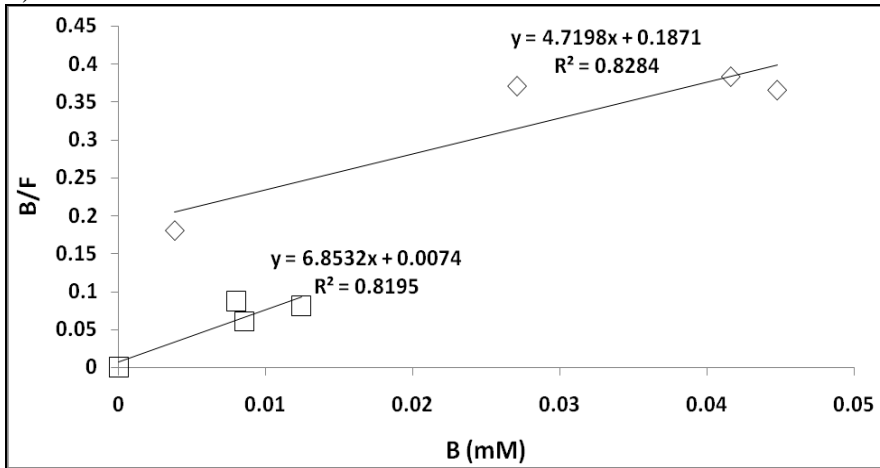


Figure A.1.7: Rebinding Isotherms of Testosterone Recognitive and Control Poly(MAA-co-EGDMA) at 90% Crosslinking. Poly(MAA-co-EGDMA) Recognitive Network (\diamond) and Control Network (\square). a) The Freundlich Isotherm; b) Langmuir Isotherm; c) Scatchard Plot. According to the R^2 values for both the testosterone and control networks, the Freundlich Isotherm was used to analyze the rebinding data to obtain the affinity constants for each system. B is the bound concentration of testosterone, F and T represents the equilibrium concentration of testosterone (T= 25°C).

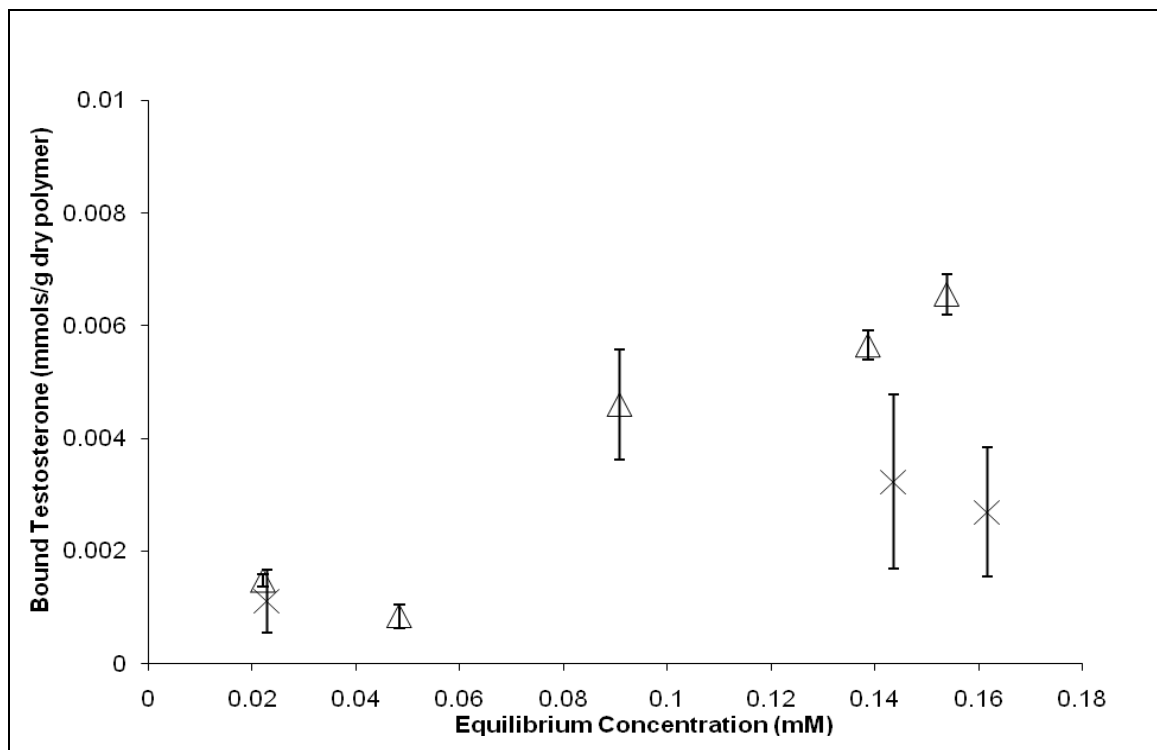


Figure A.1.8: Testosterone Equilibrium Binding Isotherms of Poly(MAA-*co*-PEG200DMA) at 77% Feed Crosslinking. Poly(MAA-*co*-EGDMA) Recognitive Network (Δ) and Control Network (x). Error bars represent standard deviation of four replicates ($T=25^{\circ}\text{C}$).

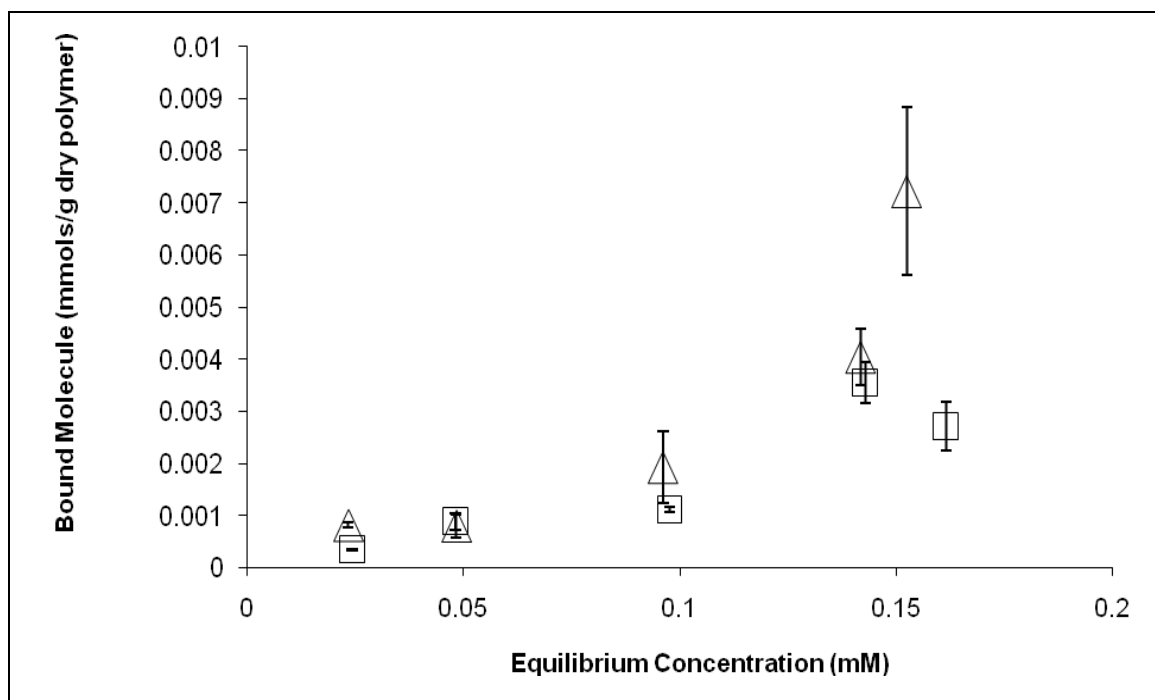


Figure A.1.9: Progesterone Equilibrium Binding Isotherms of Poly(MAA-co-EGDMA) at 77% Feed Crosslinking. Poly(MAA-co-EGDMA) Recognitive Network (◇) and Control Network (□). Error bars represent standard deviation of four replicates (T= 25°C).

A-2 Data from the Template Release Studies

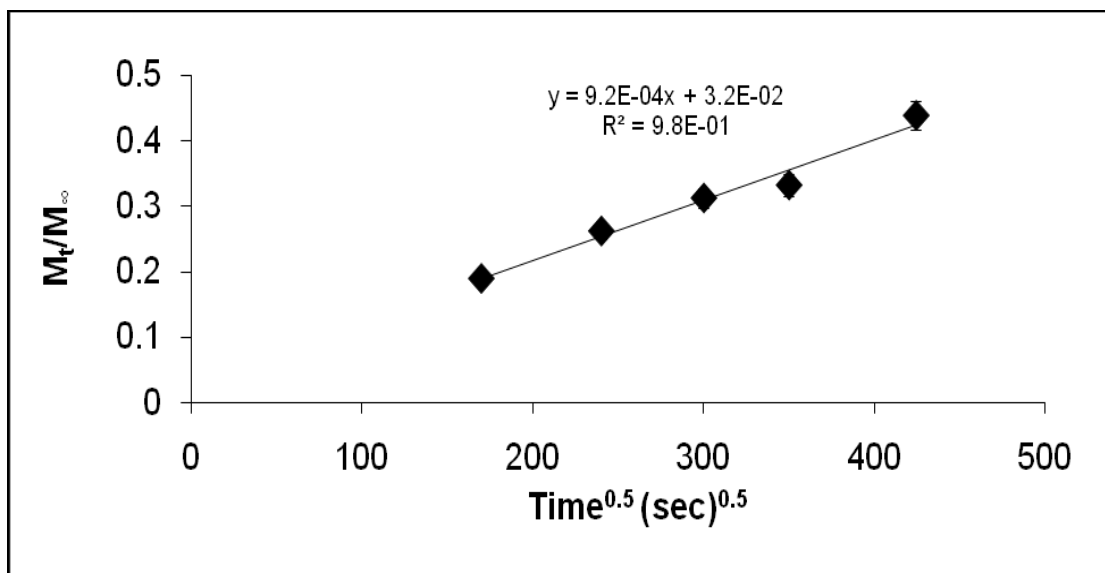


Figure A.2.1: Linear Regression Fractional Mass of Testosterone Released from Testosterone Recognitive Poly(MAA-co-EGDMA) Network at 77% Crosslinking.

The slope of the line was used in the calculation of the diffusion coefficient.

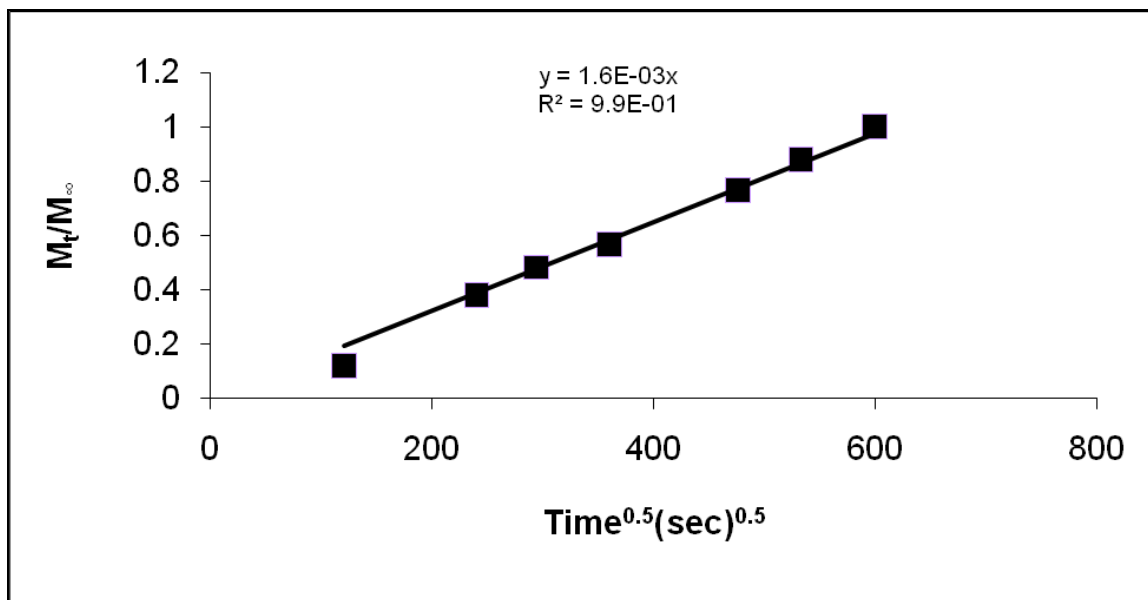


Figure A.2. 2: Linear Regression Fractional Mass of Testosterone Released from the Control Poly(MAA-*co*-EGDMA) Network at 77% Crosslinking. The slope of the line was used in the calculation of the diffusion coefficient.

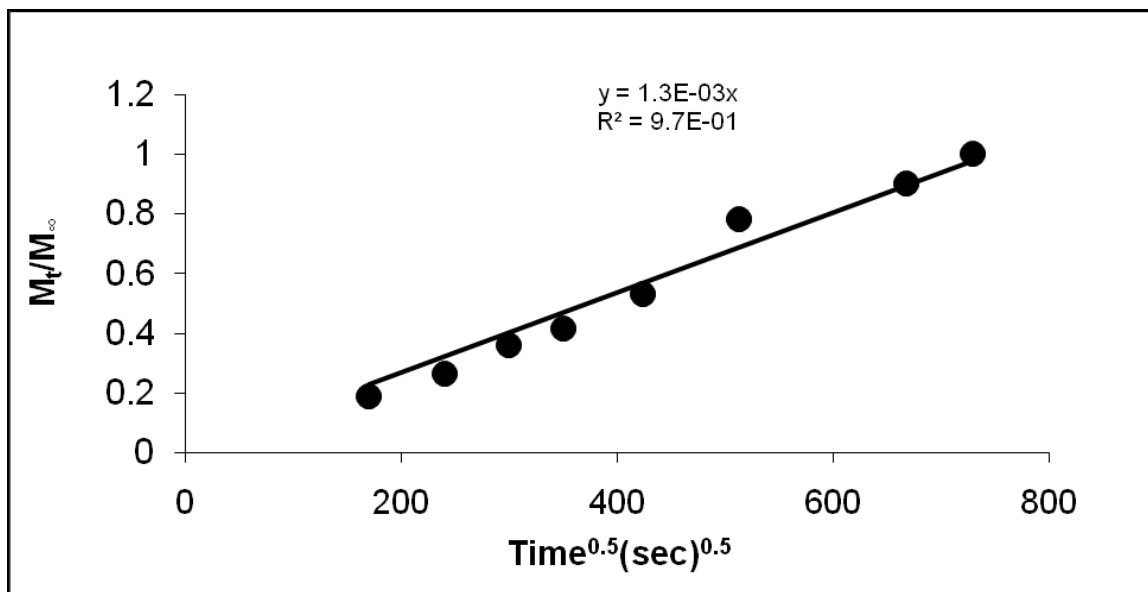


Figure A.2.3: Linear Regression Mass Fraction of Testosterone Released from Testosterone Recognitive Poly(MAA-co-EGDMA) Network at 50% Crosslinking.

The slope of the line was used in the calculation of the diffusion coefficient.

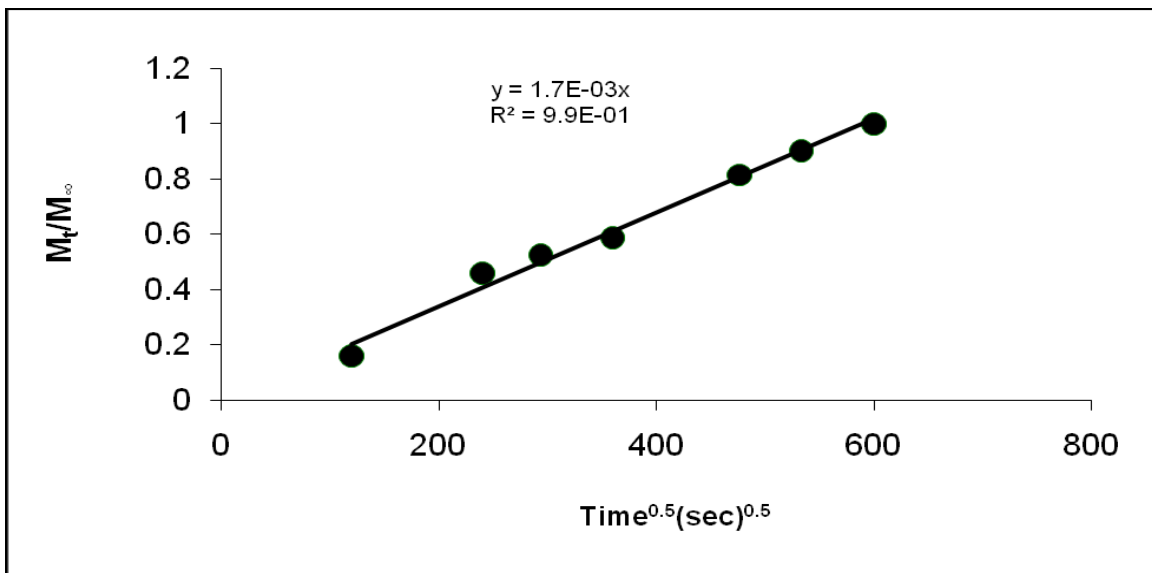


Figure A.2. 4: Linear Regression Fractional Mass of Testosterone Released from the Control Poly(MAA-*co*-EGDMA) Network at 50% Crosslinking. The slope of the line was used in the calculation of the diffusion coefficient.

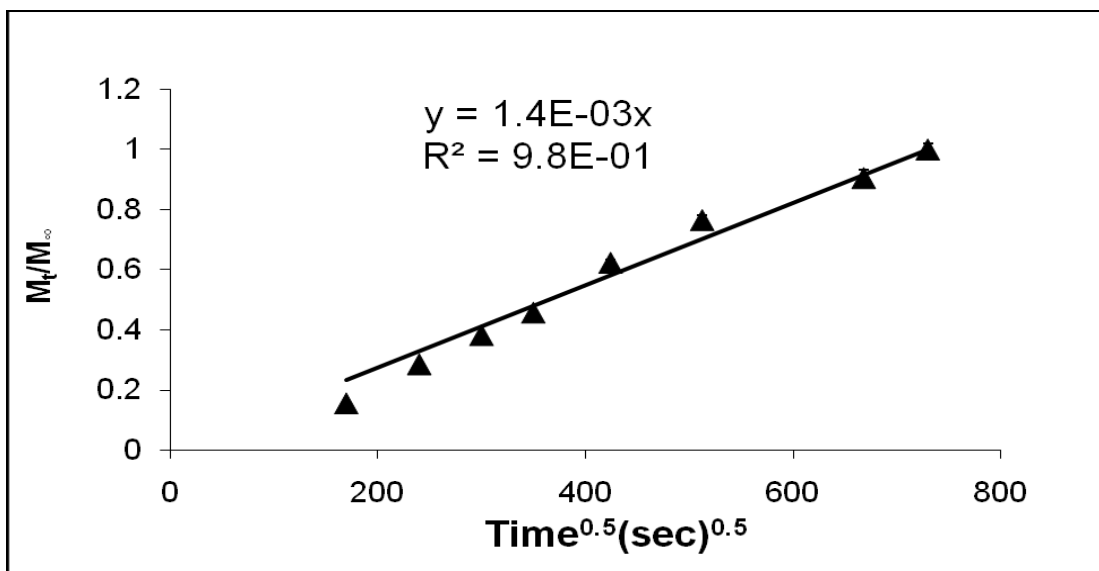


Figure A.2. 5: Linear Regression Fractional Mass of Testosterone Released from Testosterone Recognitive Poly(MAA-co-PEG200DMA) Network at 77% Crosslinking. The slope of the line was used in the calculation of the diffusion coefficient.

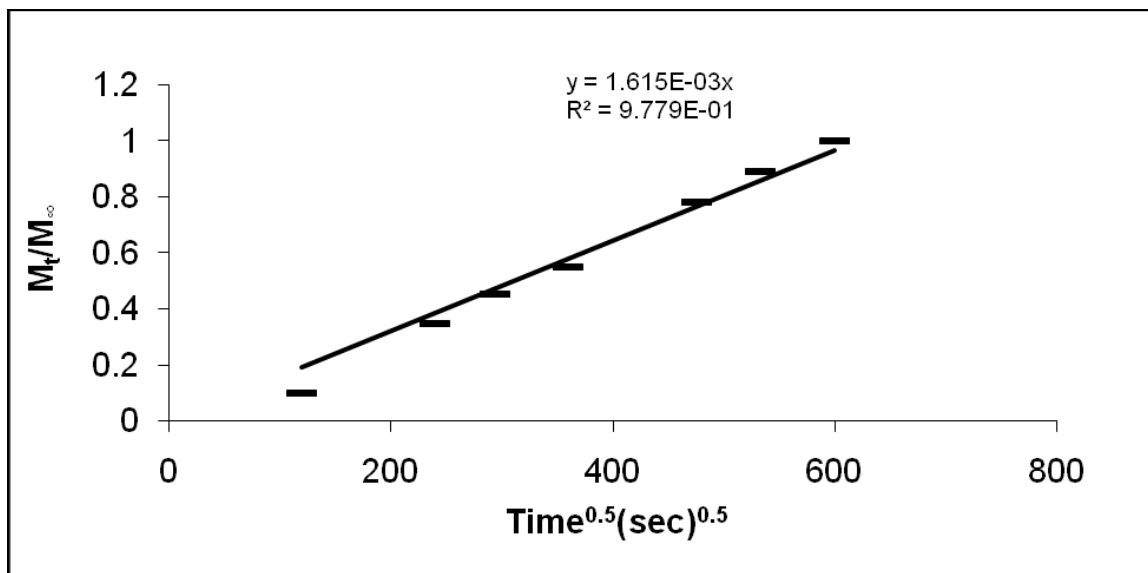


Figure A.2. 6: Linear Regression Fractional Mass of Testosterone Released from the Control Poly(MAA-co-PEG200DMA) Network at 77% Crosslinking. The slope of the line was used in the calculation of the diffusion coefficient.

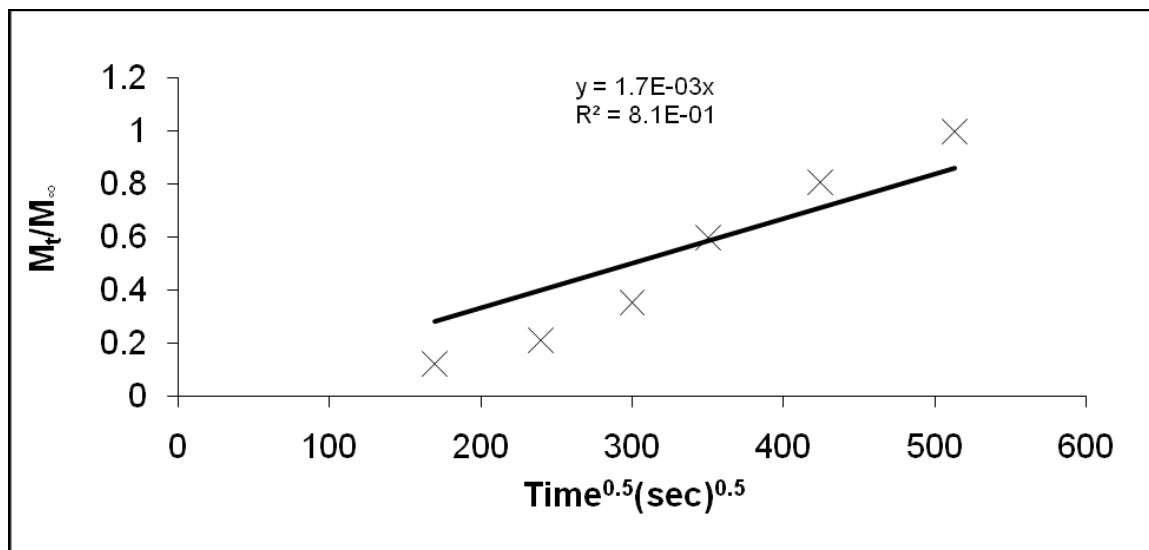


Figure A.2. 7: Linear Regression Fractional Mass of Testosterone Released from Testosterone Recognitive Poly(MAA-co-PEG200DMA) Network at 50% Crosslinking. The slope of the line was used in the calculation of the diffusion coefficient.

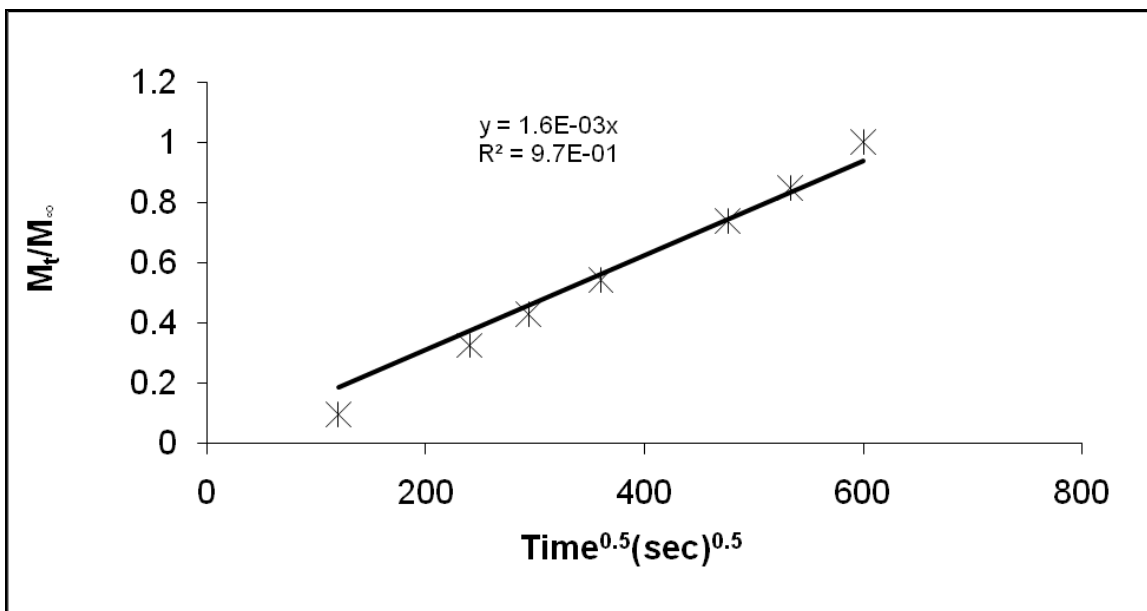


Figure A.2. 8: Linear Regression Fractional Mass of Testosterone Released from the Control Poly(MAA-co-PEG200DMA) Network at 50% Crosslinking. The slope of the line was used in the calculation of the diffusion coefficient.

APPENDIX B

Appendix B gives an overview of the error analysis used in the dissertation.

B-1. Error Analysis

Average values of multiple experiments were reported with their corresponding standard deviations. When multiplying or dividing quantities, the fractional standard deviations were squared, added, and then the square root of the sum was used to calculate the fractional total deviation. For example, consider $A \pm dA$ and $B \pm dB$, where dA and dB are the corresponding standard deviations. To calculate the multiplication of A and B (i.e., $X = A \times B$ with total error $\pm dX$) equation E.1 was used.

$$\frac{dx}{x} = \sqrt{\left(\frac{dA}{A}\right)^2 + \left(\frac{dB}{B}\right)^2} + \dots \quad (\text{E.1})$$

For addition or subtraction of average values with standard deviations, sum of squares analysis was also used (Eqn.E.2).

$$dx = \sqrt{(dA)^2 + (dB)^2} + \dots \quad (\text{E.2})$$

Sample average values were calculated where appropriate with 95% confidence limits for the mean. For example consider, equation E.3.

$$\bar{Y} \pm \frac{t_{(\alpha/2, n-1)} s}{\sqrt{N}} \quad (\text{E.3})$$

where \bar{Y} is the sample mean, $t_{(\alpha/2, n-1)}$ is the upper critical value of the t -distribution with $n-1$ degrees of freedom, s is the standard deviation, and N is the number of observations.